

2

NAVAL POSTGRADUATE SCHOOL

Monterey, California



THESIS

LOW FREQUENCY
GEOMAGNETIC FLUCTUATIONS (0.025 to 20 Hz)
ON THE FLOOR OF MONTEREY BAY

by

Morgan P. Ames, Jr.

and

Louis McBane Vehslage

December 1981

Thesis Advisor:

O. Heinz

DTIC
ELECTE

MAY 17 1982

A

Approved for public release; distribution unlimited.

ADA 114474

DTIC FILE COPY

82 05 17 0000

UNCLASSIFIED

SECURITY CLASSIFICATION OF THIS PAGE (When Data Entered)

REPORT DOCUMENTATION PAGE		READ INSTRUCTIONS BEFORE COMPLETING FORM
1. REPORT NUMBER	2. GOVT ACCESSION NO. AD-A114	3. RECIPIENT'S CATALOG NUMBER 474
4. TITLE (and Subtitle) Low Frequency Geomagnetic Fluctuations (0.025 to 20 Hz) on the Floor of Monterey Bay		5. TYPE OF REPORT & PERIOD COVERED Master's Thesis December 1981
7. AUTHOR(s) Morgan P. Ames Jr. Louis M. Vehslage		6. PERFORMING ORG. REPORT NUMBER
9. PERFORMING ORGANIZATION NAME AND ADDRESS Naval Postgraduate School Monterey, CA 93940		8. CONTRACT OR GRANT NUMBER(s)
11. CONTROLLING OFFICE NAME AND ADDRESS Naval Postgraduate School Monterey, CA 93940		10. PROGRAM ELEMENT, PROJECT, TASK AREA & WORK UNIT NUMBERS
14. MONITORING AGENCY NAME & ADDRESS (if different from Controlling Office) Naval Postgraduate School Monterey, California 93940		12. REPORT DATE December 1981
		13. NUMBER OF PAGES 107
		15. SECURITY CLASS. (of this report) UNCLASSIFIED
		15a. DECLASSIFICATION/DOWNGRADING SCHEDULE
16. DISTRIBUTION STATEMENT (of this Report) Approved for public release; distribution unlimited		
17. DISTRIBUTION STATEMENT (of the abstract entered in Block 20, if different from Report)		
18. SUPPLEMENTARY NOTES		
19. KEY WORDS (Continue on reverse side if necessary and identify by block number) Low Frequency Geomagnetic Measurements Geomagnetic Fluctuations in an Ocean Environment		
20. ABSTRACT (Continue on reverse side if necessary and identify by block number) Two coil antennas consisting of 5460 turns of copper wire were utilized to measure the vertical component and a horizontal component of the fluctuations of the geomagnetic field on the floor of Monterey Bay at a depth of approximately seventy meters. The results indicate that the power spectral density of the fluctuations varies from $1.6 \times 10^3 \text{ nT}^2/\text{Hz}$ at 0.01 Hz to $8 \times 10^{-8} \text{ nT}^2/\text{Hz}$ at 20 Hz for the horizontal component and from (continued on next page)		

DD FORM 1 JAN 73 1473

EDITION OF 1 NOV 66 IS OBSOLETE
S/N 0102-014-6601

UNCLASSIFIED

SECURITY CLASSIFICATION OF THIS PAGE (When Data Entered)

UNCLASSIFIED

SECURITY CLASSIFICATION OF THIS PAGE/When Data Entered

Item 20. (contd.)

$3.2 \times 10^2 \text{ nT}^2/\text{Hz}$ at 0.01 Hz to $6.3 \times 10^{-6} \text{ nT}/\text{Hz}$ at 20 Hz for the vertical. Both components exhibit a monotonic decrease of about 20 dB/decade as the frequency increases, except in the 8-20 Hz region in which the Schumann resonances occur. Measurements of the power spectral density for the vertical component show relatively small excursions from average measurements as a function of wave action, while the horizontal power spectral density varies greatly throughout the day and as a function of seawater motions.

Accession For	
DTIC GRA&I	<input checked="" type="checkbox"/>
DTIC TAB	<input type="checkbox"/>
Unannounced	<input type="checkbox"/>
Justification	
By	
Distribution/	
Availability Codes	
Avail and/or	
Dist	



Approved for public release; distribution unlimited

Low Frequency Geomagnetic Fluctuations (0.025 to 20 Hz)
On the Floor of Monterey Bay

by

Morgan P. Ames, Jr.
Lieutenant, United States Navy
B.S., United States Naval Academy 1974

and

Louis M. Vehslage
Lieutenant, United States Navy
B.A., Ohio State University 1975

Submitted in partial fulfillment of the
requirements for the degree of

MASTER OF SCIENCE IN ENGINEERING SCIENCE

from the

NAVAL POSTGRADUATE SCHOOL
December 1981

Authors:

Morgan P. Ames, Jr.
Louis M. Vehslage

Approved by:

Oh Heinz
Carl M. [unclear]
Jim Dyer
William M. Toller

Thesis Advisor
Second Reader
Chairman, Department of Physics and Chemistry
Dean of Science and Engineering

ABSTRACT

Two coil antennas consisting of 5460 turns of copper wire were utilized to measure the vertical component and a horizontal component of the fluctuations of the geomagnetic field on the floor of Monterey Bay at a depth of approximately seventy meters. The results indicate that the power spectral density of the fluctuations varies from $1.6 \times 10^3 \text{ nT}^2/\text{Hz}$ at 0.01 Hz to $8 \times 10^{-8} \text{ nT}^2/\text{Hz}$ at 20 Hz for the horizontal component and from $3.2 \times 10^2 \text{ nT}^2/\text{Hz}$ at 0.01 Hz to $6.3 \times 10^{-6} \text{ nT}^2/\text{Hz}$ at 20 Hz for the vertical. Both components exhibit a monotonic decrease of about 20 dB/decade as the frequency increases, except in the 8-20 Hz region in which the Schumann resonances occur. Measurements of the power spectral density for the vertical component show relatively small excursions from average measurements as a function of wave action, while the horizontal power spectral density varies greatly throughout the day and as a function of seawater motions.

TABLE OF CONTENTS

I.	INTRODUCTION	11
II.	BACKGROUND	13
	A. ORIGIN OF THE MAIN GEOMAGNETIC FIELD	13
	B. TIME VARIATIONS OF THE GEOMAGNETIC FIELD	17
	C. ELECTROMAGNETIC PROPAGATION IN LAYERED CONDUCTING MEDIA	26
	D. REVIEW OF PREVIOUS WORK	29
III.	EXPERIMENTAL EQUIPMENT AND TESTS	32
	A. EQUIPMENT CONFIGURATION	32
	1. DATA COLLECTION EQUIPMENT	34
	a. COIL ANTENNA SENSOR	34
	b. PREAMPLIFIER	36
	c. VARIABLE GAIN AMPLIFIER	37
	d. VOLTAGE CONTROLLED OSCILLATOR (VCO)	37
	e. REFERENCE OSCILLATOR	37
	f. ANALOG CASSETTE RECORDERS	38
	g. TIMER	38
	h. DC POWER SUPPLIES	39
	2. DATA ANALYSIS EQUIPMENT	39
	a. MIXER	39
	b. AMPLIFIER	41
	c. FREQUENCY-TO-VOLTAGE CONVERTER (FVC)	41
	d. DIFFERENTIAL AMPLIFIER	41

e. SPECTRUM ANALYZER -----	42
f. STRIP CHART RECORDER -----	42
B. SENSOR SENSITIVITY -----	42
1. THEORETICAL SENSOR SENSITIVITY -----	42
2. EXPERIMENTAL DETERMINATION OF SENSOR SENSITIVITY -----	44
C. SYSTEM TRANSFER FUNCTION -----	47
D. POWER SPECTRAL DENSITY CORRECTIONS -----	49
E. SYSTEM NOISE -----	52
IV. EXPERIMENTAL RESULTS -----	55
A. INTRODUCTION -----	55
B. DISCUSSION AND CORRELATION OF DATA -----	56
V. EQUIPMENT/SYSTEM RECOMMENDATIONS -----	64
LIST OF REFERENCES -----	66
APPENDIX A -----	68
A. EQUIPMENT SCHEMATICS -----	68
APPENDIX B -----	74
A. SYSTEM AND EQUIPMENT USAGE -----	74
APPENDIX C -----	77
A. THEORETICAL SENSOR SENSITIVITY -----	77
APPENDIX D -----	78
A. TRANSFER FUNCTION USAGE -----	78
APPENDIX E -----	80
A. DATA CURVES -----	80
INITIAL DISTRIBUTION LIST -----	105

LIST OF FIGURES

2.1	Power Spectrum of Geomagnetic Disturbances Observed on the Surface of the Earth -----	18
2.2	Field Strength of Micropulsations -----	22
2.3	Induced Magnetic Field Per Meter Amplitude of the Surface Wave -----	25
2.4	Attenuation of Electromagnetic Waves -----	27
2.5	Induced Magnetic Field -----	28
3.1	Diagram for Ocean Floor Measurements -----	33
3.2	Data Acquisition System Schematic -----	35
3.3	Sensor Dimensions -----	36
3.4	Data Analysis System Schematic -----	40
3.5	emf vs Signal Frequency for a Signal of 1 nT -----	43
3.6	Test Coil System Circuitry -----	45
3.7	Experimental Sensor Sensitivity -----	46
3.8	Transfer Function Components -----	47
3.9	Preamplifier Gain Characteristics -----	48
3.10	VCO/FVC Gain Characteristics -----	50
3.11	System Transfer Functions -----	51
3.12	Horizontal System Noise -----	53
3.13	Vertical System Noise -----	54
4.1	Average Power Spectral Data (horiz) -----	58
4.2	Average Power Spectral Data (vert) -----	59
4.3	Average Land Data Curves -----	63

A.1	Preamplifier Schematic -----	69
A.2	Timer Schematic -----	70
A.3	Mixer Schematic -----	71
A.4	Reference Oscillator Schematic -----	72
A.5	VCO Schematic -----	73
E.1	Data Curve (9/20/81, horiz., .1-20 Hz) -----	81
E.2	Data Curve (9/20/81, vert., .1-20 Hz) -----	82
E.3	Data Curve (9/20/81, horiz., .1-20 Hz) -----	83
E.4	Data Curve (9/20/81, vert., .1-20 Hz) -----	84
E.5	Data Curve (9/20/81, horiz., .1-20 Hz) -----	85
E.6	Data Curve (9/20/81, vert., .1-20 Hz) -----	86
E.7	Data Curve (9/24/81, horiz., .1-20 Hz) -----	87
E.8	Data Curve (9/24/81, vert., .1-20 Hz) -----	88
E.9	Data Curve (9/25/81, horiz., .1-20 Hz) -----	89
E.10	Data Curve (9/25/81, vert., .1-20 Hz) -----	90
E.11	Data Curve (9/25/81, horiz., .1-20 Hz) -----	91
E.12	Data Curve (9/20/81, horiz., .025-5 Hz) -----	92
E.13	Data Curve (9/20/81, vert., .025-5 Hz) -----	93
E.14	Data Curve (9/20/81, horiz., .025-5 Hz) -----	94
E.15	Data Curve (9/20/81, vert., .025-5 Hz) -----	95
E.16	Data Curve (9/20/81, horiz., .025-5 Hz) -----	96
E.17	Data Curve (9/20/81, vert., .025-5 Hz) -----	97
E.18	Data Curve (9/24/81, horiz., .025-5 Hz) -----	98
E.19	Data Curve (9/24/81, vert., .025-5 Hz) -----	99
E.20	Data Curve (9/25/81, horiz., .025-5 Hz) -----	100

E.21	Data Curve (9/25/81, vert., .025-5 Hz)	-----	101
E.22	Data Curve (9/25/81, horiz., .025-5 Hz)	-----	102
E.23	Data Curve (9/25/81, Land Data, .1-20 Hz)	-----	103
E.24	Data Curve (9/25/81, Land Data, .1-20 Hz)	-----	104

ACKNOWLEDGEMENTS

We owe a special gratitude to our advisors, Dr. Otto Heinz and Dr. Paul H. Moose for their guidance, cooperation and assistance during this research project. Next, appreciation is extended to Mr. Robert Smith of the Research Department for his technical expertise in the design and construction of many of the electronic components and to Mr. Thomas Maris of the Physics and Chemistry Department for the design and construction of the sensor support stand. A special thanks is extended to Miss Ginger Kelley for her efforts in the typing of this thesis. Finally, we are appreciative of Captain Woodrow Reynolds, Master of the Research Vessel Acania, and his crew for the professional handling of our system during deployment and recovery operations and for the escape from academia that the underway periods on Monterey Bay provided.

I. INTRODUCTION

This thesis research is part of a continuing effort by this institution to obtain a long term data base for the improved understanding and interpretation of electromagnetic noise in the vicinity of the sea floor. The overall project emphasizes the importance of obtaining measurements of geomagnetic fluctuations on the sea floor over a period of several years at various locations and depths. Primary objectives include the interpretation of signals covering four decades of frequency, from 0.01 Hz to 100 Hz through the use of total field magnetometers, induction coils and ULF/ELF receivers.

The magnetic noise in the sea is of interest both from a geophysical viewpoint as well as for naval applications. In addition to undersea field magnetometry, some areas of current geophysical interest are the measurement of marine geomagnetic anomalies near centers of seafloor spreading, characterization of magnetic fields induced by ocean waves, geophysical exploration and the utilization of low frequency waveguides present under the seafloor. Applications of interest to the Navy are in the areas of mine warfare, submarine detection, submarine communications using a superconducting quantum interference device (SQUID) as the sensing element for an extreme low frequency (ELF) receiving antenna system, and

possibly as a means of remote verification of underground nuclear test detonations.

The particular objectives of this thesis research are to collect two component (horizontal and vertical) field fluctuation data from the floor of Monterey Bay and to evaluate the relationship, if any, between them. A secondary objective is to compare seafloor data with simultaneous data obtained at a remote land site by other experimenters.

II. BACKGROUND

A. ORIGIN OF THE MAIN GEOMAGNETIC FIELD

The earth's main field is approximately 50,000 nT¹ in strength and its shape may be approximated as being that of an almost terrestrially centered dipole magnet with its axis at an angle of 11.5 degrees to the rotation axis of the earth. Actually, its source is located in the earth's molten core, which is a conducting fluid subject to both differential rotation and convective circulation. The core is a very good electrical conductor and is believed to have a conductivity of about 10 siemens per meter. As a result of viscous forces and temperature gradients in the molten core there is both differential rotation, since the interior rotates faster than the outer portion of the core, and turbulent upwelling due to thermal convection. Several energy sources are available in the core and some of the mechanisms by which energy can be generated are radioactive decay, gravitational contraction, and perhaps, high pressure phase transitions.

[Ref. 1]

A simple self sustaining dynamo may be represented by a loop of wire in which a current flows, inducing a magnetic field, and a conducting disk coaxially located parallel to

¹1 nanotesla (nT) = 10^{-9} Tesla = 10^{-5} Gauss (G) = 1 Gamma (γ)
1 Tesla = 1 volt second / meter = 10^4 Gauss

and immediately above the loop rotating across the magnetic field to generate an electromotive force that drives the current in the loop. In this manner an initial "seed" field can be augmented by this feedback arrangement and would continue to grow indefinitely, so long as conditions remained the same. Of course, this is not possible since power is required to maintain the conducting disk's rotation. Depending upon the conductivity of the disk, the dynamo would not function unless either its rotation rate were sufficiently fast (faster spin rates are required for lower conductivity disks) or it is scaled up to an enormous size. Should the latter solution be accomplished, scaling it up to the size of the earth's radius, only very slow angular velocity would be required, on the order of one complete rotation about its axis every six hundred years. However since the earth does rotate roughly once in each twenty-four hour period there is more than enough energy available to support the internal dynamo.

Any dynamo theory of the geomagnetic field postulates that the fluid core is moving in magnetic fields that generate currents to support and amplify the magnetic fields. Although the dynamo concept is generally accepted, the details of the fluid motion of the earth's conductive core and its interaction with the magnetic field are not fully understood. Neither is the origin of the earth's "seed" field completely understood. It is assumed that the

earth initially had an established symmetric field of external origin, perhaps due to the solar magnetic field, and that the field was "frozen" into the earth's highly conductive core during its formation.

The first proposal of a dynamo origin of the field was made by Elsasser (1946), who provided the first step of the regenerative process. Tidal deceleration of the mantle was taken to be the energy source making the core fluid circulate eastward (as it experiences differential rotation). ...In simple patterns of differential rotation, the inner parts of the fluid core, nearest the axis of rotation, have a higher angular velocity than the outer parts because of a tendency for conservation of angular momentum. The inner regions then rotate eastward deep into the core from north to south, it may be dragged eastward where it approaches nearest the center into the shape of a bent hairpin wrapped at least part way around the (spin) axis... (As differential rotation continues the wrapped flux lines eventually disconnect) generating a toroidal or east-west (aximuthal) field from a poloidal initial poloidal field, a step of amplification.

The other step, a feedback mechanism, was provided by Bullard (1949). He postulated convective flow including radial currents presumably driven by a central radioactive heat source. [Ref. 2]

The next refinement was introduced by Parker (1955), who considered a random distribution of a few large upward vortices, as well as the possibility of many smaller upward vortices. He showed that their cyclonic helicity, arising from both the Coriolis force and an opposing ring current, twists the azimuthal toroidal field in such a way as to cause it to wind itself up into a helical toroid. The toroidal magnetic field is thus replaced by a toroidal helix which winds itself tighter and tighter until eventually, diffusion allows the helix to break up into north-south eddy rings.

There have since (1955) been analyzed a number of interesting variations of this theme, each of them postulating some either random or systematic distribution of vortices having preponderantly left-handed helicity in the Northern Hemisphere and right-handed helicity in the southern as a result of Coriolis force. Basic to all this is the way a twisting stream of fluid crossing a magnetic field distorts that field to produce a circulation of the field about its original direction, the sense of the circulation of the field depending on the helicity of the stream. The toroidal field is eastward in the Northern Hemisphere, westward in the Southern... thus a westward toroidal current is generated in each (hemisphere) and this is the correct sense to generate the original poloidal field. [Ref. 3]

Since the poloidal field closely resembles that of a dipole, the earth's main field may be represented simplistically by a dipole magnet, almost terrestrially centered, that is decreasing in intensity about 15 nT per year while moving westward at a rate of about 0.18 degrees each year. To illustrate this point, note that the line of zero declination was in Europe five centuries ago and is now in America. The nondipole portion of the magnetic field has a total intensity of about 5,000 nT and is changing at a rate of about 50 nT per year. The sense of the geomagnetic field lines is southward near the earth's center emerging in the southern magnetic hemisphere then northward outside, external to the surface of the earth to the conjugate point in the northern hemisphere. A unique feature of the ring current in the earth's core creating a new dipole field is that its magnetic polarity is reversed. Thus the earth's magnetic dynamo is self-sustaining with periodic reversals in its magnetic field.

B. TIME VARIATIONS OF THE GEOMAGNETIC FIELD

As discussed in the previous section, secular variations of the earth's main magnetic field have characteristic times on the order of thousands of years. Superimposed on these very slow field variations is a continuous spectrum of fluctuations of higher frequencies as depicted in Figure 2.1. The sources of these variations are found external to the surface of the earth, and include diurnal variations, variations due to geomagnetic storms, micropulsations, and in the ocean variations due to ocean waves.

Diurnal variations exhibit fluctuations in field intensity of between 20 and 50 nT. They occur on a daily basis and are caused by ionospheric current systems, which are initiated by radial convection in the conductive upper atmosphere. The vertical motion of the atmosphere occurs as a result of pressure and temperature differentials produced by solar heating. These combine with the Coriolis force and very high wind velocities in the ionosphere to produce the transport of charged particles through the earth's magnetic field.

The ionospheric current distribution remains stationary with respect to the sun while the earth rotates beneath it once each twenty-four hour period. These currents are limited to that side of the earth illuminated by the sun and are centered on the meridian that represents local noon.

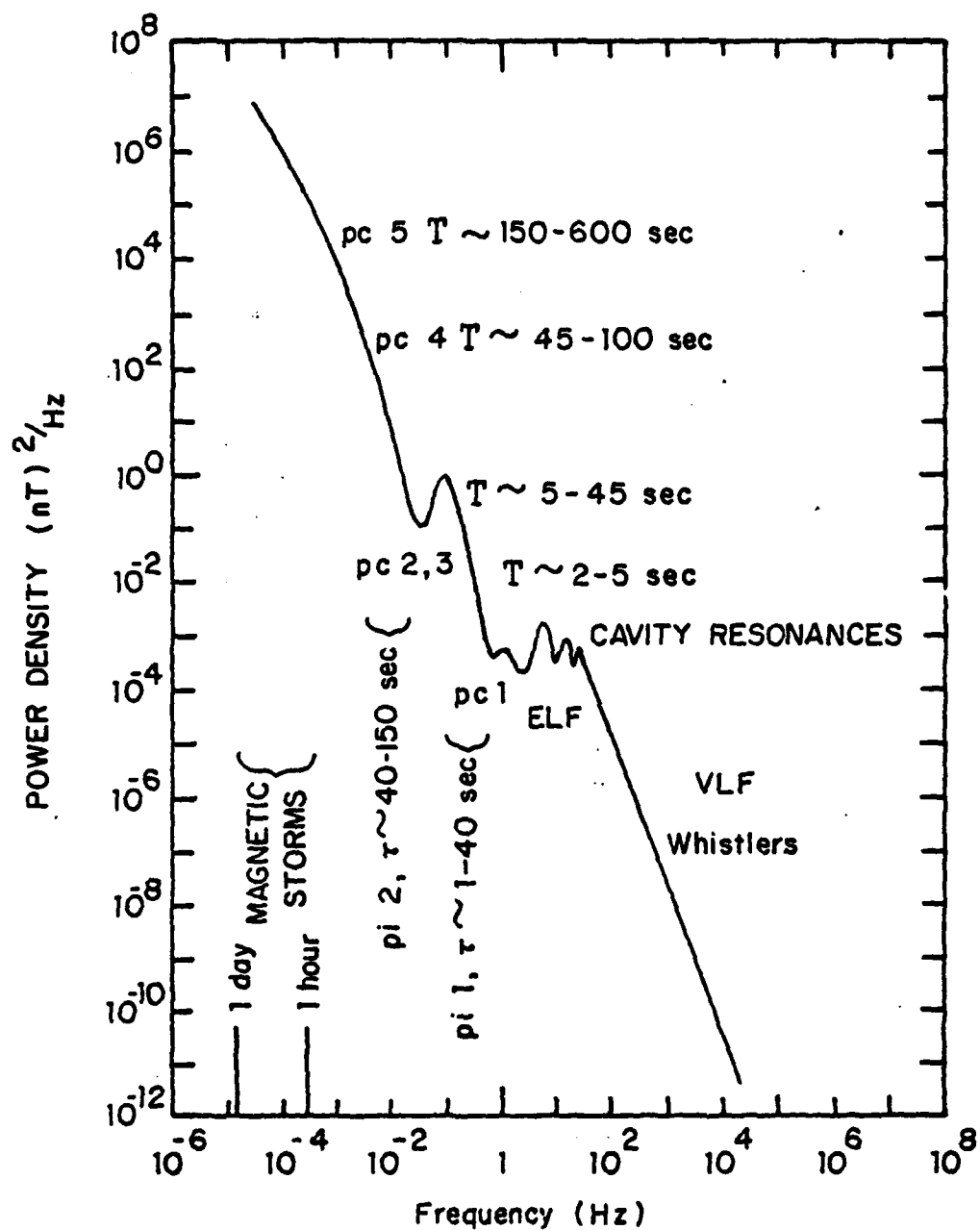


Figure 2.1 Power Spectrum of Geomagnetic Disturbances Observed on the Surface of the Earth.

[Cladis, Davidson, and Newkirk 1971]

Larger variations, which exhibit definite characteristic phases, are due to magnetic storms. They are the result of solar flare activity, which radiates energy in the form of an intense burst of plasma particles. The impact of this plasma stream on the outer boundary of the magnetosphere produces a compression of the magnetosphere that registers itself upon the surface of the earth as an increase in the magnetic field intensity on the order of approximately 50 nT over the space of about five minutes. A new equilibrium is reached between the magnetosphere and the engulfing solar plasma stream and this equilibrium is maintained until the plasma cloud has blown completely past the earth. The magnetic field intensity decreases to values that are typically several hundred nanoteslas below the prestorm values, due to an increase of the trapped particulate population from the plasma cloud, and the acceleration of previously trapped electrons and ions producing a westward ring current, which circles the earth at several earth radii. This magnetic field strength recovers back to its prestorm equilibrium as the ring currents gradually dissipate over the next several days.

In addition to the major variations discussed above, there also exists a wide range of smaller disturbances or electromagnetic perturbations that propagate through the magnetosphere as hydromagnetic waves both along and across the magnetic field lines. The resultant variations of the

earth's magnetic field are called micropulsations. These geomagnetic micropulsations are produced as a result of wave-particle interactions in the magnetosphere. [Ref. 4] As they propagate through the conductive layers of the atmosphere, they are transformed into electromagnetic waves, which may be detected on the surface of the earth as magnetic field pulsations. These micropulsations are divided depending on their appearance into one of two types: continuous or irregular.

Smoothly varying, periodic pulsations are classified as continuous (Pc) micropulsations. This distinct periodicity suggests that some kind of resonance occurs within the magnetospheric cavity. One model proposed by Jacobs (1963) describes the resonance as a result of an oscillating hydromagnetic wave composed of bunches of ions trapped in the magnetosphere which "bounce" back and forth between the hemispheres while spiralling about a line of force between two conjugate points on the earth's surface. [Ref. 5]

These continuous micropulsations are further divided according to their periods as follows: (see Figure 2.2)

1. Pc 1: (0.15 - 5 seconds)

More commonly known as "Pearls" they are generated by the cyclotron instability of energetic protons. These are associated with solar disturbances and have been studied as a means for possible prediction of impending magnetic storm activity since they

demonstrate an increase in activity one to two hours before and four to seven days after a magnetic storm. [Ref. 6] They occur during the daytime in the auroral zone and during night and early morning hours in the midlatitudes. They have an average amplitude of approximately 0.05 - 0.1 nT.

2. Pc 2: (5 - 10 seconds)

These are diurnal phenomena which show some correlation with solar activity and seasonal effects. They are noted for a decrease in their period as magnetic activity increases, for example, at sunset. The average amplitude is in the range of 0.1 - 1 nT.

3. Pc 3: (10 - 45 seconds)

Except for the difference in period length, these pulsations have characteristics similar to those of the Pc 2 pulsations.

4. Pc 4: (45 - 150 seconds)

These pulsations are associated with sunspot activity and have been observed to change their period seasonally. They occur for the most part during daylight hours and have an average amplitude between 0.1 - 1 nT.

5. Pc 5: (150 - 600 seconds)

These are large amplitude pulsations which usually occur during morning and evening hours and have typical amplitudes of 1 - 10 nT but on occasion have been

observed to vary by several hundred nanoteslas during the magnetically active periods of sunrise and sunset. The duration of their period bears a strong dependent on geomagnetic latitude.

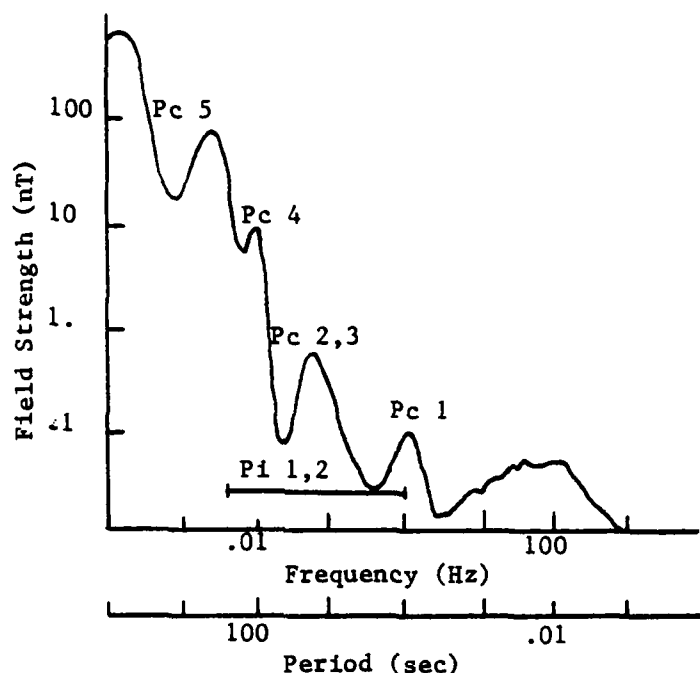


Figure 2.2. Field Strength of Micropulsations [Campbell 1966]

Irregular (Pi) micropulsations are associated with polar magnetic disturbances and are observed as nighttime phenomena. It is suspected that these arise from conductivity disturbances of the ionosphere due to particle bombardment from the magnetosphere, as well as from increased solar radiation levels. These sporadic irregular pulsations are classified as follows:

1. Pi 1: (1 - 40 seconds)

These are low amplitude noise bursts which usually occur during night and early morning hours and typically vary between 0.01 - 0.1 nT. They are closely associated with auroral disturbances and may be observed in the low and middle latitudes.

2. Pi 2: (40 - 150 seconds)

These have amplitudes of 1 - 5 nT and usually occur during the evening hours and may continue throughout the night. They may occur separately or as a succession of pulsations, known as pulsation trains, which have displayed periods up to 250 seconds. In general, the periods decrease with increased magnetic activity.

The continuous micropulsations last for several hours while the irregular pulsations may vary from a few minutes to about an hour. [Ref. 7] Above 3 Hz, the most pronounced geomagnetic field variations are the earth - ionosphere cavity resonances, or Schumann resonances (see Figure 2.1), which result from disturbances resonantly excited in the concentric spherical cavity bounded by the earth and the ionosphere by lightning transients [Ref. 8]. These effects have also been observed following atmospheric detonations of nuclear devices within the cavity. [Ref. 9]

Magnetic variations due to ocean waves are caused by the mass transport of a conducting fluid, seawater, across the geomagnetic field lines inducing electric currents in

conducting medium. These currents give rise to secondary magnetic fields, which add vectorially to the quasistatic, geomagnetic field. [Ref. 10] Only the surface waves need be considered in a first approximation. Figure 2.3 is a plot for several wave periods of the induced magnetic field per meter amplitude of surface wave. [Ref. 11] This curve is based upon a surface wave travelling along the magnetic meridian and an inclination angle of the earth's main field of seventy degrees. This closely approximates the local dip angle for the field which is sixty two degrees in the Monterey Bay region. This plot demonstrates that a one meter high wave, typical of the wind-driven waves on Monterey Bay in the afternoon, produces magnetic amplitude variations on the order of one nanotesla at depths up to approximately 100 meters for a sea swell period of about 12 seconds. In this treatment, Weaver assumed an infinite ocean. In generalizing Weaver's equations to incorporate bottom reflection and transmission, it was found that the effect of the bottom decreased the magnitude of the induced magnetic field by less than 3 dB for frequencies greater than 0.016 Hz in water depths less than 500 meters. [Ref. 12] For swell periods of less than twenty seconds, the bottom effect becomes negligible at depths greater than a few hundred meters.

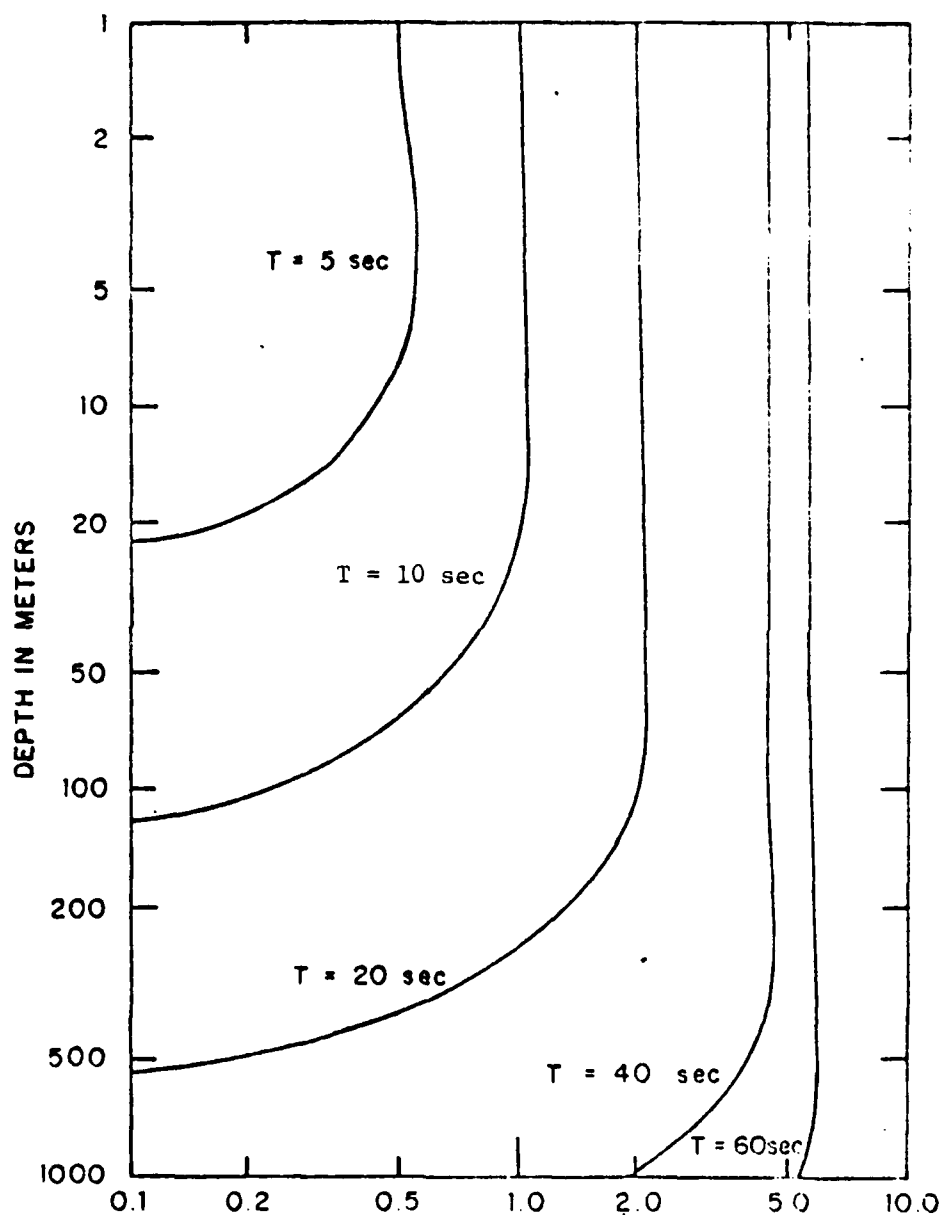


Figure 2.3. Induced Magnetic Field per Meter Amplitude of the Surface Wave.

[Weaver 1965]

C. ELECTROMAGNETIC PROPAGATION IN LAYERED CONDUCTING MEDIA

In seawater, the electrical conductivity varies from three to six Siemens per meter. If the case of an infinitely deep ocean and an average conductivity of four siemens per meter is assumed, then for every factor of one hundred decrease in frequency, the skin depth increases by a factor of ten as shown in Figure 2.4.

To fully explain electromagnetic wave propagation in the sea, consideration must be given to the effects and interaction of the seawater, ocean floor and air-sea surface interface. A physical model for a layered conducting media was developed in previous work by Moose and Chaffee (1979). The results of this model provide a relationship to obtain the ratio of induced to incident magnetic field amplitude as a function of seawater conductivity, water depth, seafloor conductivity and frequency. The resultant curves, which are depicted in Figure 2.5, clearly indicate that in shallow water the ocean serves as a thin layer in the model and the curve is affected by the conductivity of the earth's crust and mantle as reflections occur within the first skin depth. In the deep ocean case, the curves begin to conform to the ratio of induced to incident magnetic field which applies when only considering skin depth effects. Since the seafloor is no longer in close proximity to the surface, the reflections of electromagnetic waves in the sea no longer dominate, thus the attenuation per wavelength of the magnetic field ratio becomes constant.

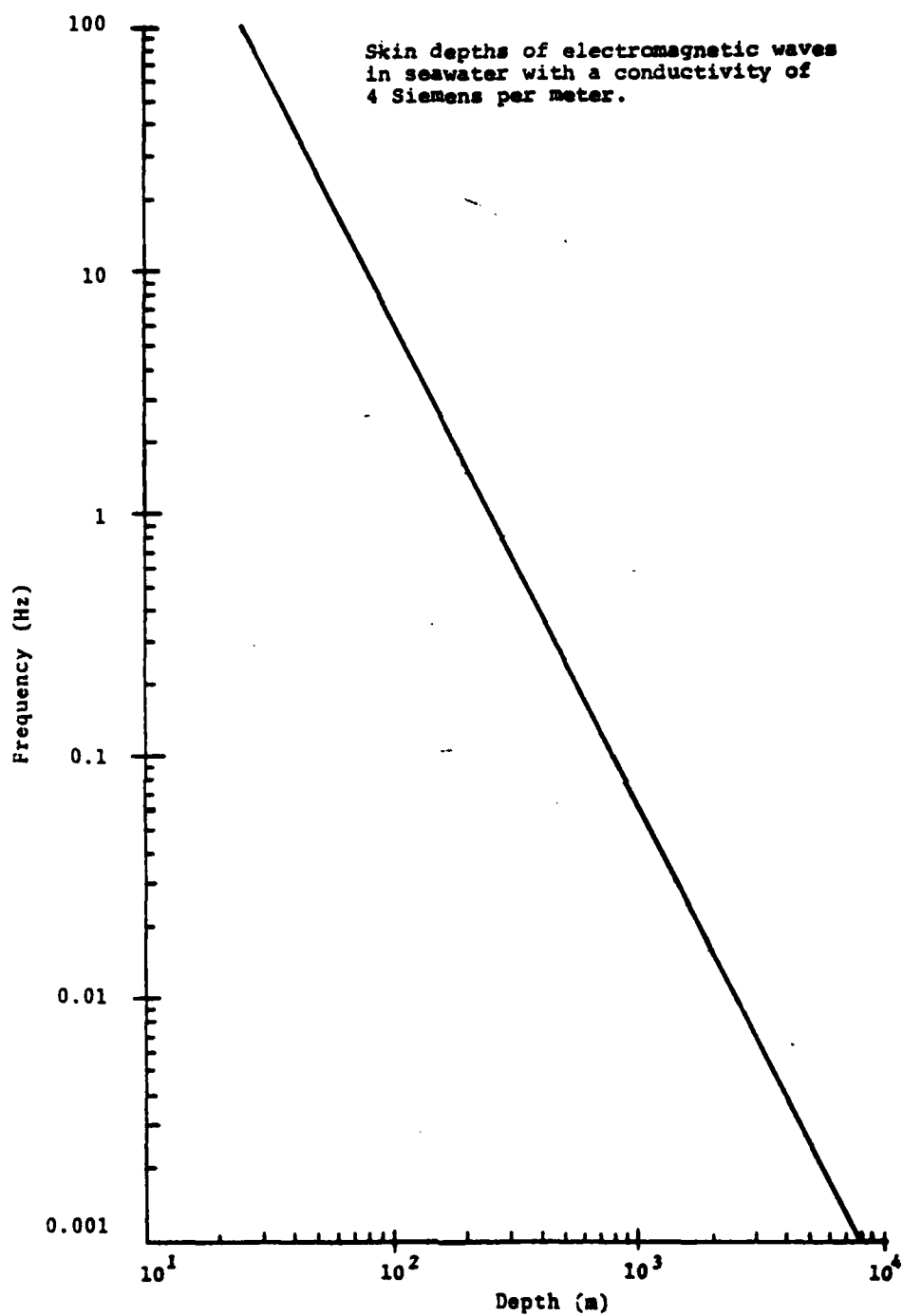


Figure 2.4. Attenuation of Electromagnetic Waves

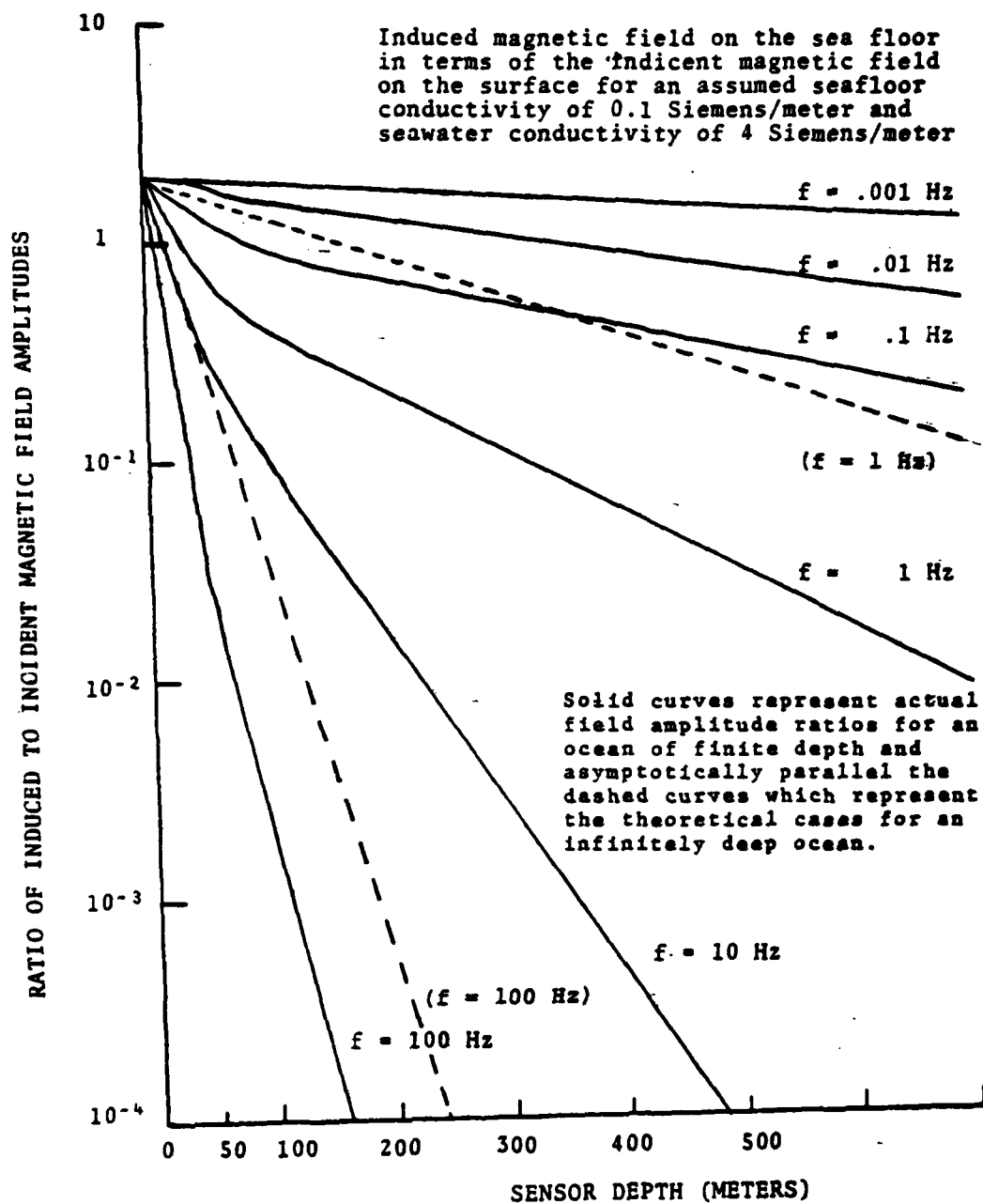


Figure 2.5. Induced Magnetic Field

D. REVIEW OF PREVIOUS WORK

Several studies have been undertaken in the detection and prediction of low frequency (i.e. less than 100 Hz) geomagnetic variations both on land and in the sea over the past two decades. Experiments by Horton and Hoffman (1962), Santirocco and Parker (1963), and Davidson (1964) demonstrated that the power spectral density of the geomagnetic field decreases monotonically by 6 dB per octave, or 20 dB per decade, between 10^{-4} and 1.0 Hz. Between 1 and 40 Hz, the spectrum levels off and is dominated by the Schumann resonances. [Ref. 13] There are indications of a general increase in background activity between 20 and 70 Hz with a continuation of the decrease in the power density above 80 Hz. [Ref. 14] More recently obtained spectra indicate that the general decline in the power density observed at frequencies below 5 Hz continues through 70 Hz. [Ref. 15] This general decline may continue on to higher frequencies with the Schumann resonance activity superimposed onto the declining magnetic background. [Ref. 16]

High sensitivity measurements of the field variations on land were made in the 0.1 to 14 Hz frequency band through the use of a superconducting magnetometer. Although this work concentrated on Pc 1 micropulsations, it not only provides an excellent reference for the slope of the power spectral density of north-south component field fluctuations, but also exhibited an overall decline in the amplitude of

nighttime events relative to those that occurred during daylight hours. Additionally, it demonstrated that the increase or decrease, respectively, of the amplitude of the power spectrum lagged both sunrise and sunset by approximately three hours. Hence, there is a steady decline of the background magnetic activity at a rate of 6 dB per octave which extends over almost six decades of frequency, 10^{-4} to 100 Hz. [Ref. 17] Further investigations of the low frequency variations in the range of 0.1 to 10 Hz and 0.4 to 40 Hz were undertaken near Monterey, California on land using a cesium vapor magnetometer and determined to be in concurrence with earlier measurements. [Ref. 18]

Measurements of time variations of the geomagnetic field were performed underwater, on the floor of Monterey Bay, at depths of 100 - 200 meters. The measurements, obtained using a cesium vapor, total field magnetometer, were in the frequency range of 0.01 to 3 Hz. From these measurements, the power spectrum of typical fluctuations was observed to vary from $1 \text{ nT}^2/\text{Hz}$ to $10^{-5} \text{ nT}^2/\text{Hz}$, monotonically decreasing over the frequency range. Additionally, observations were made of the influence of ocean waves and swell on the geomagnetic power density spectrum. [Ref. 19]

Horizontal components of the geomagnetic field fluctuations were measured, both on land and in the sea, through the use of a coil antenna. An attempt was made to measure the vertical component of the field fluctuations and upper limits

of 10^{-3} nT²/Hz and 10^{-6} nT²/Hz at one and ten hertz, respectively, were placed on the power spectral density.

[Ref. 20]

Most recently, a cesium vapor magnetometer was utilized to measure field fluctuations on land, as well as, on the seafloor. This data revealed that the decline in the power spectrum, below five hertz, was approximately 30 dB per decade; and that a relationship exists according to which the fall-off of the power spectrum was greater during periods of increased geomagnetic activity. [Ref. 21] This observation conforms with that of Nishida (1978), who determined that more active geomagnetic days manifest themselves by attenuating the higher frequency pulsations and enhancing the lower frequencies. McKinley and Santos (1980) observed that the power spectrum for the land and sea measurements were roughly parallel with the exception of the sea swell generated peak and noted that the undersea curves have a higher power density than the land data in the same frequency range. McKinley and Santos also made comparative measurements of the power spectrum for nighttime and daylight hours. They observed that the power density decreases shortly after nightfall and that an upward shift in the Pc 3 micropulsations occurs during the transition from day to night. This transition was observed to lag local sunrise and sunset by three hours and is related to the increased prominence of the higher nocturnal frequencies of the Pc 3 pulsations.

III. EXPERIMENTAL EQUIPMENT AND TESTS

A. EQUIPMENT CONFIGURATION

The general layout for component measurements of fluctuations of the earth's magnetic field is shown in Figure 3.1.

The sensors and data collection equipment were housed in Benthos glass spheres with a 0.404 meter inner diameter. The instrumentation and sensor spheres were connected by two 30 meter long, coaxial cables terminated with Brantner type sea connectors and Benthos sphere penetrators through the glass walls to the enclosed equipment.

The non-metallic stand permitted ease of deployment and provided structural support and protection for the sensor spheres. Sensor stand design called for a light, free-flooding structure with removable strap-on weights to obtain the required negative buoyancy, but still allow for portability and ease of handling in system deployment. A non-metallic material was necessary in the stand construction to avoid the effects of induced currents due to electrochemical reactions at the interface of a metal surface and the electrically conductive seawater. The stand was constructed of light-weight, high-strength, Acrylonitrile-Butadiene-Styrene (ABS) piping which is well suited for this application. The weights were fashioned from lengths of ABS piping filled with lead, sand, and transformer oil. The piping was then capped off at the

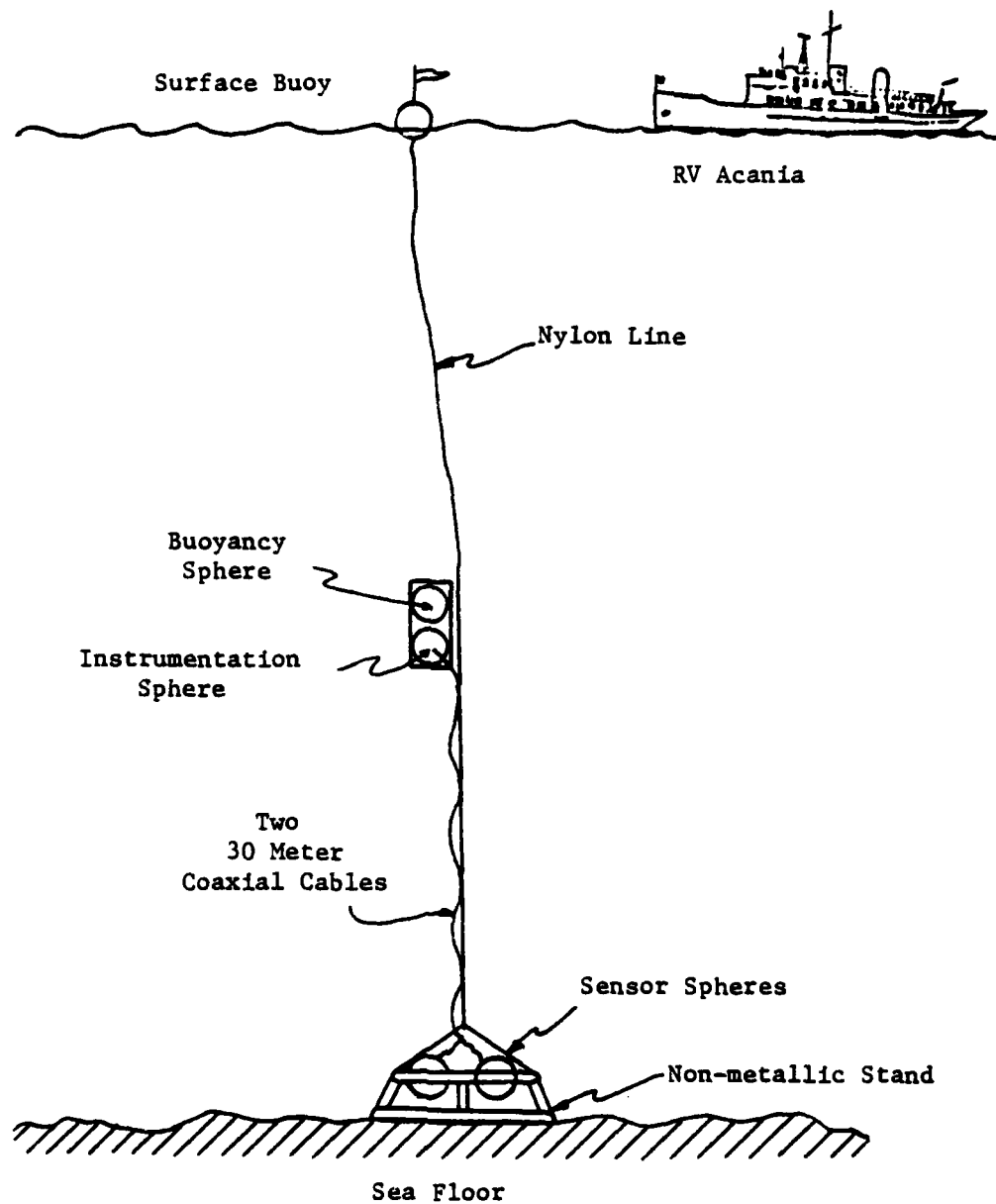


Figure 3.1. Diagram for Ocean Floor Measurements

ends to provide a watertight, non-metallic and compact means of adding the necessary negative bouancy to the stand.

1. Data Collection Equipment

The acquisition system illustrated in Figure 3.2 reveals the following major components:

1. coil antenna sensors (2)
2. preamplifiers (2)
3. variable gain amplifiers (2)
4. voltage controlled oscillators (2)
5. reference oscillator (1)
6. analog cassette tape recorders (2)
7. timer (1)

The system components are discussed in the following subsections:

- a. Coil Antenna Sensor

Each sensor is a continously wound coil antenna manufactured from 5460 turns of 18 gauge copper magnet wire by Elma Engineering of Palo Alto, California. The coils weight approximately 100 pounds each with dimensions as depicted in Figure 3.3. The average enclosed area of each coil is 0.0824 square meters which was determined by taking the average of the areas obtained by computing the area for both the inner radius and the outer radius. The dimensions of the sensor are constrained by the amount of volume in the glass spheres available to house the coil. The coil resistance is 120 ohms with a self-inductance of approximately 9.31 henries.

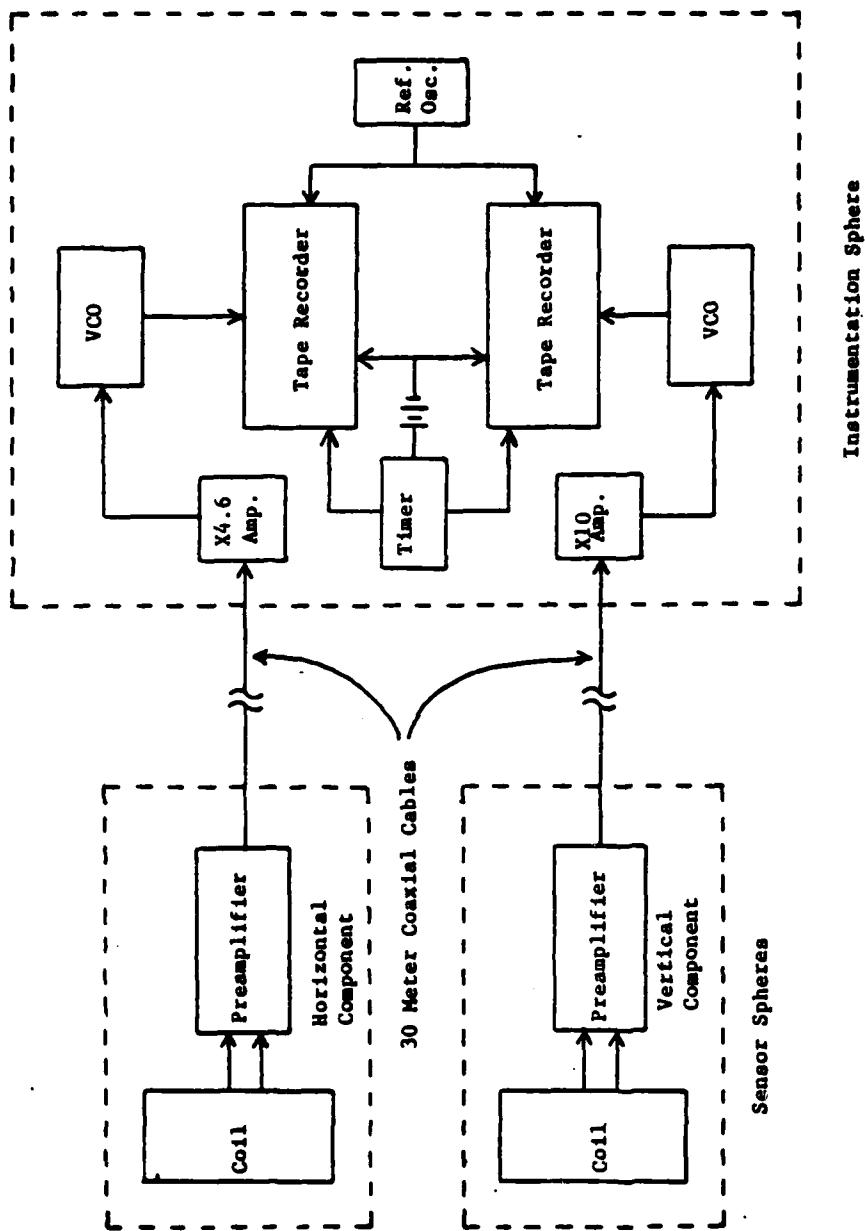


Figure 3.2. Data Acquisition System Schematic

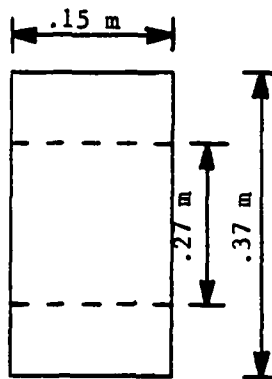


Figure 3.3. Sensor Dimensions

b. Preamplifier

The preamplifier selected for use in the sensor sphere was the model 13-10A low noise ELF amplifier manufactured by Dr. Alan Phillips of SRI International. The final stage of the amplifier contains an active low-pass filter with a cutoff frequency at 20 Hz. In addition to actively rejecting frequencies above 20 Hz through this filtering, the mere fact that the system was operationally employed at 70 meters depth provides protection from frequencies above 20 Hz which do not penetrate significantly below their skin depth (see Figure 2.4) Such filtering is necessary to reject the efforts of 60 Hz signals and harmonics due to the presence of power lines. The overall preamplifier gain is approximately 55 dB. Figure 3.9 displays the gain and filtering characteristics of the model 13-10A preamplifier. A schematic diagram of the preamplifier circuit is contained in Appendix A. The preamplifier was powered by two 12 volt mercury batteries.

c. Variable Gain Amplifier

An amplifier between the preamplifier and the voltage controlled oscillator was required to measure the horizontal and vertical components. Now that a satisfactory level of gain ($\times 4.6$ for the horizontal system and $\times 10$ for the vertical system) has been established, this extra amplifier could be eliminated and compensated for by increasing the conversion factor used in the voltage controlled oscillator by the appropriate amount. This will reduce the power requirements in the instrumentation sphere and lower the system noise floor thereby improving the signal to noise ratio of the recorded data.

d. Voltage Controlled Oscillator (VCO)

The VCO is used to convert low frequency analog voltages originating in the sensor, into a signal of varying frequency centered at 1500 ± 500 Hz. The VCO conversion factor used for converting the amplified emf generated by the induction coil (see equation 3-1) for both systems was 33 Hz/mV. A schematic diagram of the VCO is included in Appendix A.

e. Reference Oscillator

A reference signal of 2 KHz was recorded simultaneously on a separate channel on each recorder. This reference signal can then be used during playback through a mixer to reduce tape recorder noise. This recorder noise reduction was found to be on the order of 10 dB. The circuit schematic for the reference oscillator is contained in Appendix A.

f. Analog Cassette Recorders

Two Marantz CD-320 cassette two-channel tape recorders were utilized to record the VCO signals of both horizontal and vertical components with the 2 KHz reference signal on the remaining channel of each recorder. The recorders were powered by a 6 VDC Gould Gelyte battery. The tape recorder characteristics are as follows:

1. Tape speed: 1-7/8 ips
2. Frequency response: 40 Hz to 12 KHz
3. Signal to noise ratio: 50 dB
4. Wow and flutter: .12%

g. Timer

To effect accurate timing for correlation of data and to maximize the limited data acquisition time of 30 minutes, a timer was designed and assembled around the Toshiba model LC-1019MN Electronic Memo Note III liquid crystal calculator. This model has a programmable clock function which allows information to be stored and held until recall using alpha-numerica notation. When a time is set with the information (i.e. "ON"), an alarm will sound at the preset time. A latching circuit was designed to sense this alarm current and operate a relay to provide power to the data collection equipment. Thirty such alarm times may be programmed using this timing system. A schematic of the timer is provided in Appendix A.

h. DC Power Supplies

Gould Gelyte rechargeable batteries were utilized for all power requirements within the instrumentation sphere. The various size and ampere-hour ratings were matched to the current and voltage requirements of the various components.

Eveready mercury batteries were employed in the sensor spheres to power the preamplifiers because of their small size and constant, stable voltage characteristics.

2. Data Analysis Equipment

The analysis system illustrated in Figure 3.4 contains the following major components:

1. Cassette tape recorder
2. Mixer
3. X5 amplifier
4. Frequency to voltage converter (Discriminator)
5. Differential amplifier
6. Spectrum analyzer

The tape recorder and associated DC power supplies are the same components used in the data collection system discussed above. A description of those components which have not been discussed previously follows:

a. Mixer

The mixer produces a difference frequency (0-1000 Hz) by accepting the recorded data and reference signals from the tape recorder. The mixer circuit also incorporates a low pass filter on the output with a cutoff frequency of

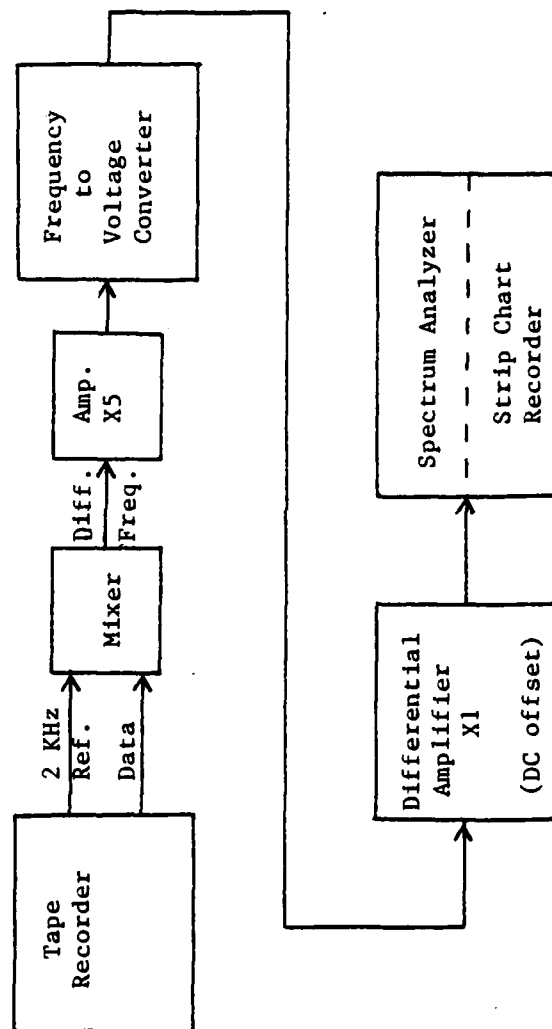


Figure 3.4. Data Analysis System Schematic

1200 Hz which serves to eliminate unwanted harmonics of the difference frequency. The mixer circuit schematic is in Appendix A.

b. Amplifier

An amplifier with a gain of five was required to boost the signal output of the mixer to a sufficient level to drive the frequency-to-voltage converter.

c. Frequency-to-Voltage Converter (FVC)

The FVC of discriminator converts the amplified difference frequency signal from the mixer back into an analog voltage. This signal of varying voltage represents the magnetic field fluctuations detected by the sensor. The FVC (Anadex model PI-375S0 is powered by 24 VDC using Gelyte batteries and has the following characteristics:

1. Input frequency range: 0-2000 Hz (input is transformer coupled)
2. Output DC voltage: 0-10 volts full scale (outputs isolated with respect to input and power supplies)
3. Conversion factor: 4.91 mV/Hz

d. Differential Amplifier

The discriminator output is a positive DC voltage which requires a DC offset to increase the input sensitivity of the spectrum analyzer. A gain setting of one on the differential amplifier (Tektronix model AM-502) provided this function.

e. Spectrum Analyzer

Spectral analysis was accomplished using a Mini-Ubiquitous model 440S with the following characteristics:

1. DC coupling necessary for low frequency application
2. Hanning weighting for increased effective resolution for continuous signals
3. Five analysis ranges between 0-20 Hz, each with 400 resolution elements
4. Built-in CRT display and output modes for standard X-Y plotters
5. Linear or logarithmic scales

f. Strip Chart Recorder

Various strip chart recorders were employed to provide hard-copy, time-function displays of recorded data periods. These proved to be particularly useful in both data correlation and the discernment of significant geomagnetic events.

B. SENSOR SENSITIVITY

1. Theoretical Sensor Sensitivity

The magnitude of the electromotive force (emf) induced in the sensor coil (derived in Appendix C) is found using the following equation:

$$\text{emf} = NB_0 (2\pi f)A \quad (3-1)$$

where:

1. A = area enclosed by the coil
2. B = magnitude of the magnetic vector field as a function of spatial coordinates only.

3. N = number of turns of wire in the coil sensor connected in series.
4. f = specific frequency (shows frequency dependence of coil).

The coil sensor's open circuit voltage or sensitivity can now be calculated applying equation (3-1) and sensor specifications for a 1 nT field at a frequency of 1 Hz to produce an emf = 2.8264 μ V and finally $20 \log(\text{emf}) = -100.98$ db (re: 1 volt). A curve of the expected sensor sensitivity for a 1 nT field in a frequency range (.001-100 Hz) is depicted in Figure 3.5.

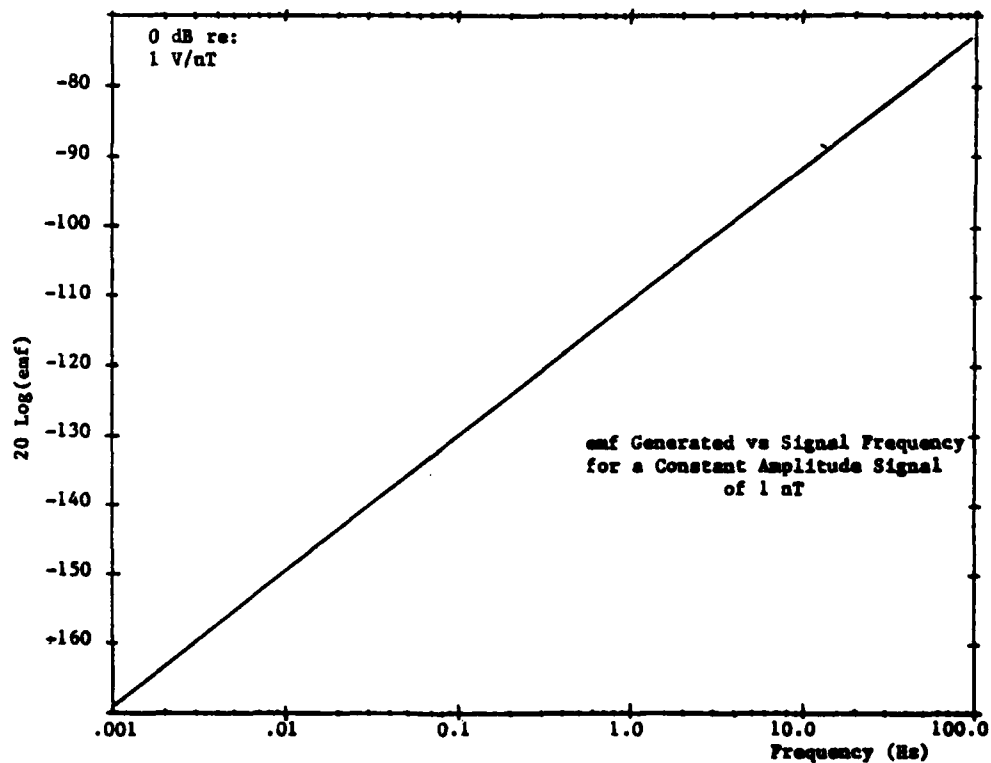


Figure 3.5. emf vs Signal Frequency for a Signal of 1 nT

2. Experimental Determination of Sensor Sensitivity

The method used to measure sensor sensitivity consisted of creating a known magnetic field at the sensor, utilizing a coaxially located driving coil and measuring the induced electromotive force at the output of the sensor.

The magnetic field produced by a circular coil consisting of N turns at a point Z meters from the driving coil along the axis of symmetry of both coils can be calculated from the Biot-Savart Law as follows:

$$\vec{B}(Z) = \frac{2 N I r^2 (10^2)}{(Z^2 + r^2)^{3/2}} \hat{K} \quad (3-2)$$

The test coil used to induce the field at the sensor had the following specifications:

1. N = 84 turns
2. r = .1577m (computed from average area)
3. Inductance = 4.6 millihenries
4. Resistance = 1.4 ohms

Inserting these specifications and rearranging equation (3-2), a relation for calculating the required current through the test coil to produce a known field at a given distance can be determined.

$$I_{rms} = \frac{(Z^2 + r^2)^{3/2}}{1.68(10^4)r^2} B_{rms} \quad (3-3)$$

The current to establish a known field was produced using the circuitry depicted in Figure 3.6.

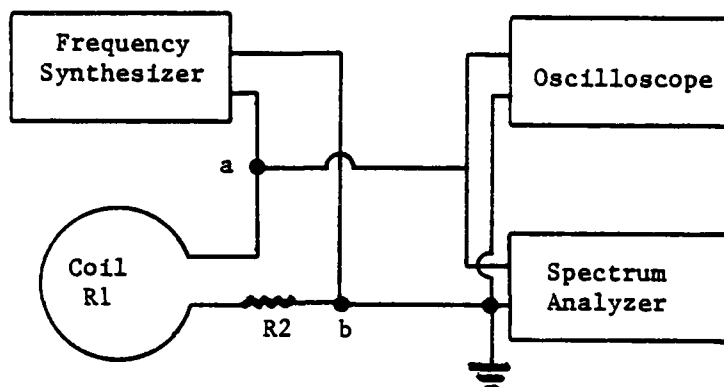


Figure 3.6. Test Coil System Circuitry

The current was produced by adjusting the signal voltage from the frequency synthesizer ($V_{a,b}$) using the relation:

$$V_{a,b} = I(R_1 + R_2) \quad (3-4)$$

where the resistance of the coil (R_1) is 1.4 ohms and a resistor (R_2) of 120.8 ohms in series was used to compute the total resistance of the circuit. A resistance greater than that provided by the coil was necessary to produce a small current in the test coil using the available test equipment. The test coil inductance can be ignored since it and the rate of change in current are small.

Using this method, the sensor sensitivity for both a 5 nT and 50 nT field was determined. A comparison of the measured readings with the theoretical sensitivity curves shown in Figure 3.7 reveals that the measured data points were within 1 dB of the theoretically predicted curves.

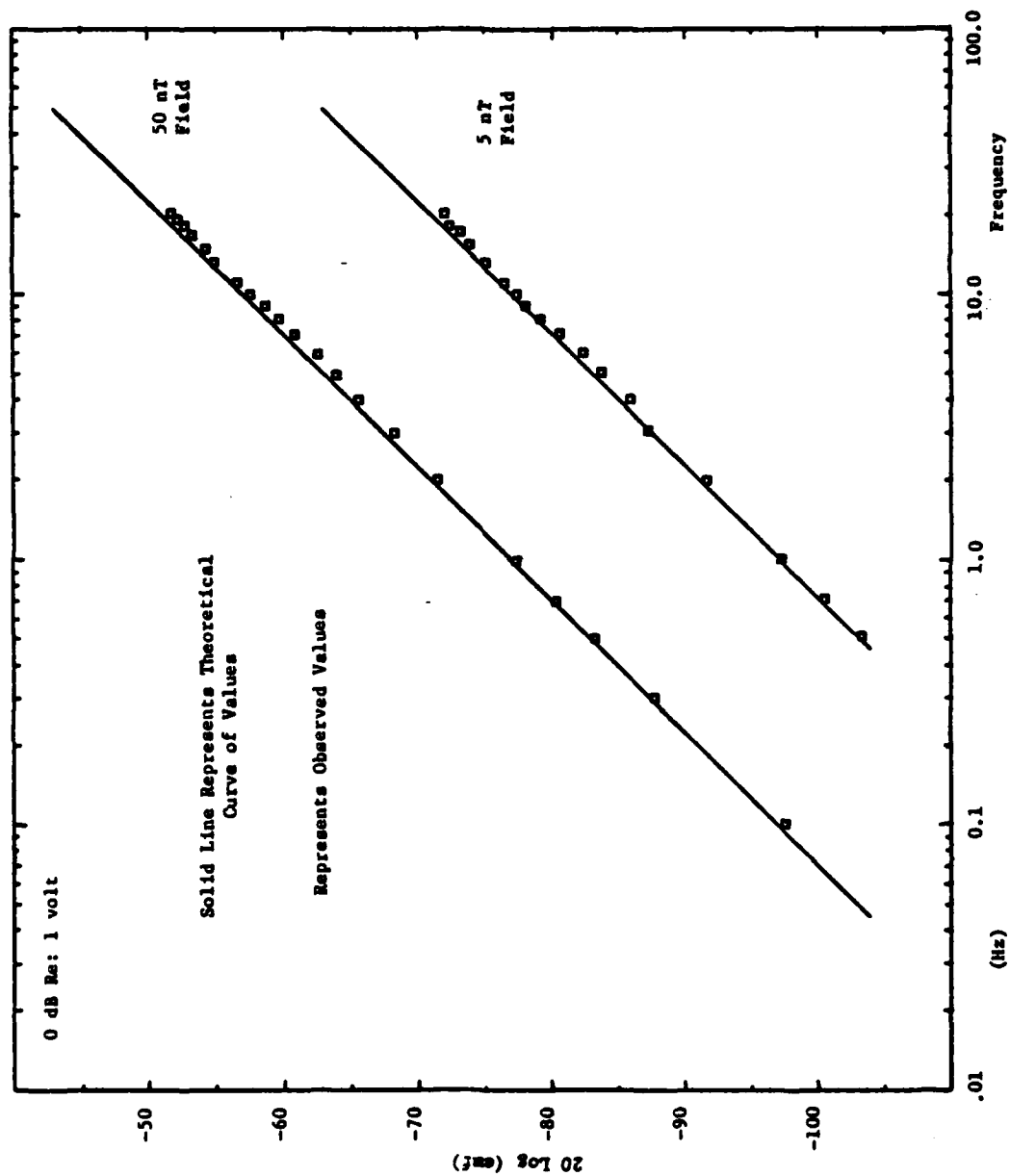


Figure 3.7. Experimental Sensor Sensitivity

C. SYSTEM TRANSFER FUNCTION

The transfer function for any one component or for the system as a whole can be determined by making frequency-response measurements. In order to experimentally determine the overall transfer function of both the horizontal and vertical systems, each system was first broken down into its component elements as shown in Figure 3.8.

The sensor sensitivity/transfer function determined in section III-B was found to be within 1 dB of the theoretical curve for a 1 nT field as shown in Figure 3.5.

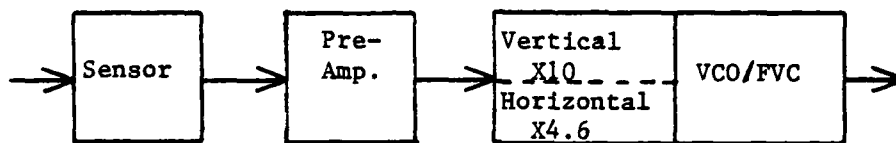


Figure 3.8. Transfer Function Components

The preamplifier is a low noise, ELF amplifier with an extremely sharp cutoff frequency at 20 Hz. The gain characteristics as a function of frequency can be seen in Figure 3.9 to display a constant gain of 55.5 dB out to 15 Hz with a slight rise in gain prior to the sharp cutoff at 20 Hz.

The variable amplifier (X10 for the vertical system and X4.6 for the horizontal system), the VCO of the data collection system and the FVC of the analysis system were placed in series and the combination was considered as a single transfer function element. The gain characteristics of these

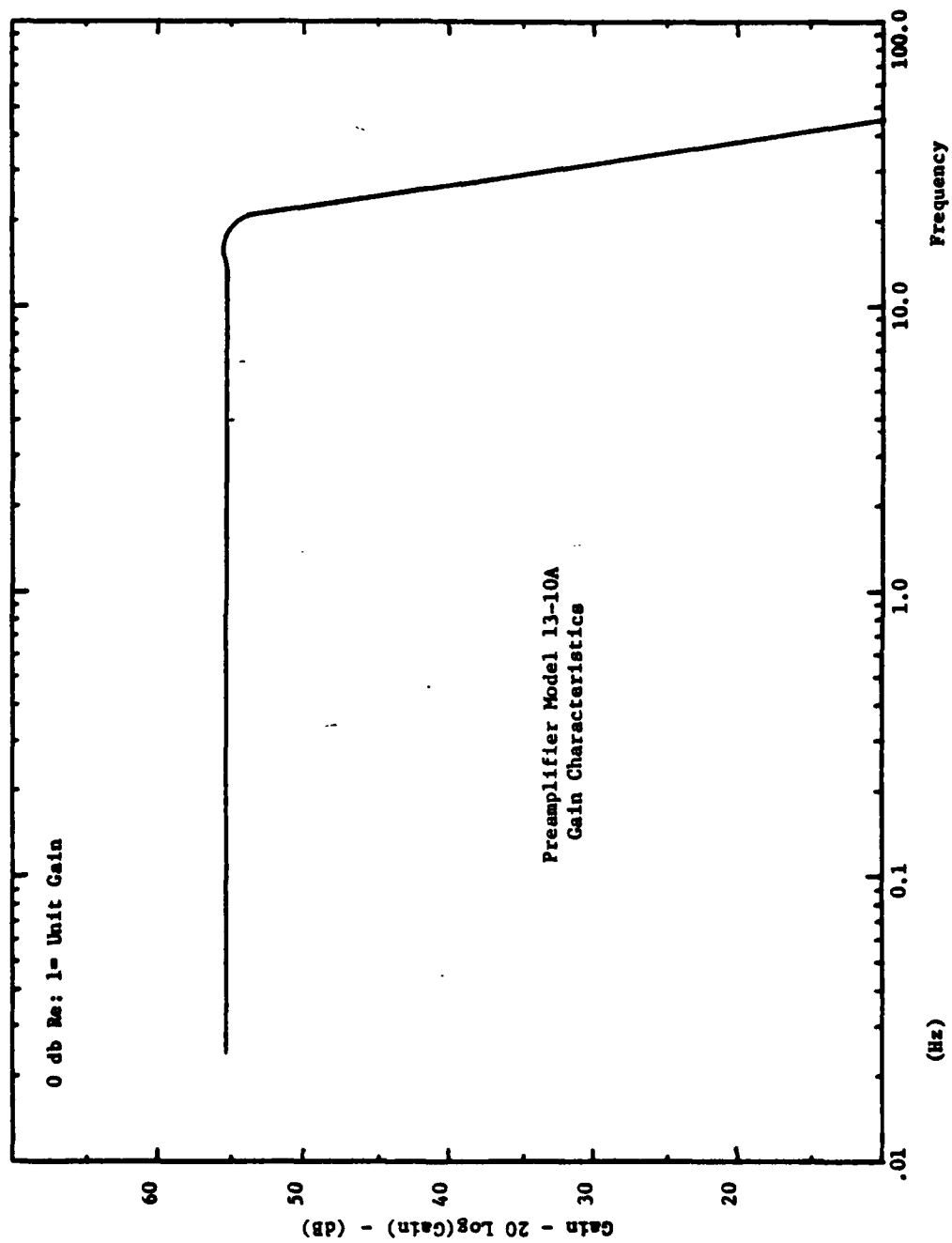


Figure 3.9. Preamplifier Gain Characteristics

combined components for both the horizontal and vertical systems are depicted in Figure 3.10.

The tape recorder is assumed to play back exactly the original recorded signal which is an acceptable assumption for an FM system. The tape recorder and other system components described in section III-A, and not shown in Figure 3.8 are not frequency dependent over the frequency ranges used in this system and may also be considered to have unity gain.

The overall system transfer functions were calculated by summing the gain contributions of the preamplifier, variable amplifier/VCO/FVC, and the sensor sensitivity at each frequency. The final transfer functions for both the horizontal and vertical systems are shown in Figure 3.11.

D. POWER SPECTRAL DENSITY CORRECTIONS

The signal presented to the spectrum analyzer by the FVC is an analog voltage signal. The spectrum analyzer provides a power spectral density which must be corrected to reflect the sensor sensitivity and system transfer function for the respective component at every frequency within the range of interest referenced to $1 \text{ nT}^2/\text{Hz}$.

The procedure which is derived in Appendix D, requires the following steps be taken to obtain the corrected power spectral density curves:

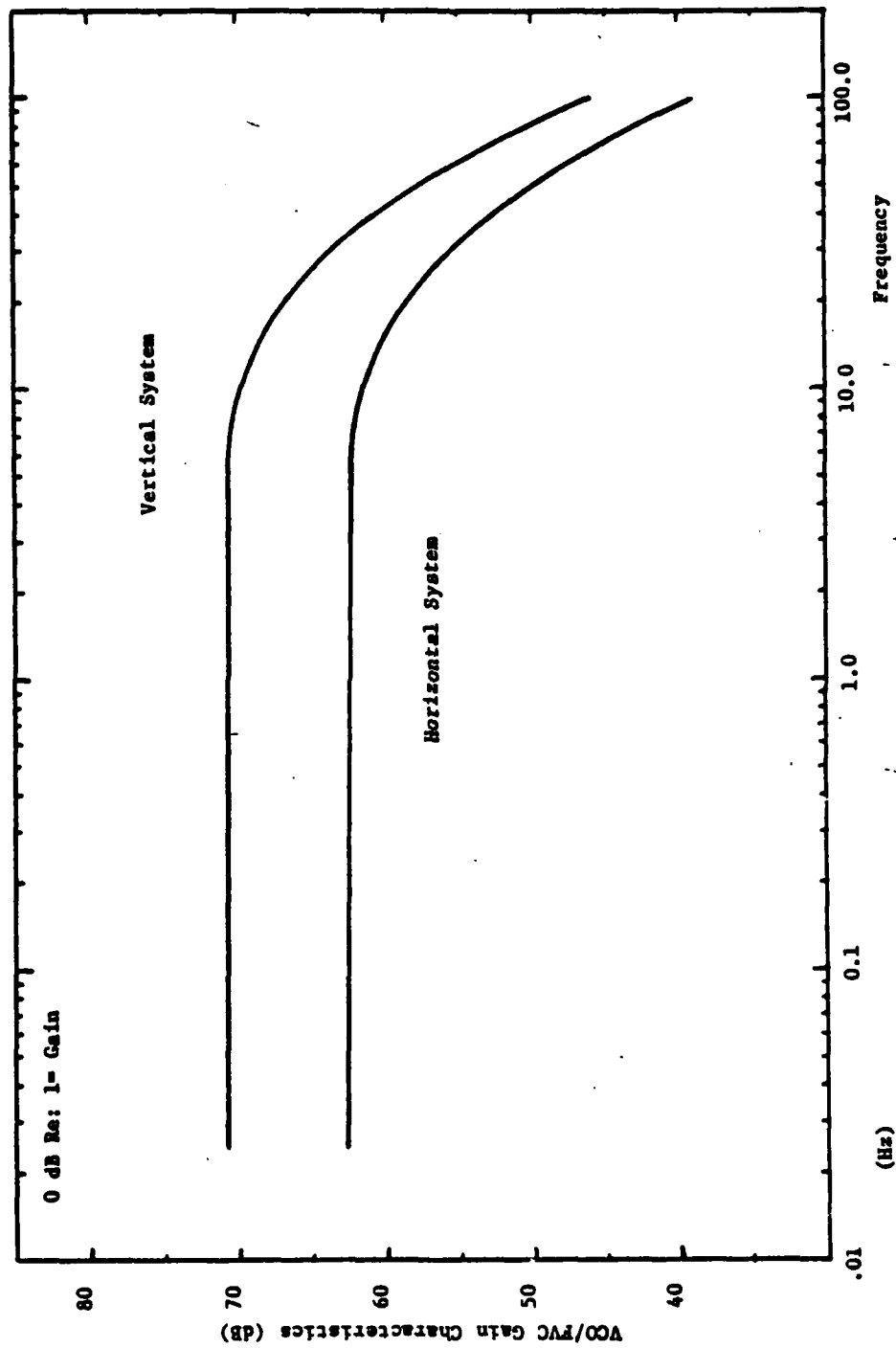


Figure 3.10. VCO/FVC Gain Characteristics

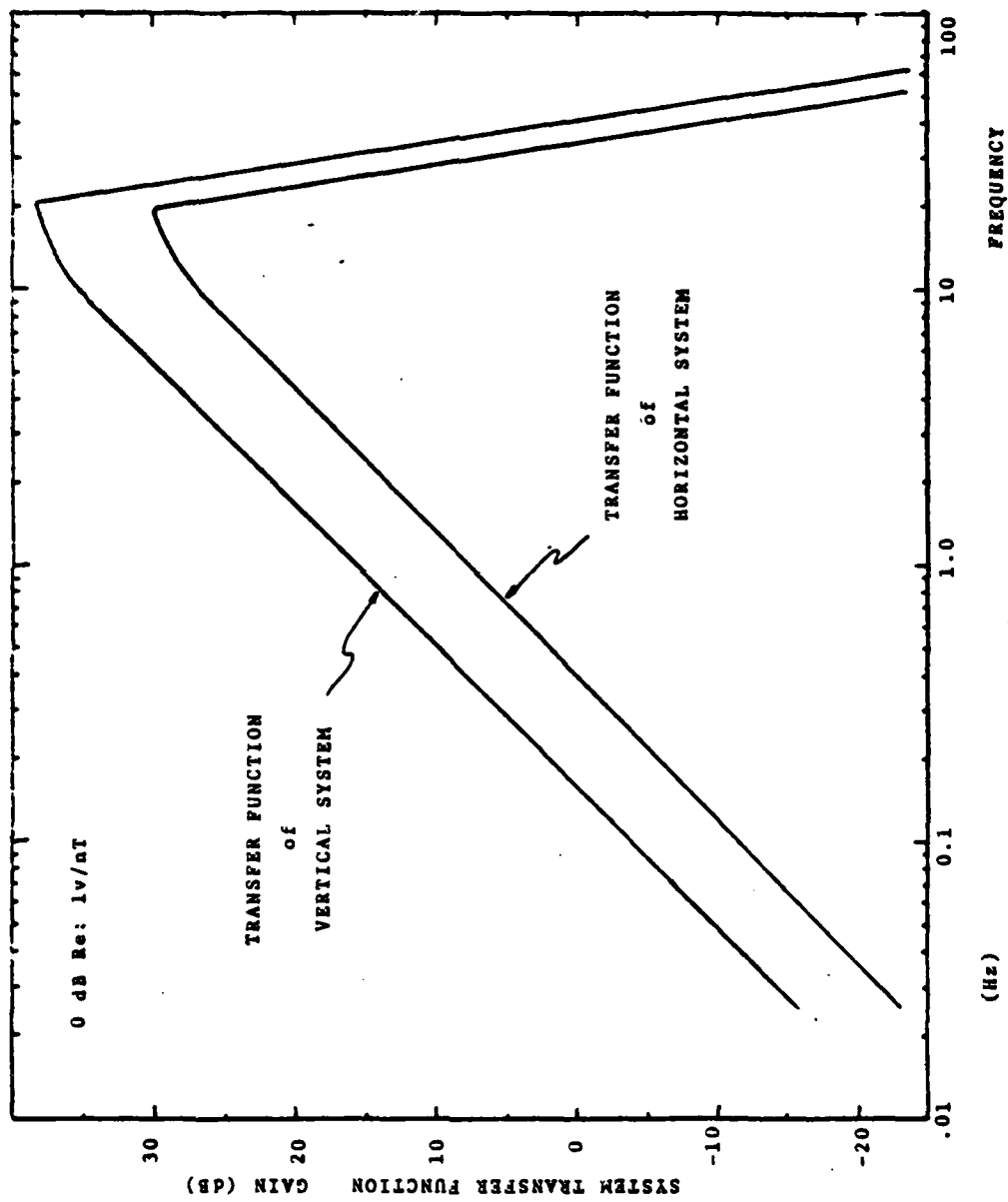


Figure 3.11. System Transfer Functions

$$p = N(\text{dB}) - (B) - 10 \text{ LOG}(BW) \quad (3-5)$$

where,

1. P = corrected power spectral density where 0 dB is referenced to $\ln T^2/\text{Hz}$
2. $N(\text{dB})$ = spectrum analyzer reading in volts (dB)
3. B = the system transfer function
4. BW = the Hanning bandwidth correction used for the particular analyzer and frequency rangw used.

E. SYSTEM NOISE

Previous work has determined that the effects of thermal noise is not a dominant factor in this system. The system noise was measured by shorting out the preamplifier input using a 120 ohm resister to match the impedance of the coil. Equipment parameters were set as in normal system operation and the curves produced in Figures 3.12 and 3.13 represent the system noise obtained in the operational environment on the seafloor for each component system. The significantly higher noise level of the vertical system was the result of poor performance of the X10 variable amplifier in that system during data acquisition.

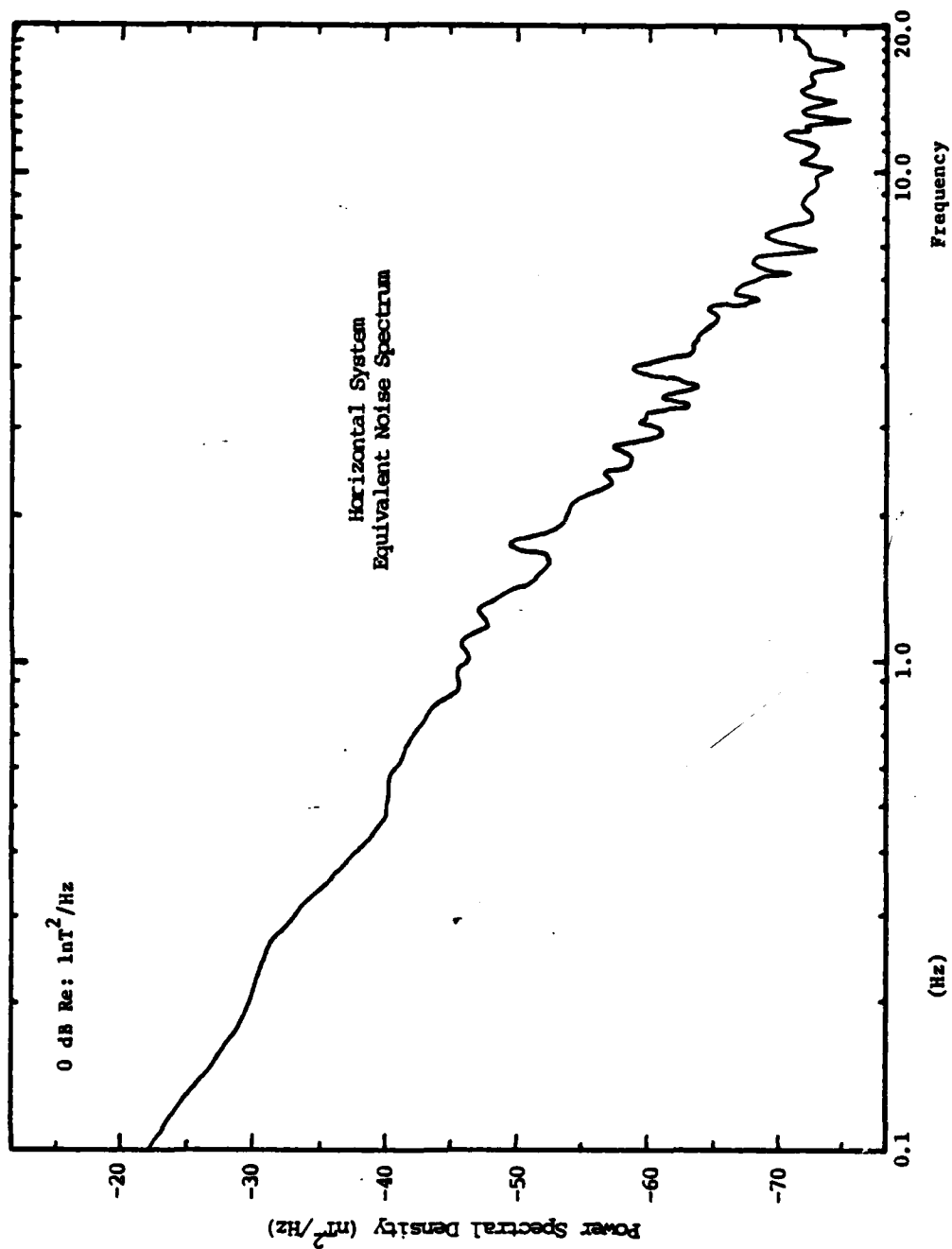


Figure 3.12. Horizontal System Noise

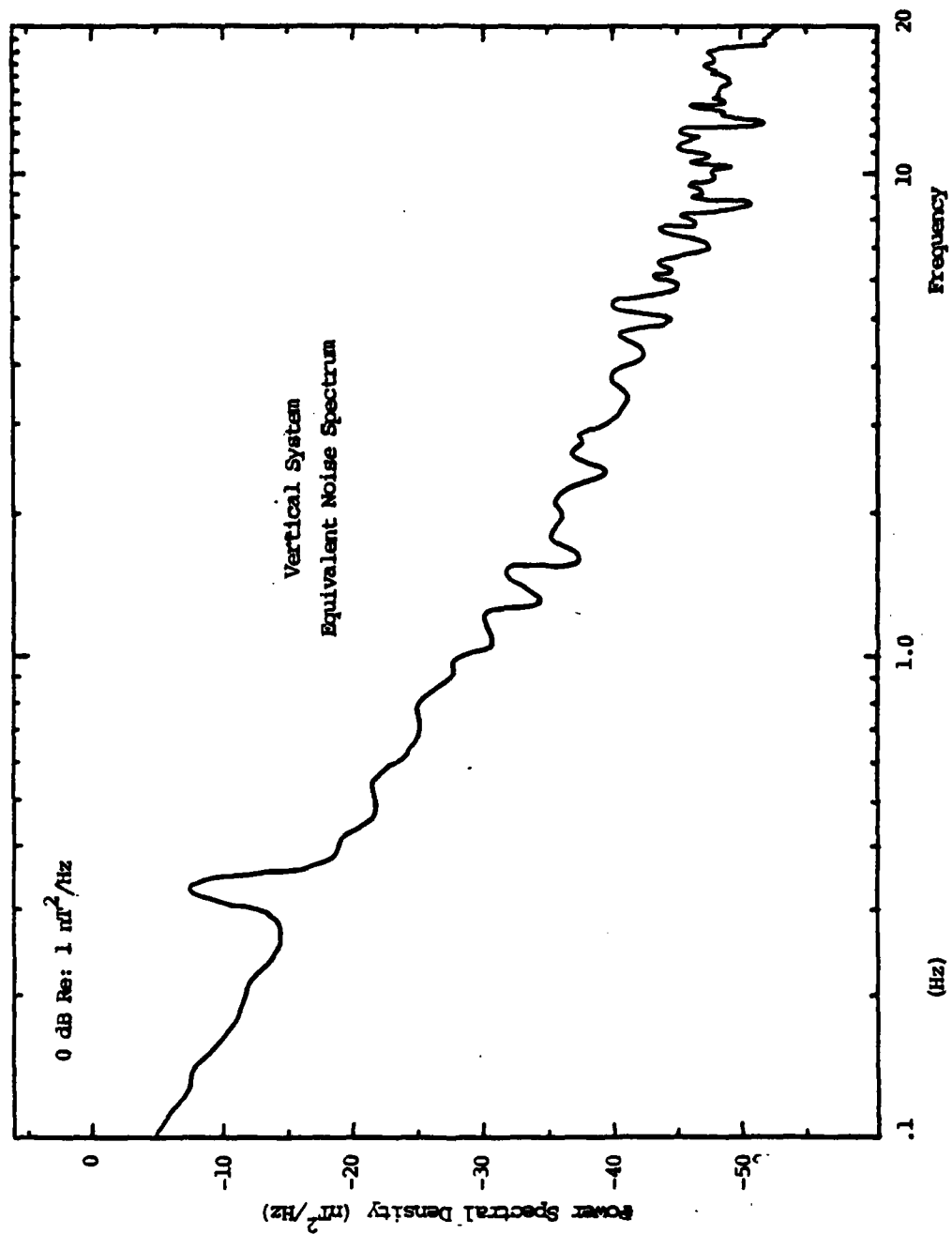


Figure 3.13. Vertical System Noise

IV. EXPERIMENTAL RESULTS

A. INTRODUCTION

The final equipment and system configuration described in section III-A was the result of experimental trial runs which yielded information on proper equipment settings as well as deficiencies in physical design and execution in system deployment. Once the system was operating as conceived, fifteen collection runs were made with the specific objective of recording simultaneous component measurements of the geomagnetic field in the vicinity of the sea floor. These measurements were made on different days at various times during both the day and night. It was felt that measurements made in such a manner would help in determining diurnal effects given the limited amount of data available.

The data was taken in the same general area at several stations within 1000 yards of Latitude 36° - 40° N, Longitude 121° - 54° W. This location was chosen since a small data base was available from previous work and because the sea floor at that location consists of sand and mud with a slope less than 0.5 degrees. During each run the water depth, time period, location, weather conditions and sea state were carefully documented to aid in analysis and correlation of data.

A representative sample of data is provided in Appendix E. This data covers various times under differing sea state conditions between 20-25 August 1981.

B. DISCUSSION AND CORRELATION OF DATA

The recorded data was frequency analyzed to examine the power spectrum of the magnetic field fluctuations. It was determined that all of the recordings were obtained during periods of low solar activity. [Ref. 22] Therefore the comparison of data recorded on separate days is justified. Certain phenomena observed in previous works were verified. For example, the fact that atmospheric electromagnetic waves are refracted vertically downward with their E and B vectors in the horizontal plane in the sea and therefore are detected in the horizontal field component was verified. Pc 1 activity was observed in horizontal component measurements (see Figure E.14 in Appendix E) and the absence of any corresponding activity in the vertical measurement for the same observation period is confirmed in Figure E.15.

Magnetic noise generated within the sea is discernible in both the horizontal and vertical components. The power density peaks between 0.07 - 0.1 Hz (see Figures E.18 and E.19) and 0.17 - 0.25 Hz (see Figures E.5 and E.6) are present in both the horizontal and vertical components and correspond to both a long period ocean swell of approximately fourteen seconds and a shorter period, wind driven wave of

four to six seconds, respectively. To be specific, it was observed in the data for the night of 24 - 25 August that the combined sea-swell conditions present at sunset subsided over the next few hours as the evening offshore breeze knocked the seas down. The recording obtained at local midnight, when the sun is over the meridian on the exact opposite side of the earth, revealed that the peak at 0.17 Hz corresponding to the wind driven waves had decayed significantly and that the peak at 0.07 Hz had increased. The internally generated noise due to the electric currents produced by seawater motions across the magnetic field are probably elliptically and/or circularly polarized in the sea.

Overall, power densities generally conformed to the observations of Barry (1979) that the power density subsides shortly after nightfall. Moreover, a comparison between the sunset and midnight data verified the observation by Nishida (1978) that the greater the geomagnetic activity, the greater will be the fall-off of the power spectra.

Several interesting observations of general trends can be made when considering the average readings of both component measurements. Figures 4.1 and 4.2 show curves depicting the average power spectral density measurements as a function of frequency with the maximum excursions above and below the average curve. These curves graphically support the theory that the horizontal component fluctuations are a composite of internal wave action effects and atmospheric

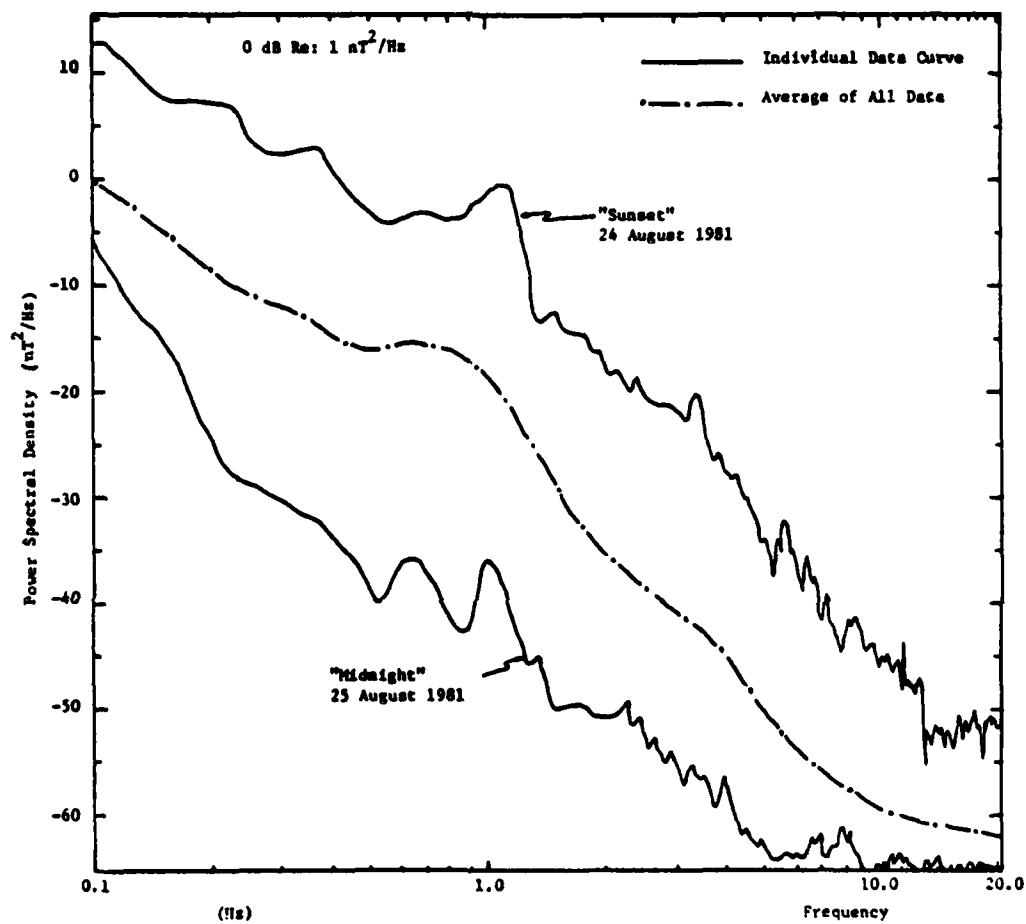


Figure 4.1. Average Power Spectral Data (horiz)

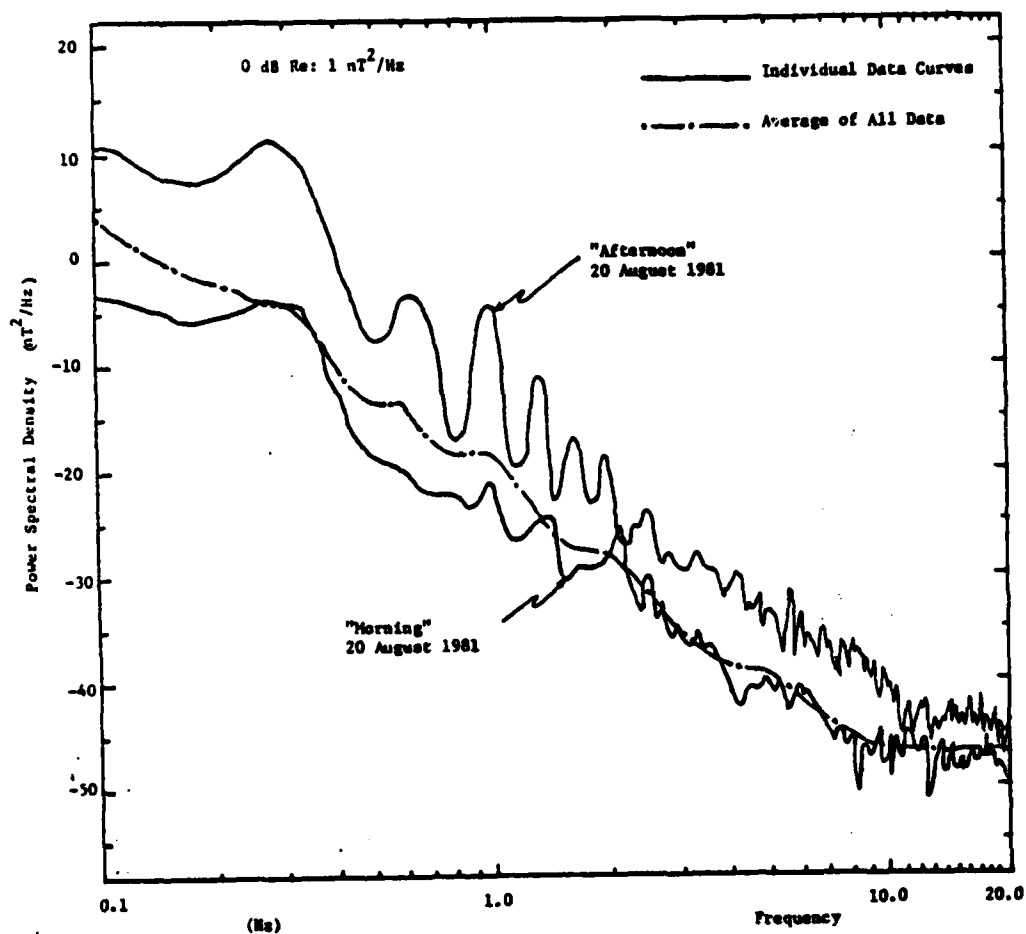


Figure 4.2. Average Power Spectral Data (vert)

related sources while the vertical component must be composed largely of internal ocean effects in that the maximum readings for each component were obtained at different, key times related to the sources of these effects. The maximum reading obtained for the horizontal system occurred at sunset when atmospheric related phenomena are high while the minimum reading was observed at local midnight during a period of minimum activity.

The maximum excursion in the vertical measurements was observed in the late afternoon when the sea state was high with swells and wind wave activity while, the minimum readings were obtained during the night and early morning hours. The wave action on Monterey Bay generally increases through the day with the maximum in the afternoon which explains why the average curve for the vertical measurements tend to be situated in closer proximity to the minimum reading.

Figures 4.1 and 4.2 show that although the spread in the horizontal component measurements is much larger than the vertical measurements, the average curves for both systems are quite comparable. This observation again supports the theory that both horizontal and vertical components are affected by seawater motions while the diurnal atmospheric effects would average out and produce only a slightly greater curve of average horizontal measurements.

The curves in Figures 4.1 and 4.2 generally show a statistical trend in the data taken in this research. There

is some uncertainty in the vertical component measurements due to the inability to perfectly orient the sensor and this may result in a small portion of the horizontal component being measured on the vertical system. In Figures E.7 and E.8 in Appendix E, the occurrence of a peak near 1 Hz might be the result of Pc 1 micropulsations which were high for both horizontal and vertical systems taken at sunset. Normally such Pc 1 occurrences should only be horizontally polarized at the sea floor as earlier discussed.

In addition, some unknown variables in the experimental situation exist due to the unpredictability of the azimuthal orientation of the horizontal system and the differences of field fluctuations due to polarization of the ionospheric sources and sea water motion effects in the horizontal plane.

Geomagnetic research was carried out in parallel at a permanent, land-based sensing station located on Chews Ridge at latitude $36^{\circ}-21.5^{\circ}$ N, longitude $121^{\circ}-34.5^{\circ}$ W. This station relayed data via a telemetry link to a receiving station located at the Naval Postgraduate School. The sensor employed at this location is a coil identical to those used in the undersea system. The coil was oriented with its axis of symmetry aligned along the magnetic east-west direction in order to obtain the magnetic fluctuations of a known component of the total magnetic field. Two hours of data were simultaneously recorded by both systems at

local sunrise, noon, sunset and midnight. Subsequent comparisons of the data revealed that the power spectral densities roughly agreed for the horizontal components of each system. The undersea power densities were consistently below those of the land station. In the neighborhood of 0.1Hz, the undersea readings were each about three decibels below those acquired on land. Thereafter, the undersea power spectra declined more rapidly than the land data for increased frequencies due to the attenuating effect of skin depth on the electromagnetic waves in the sea. Specific geomagnetic phenomena, such as Pc 1 pulsations can be identified in the power spectra of both horizontal systems (see Figures E.11 and E.24). Further observation of the geomagnetic power spectrum from the land based station reveals that the average power density spectrum for daylight hours is approximately ten decibels above the average spectrum for the nocturnal hours during the period 21 August through 9 October, 1981 (see Figure 4.3). [Ref. 24].

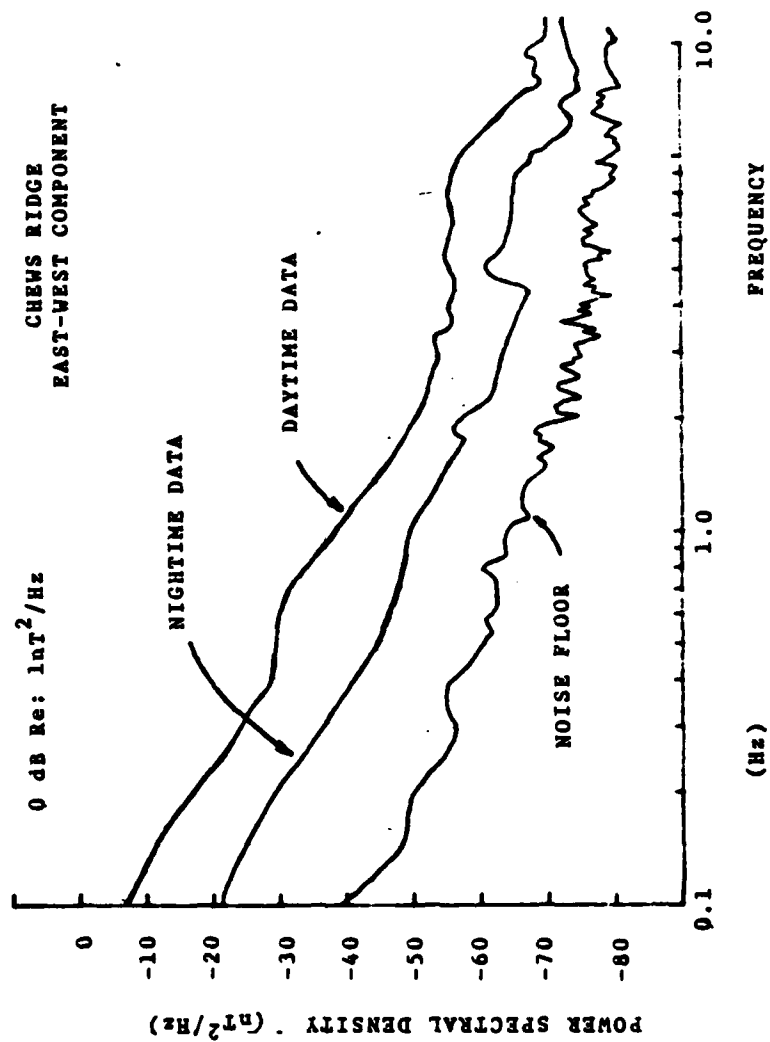


Figure 4.3. Average Land Data Curves
[Beard 1981]

V. EQUIPMENT/SYSTEM RECOMMENDATIONS

The system designed for this research was successfully employed in the continuing effort of geomagnetic data collection with the specific task of recording simultaneous component measurements of the magnetic field on the sea floor.

The data collected with the present system was somewhat limited by virtue of equipment restrictions and deployment techniques. The analog tape recorder posed the greatest limitation. A digital acquisition recorder is currently on order and will provide a means of collecting long-term data, while at the same time, remove many of the sources of equipment noise in the system. Should the analog recorder in the current system be used in future measurements, it is recommended that the variable amplifiers between the preamplifiers and voltage controlled oscillators (see section III-A) be removed. A corresponding increase in the VCO conversion factor for each system will then be necessary. Additionally, the dynamic range of the VCO's should be expanded (2000 ± 1000 Hz is recommended as opposed to 1500 ± 500 Hz) to handle the increase in sensitivity necessary for periods of low magnetic activity and still have the capability to convert the high sensor voltages during periods of high geomagnetic activity.

A better means of positioning the sensors on the bottom has yet to be devised. The ability to accurately position

and detect sensor orientation will be critical in future data acquisition and component field correlation experiments. The exact orientation method to use will be directly related to the acquisition system chosen for future measurements. Such system considerations should include the following options:

1. Small, easily deployed systems for simultaneous, short-term measurements in different locations.
2. A system for long-term measurements in a single location, but where repositioning can be affected.
3. A long-term collection station for measurements over periods of years.

A final proposal and recommendation is to engineer a collection system that incorporates a telemetry link to transmit geomagnetic and wave action data back to a receiving station on land. In the past such a system was not developed since there is concern that any cabling used from the seafloor to the surface would act as an antenna and quite likely introduce unwanted signals into the data. Currently, efforts are being made to incorporate an optical fiber link to transmit signals from the sensors to the surface for follow on telemetry to a receiving station. The use of fiber optics in such a system would alleviate concerns for the "antenna" effect and enable continuous data to be collected over long periods of time, assisting in the correlation of data received from other sea/land stations and greatly enhance the knowledge of magnetic activity on the floor of the sea.

LIST OF REFERENCES

1. Carrigan, C. R., Gubbines, D., "The Sources of the Earth's Magnetic Field", Scientific American, Feb. 1979.
2. Inglis, D. R., "Dynamic Theory of the Earth's Varying Magnetic Field", Reviews of Modern Physics, v. 53, p. 481, July 1981.
3. Ibid, p. 482.
4. Jacobs, J. A., Geomagnetic Micropulsations, Springer, New York, 1970.
5. Jacobs, J. A., Physics and Chemistry in Space, Vol. I, Roederer, Denver and Zahringer, Springer-Verlag, New York, 1970.
6. Fraser-Smith, A. C., "Short-Term Prediction and a New Method of Classification of Pc 1 Pulsation Occurences", Planet Space Science, v. 28, pp. 739-747, 1980.
7. Chaffee, E. J., Low Frequency Geomagnetic Fluctuations (.01 to 3Hz) on the Floor of Monterey Bay, M.S. Thesis, Naval Postgraduate School, Monterey, 1979.
8. Schumann, W. O. and Konig, H., "Unber die Beobachtung von Atmospherics bei geringsten Frequenzen", Naturwissen - schafften, v. 41, p. 183, 1954.
9. Balser, M. and Wagner, C. A., "Observations of Earth-Ionospheric Cavity Resonances", Nature, v. 188, p. 638, 1960.
10. Weaver, J. T., "Magnetic Variations Associated with Ocean Waves and Swell", Journal of Geophysical Research, v. 70, No. 8, pp. 1921-1929, April 1965.
11. Ibid, pp. 1921-1929.
12. U.S. Navy Mine Defense Laboratory Report No. 2743, A Study of the Electric and Magnetic Fields of Ocean Waves, by M. J. Wynn and H. W. Trantham, 1968.
13. Schumann, W. O. and Konig, H., "Uber die Beobachtung von Atmospherics bei geringsten frequenzen", Naturwissen - schafften, v. 41, p. 183, 1954.

14. Campbell, W. H. and Matsushita, S., Physics of Geomagnetic Phenomena, v. 1, 2, Academic Press, 1967.
15. Larson, T. R. and Egeland, A., "Fine Structure of the Earth-Ionosphere Cavity Resonances", Journal of Geophysical Research, v. 73, p. 4986, 1968.
16. Westerlund, S., Preliminary Results of Magnetotelluric Soundings in the Range .01-10,000 Hz, Rep. 706, Kiruna Geophys. Obs., Kiruna, Sweden, December 1970.
17. Fraser-Smith, A. C. and Buxton, J. L., "Superconducting Magnetometer Measurements of Geomagnetic Activity in the 0.1 to 14 Hz Frequency Range", Journal of Geophysical Research, v. 80, No. 27, pp. 3141-3147, August, 1975.
18. Clayton, F. W., Power Spectra of Geomagnetic Fluctuations Between 0.1 and 40 Hz., M.S. Thesis, Naval Postgraduate School, Monterey, 1979.
19. Chaffee, E. J., Low Frequency Geomagnetic Fluctuations (.01 to 3 Hz) on the Floor of Monterey Bay, M.S. Thesis, Naval Postgraduate School, Monterey, 1979.
20. McDevitt, G. R. and Homan, B. B., Low Frequency Geomagnetic Fluctuations (.04 to 25 Hz) on Land and on the Floor of Monterey Bay, M.S. Thesis, Naval Postgraduate School, Monterey, 1980.
21. McKinley, G. M. and Santos, R. M., Characteristics of Geomagnetic Power Spectra on Land and Sea in the Period Range 0.2 to 400 Seconds, M.S. Thesis, Naval Postgraduate School, Monterey, 1980.
22. U.S. Department of Commerce, Preliminary Report and Forecast of Solar-Geophysical Data, Joint National Oceanic and Atmospheric Administration - U.S. Air Force Space Environment Services Center, Boulder, Colorado, vols. 312 and 313, 25 August and 01 September 1981.
23. Beard, M. W., Power Spectra of Geomagnetic Fluctuations Between 0.02 and 20 Hz., M.S. Thesis, Naval Postgraduate School, Monterey, 1981.

APPENDIX A

A. EQUIPMENT SCHEMATICS

Much of the equipment utilized in this project was either designed and/or constructed at the Naval Postgraduate School. Equipment of this nature and not widely available commercially is presented schematically in the following figures:

1. preamplifier (Figure A.1)
2. timer (Figure A.2)
3. mixer (Figure A.3)
4. reference oscillator (Figure A.4)
5. VCO (Figure A.5)

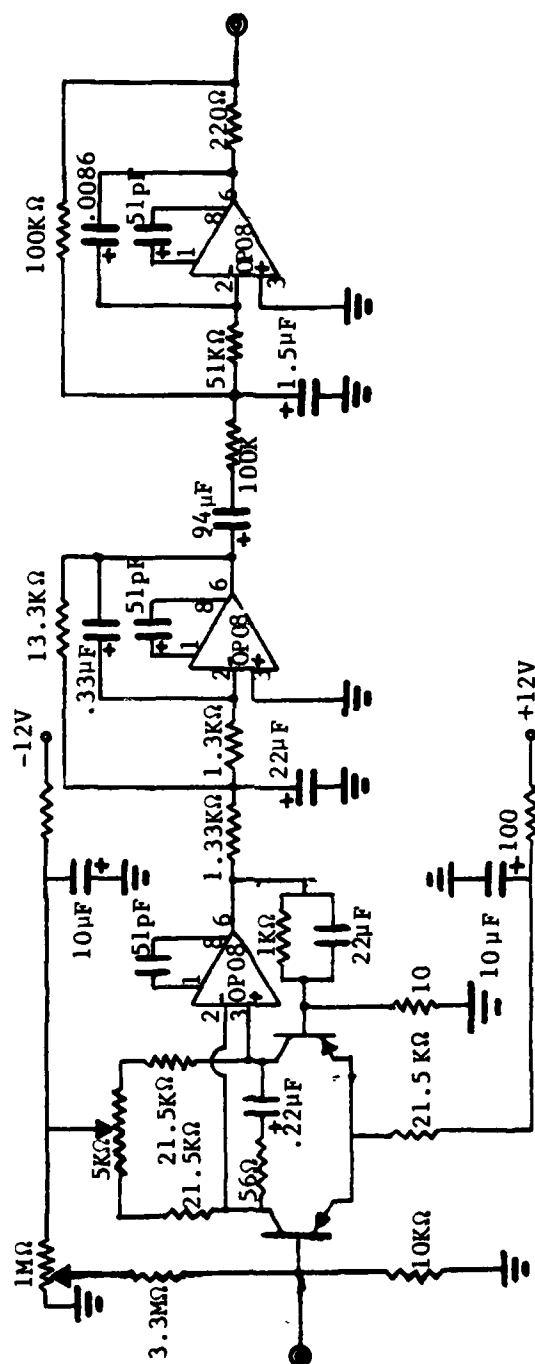


Figure A.1. Preamplifier Schematic

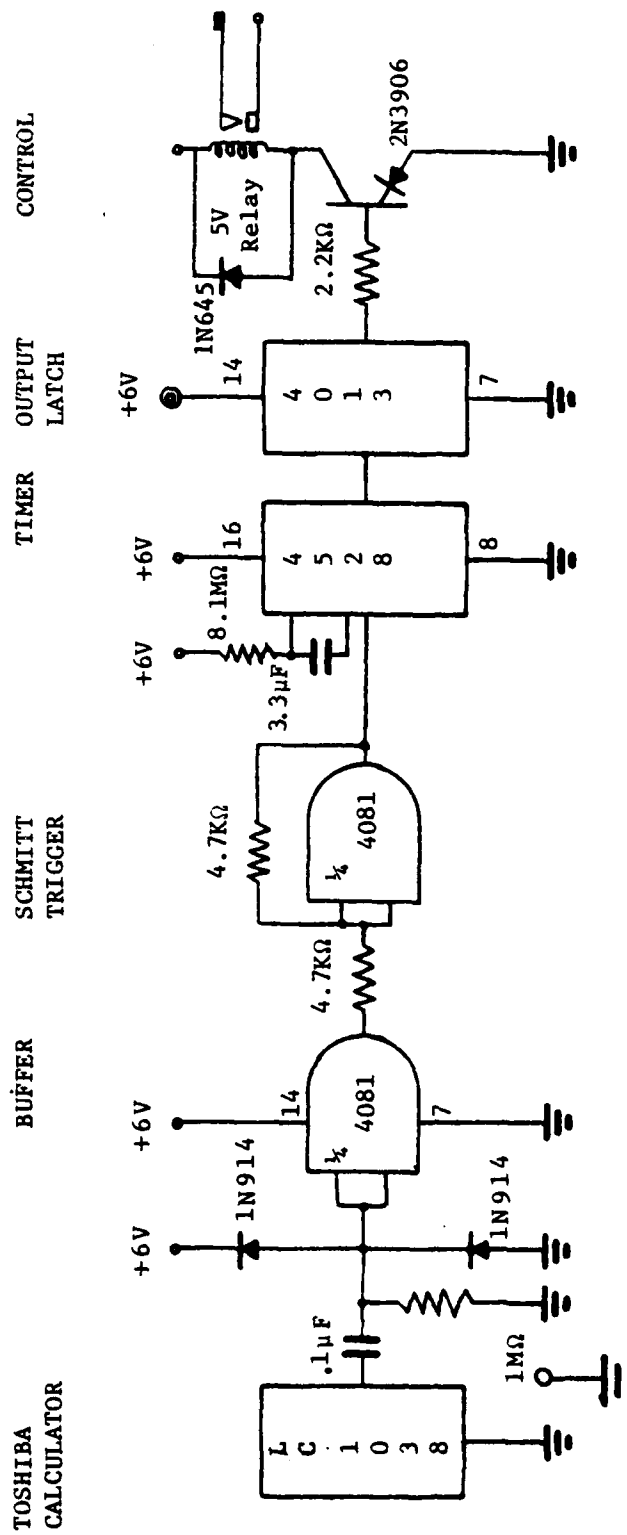


Figure A.2. Timer Schematic

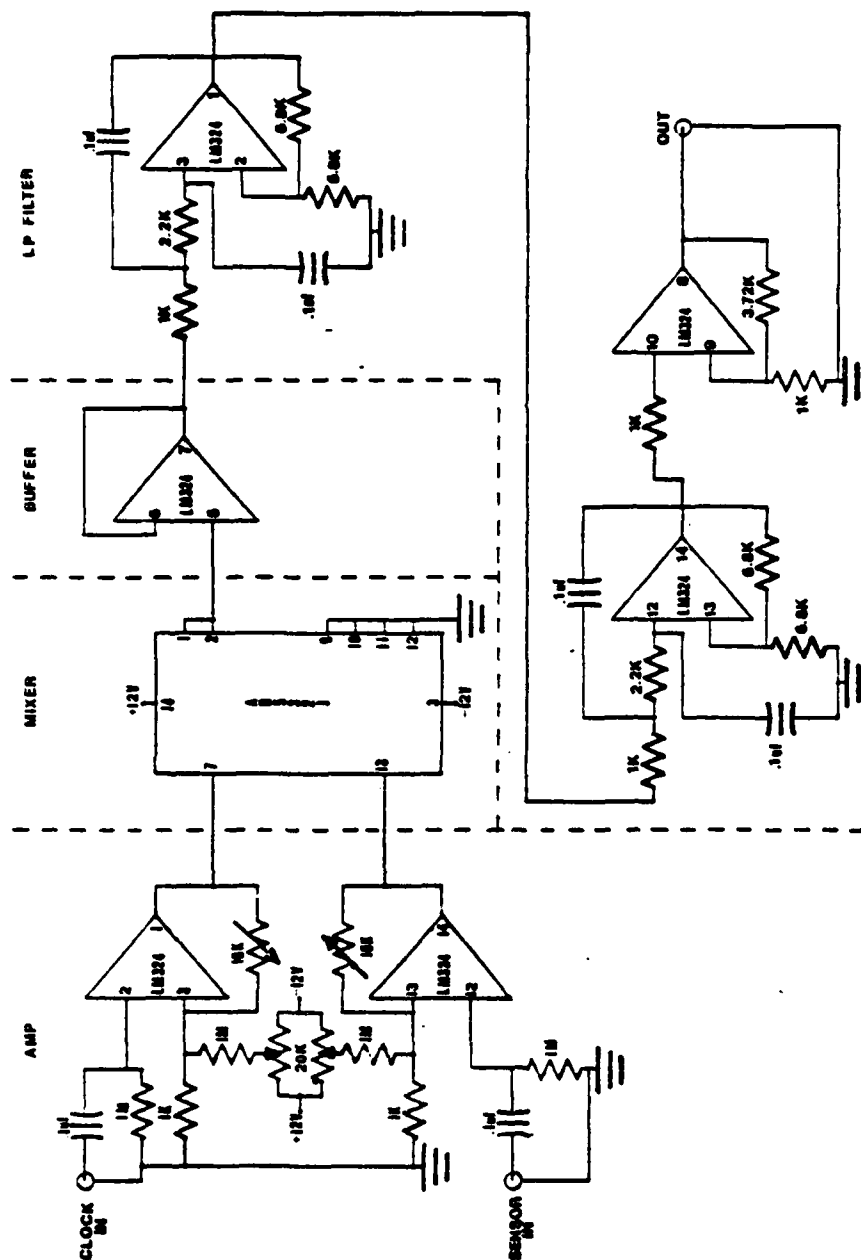


Figure A.3. Mixer Schematic

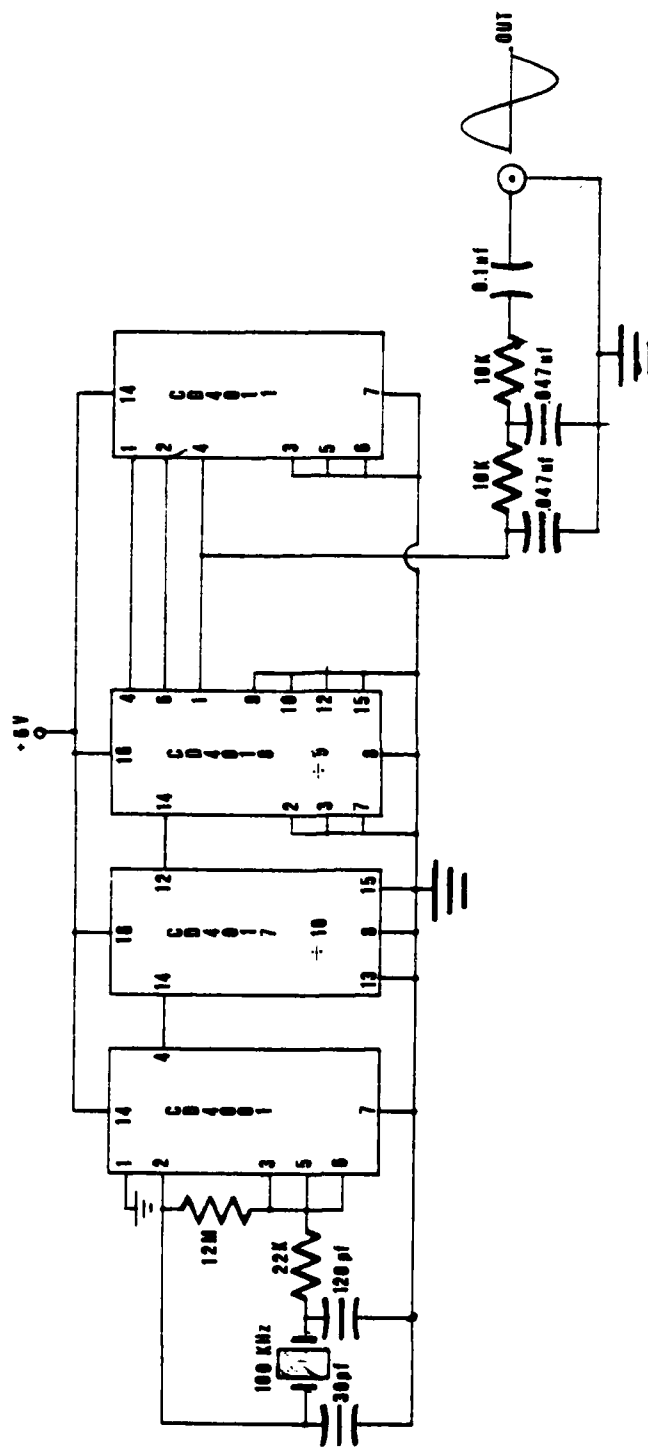


Figure A.4. Reference Oscillator Schematic

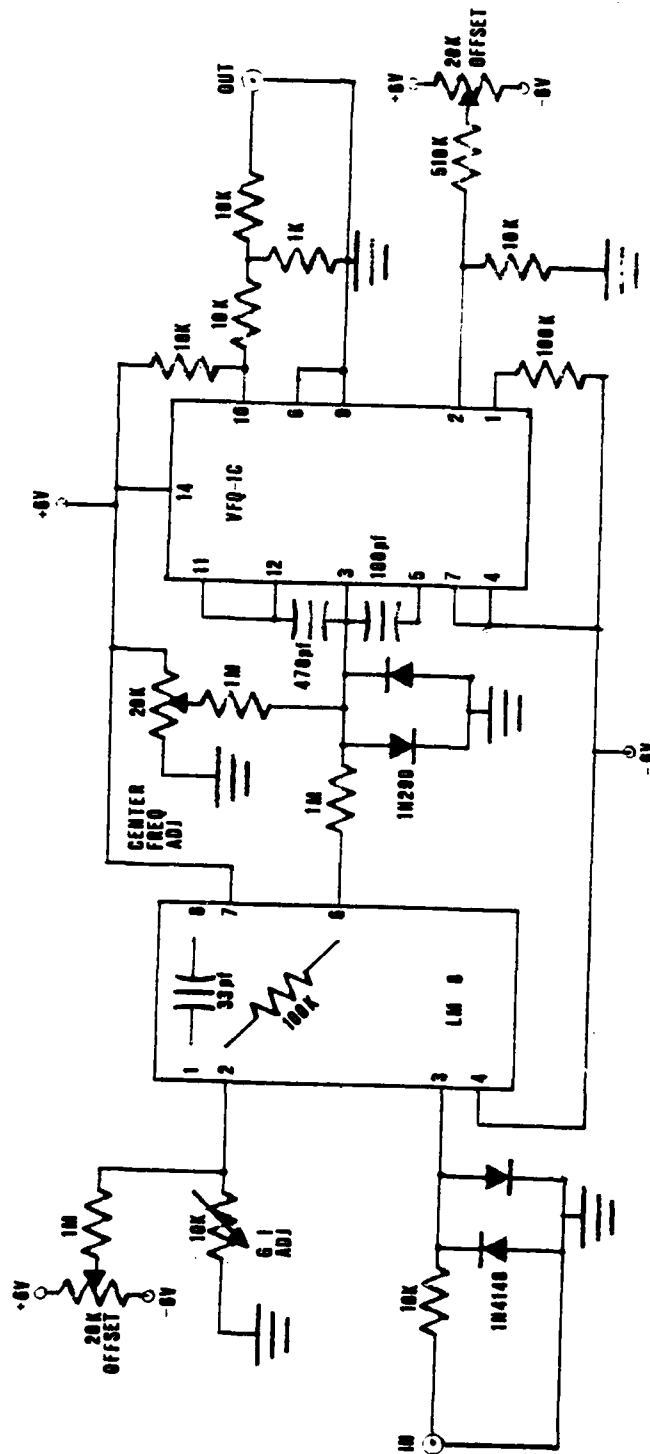


Figure A.5. VCO Schematic

APPENDIX B

A. SYSTEM AND EQUIPMENT USAGE

In order for equipment to perform and operate as designed, certain preventive maintenance measures and procedural steps should be taken. Such prudent steps, especially in under-sea research will most certainly allow maximum results and prolong equipment life.

The following list serves as a culmination of lessons-learned in previous and on-going project work:

1. Spherical glass instrument housing - the Benthos glass spheres are composed of two matched hemispheres with finely ground edges. As these edges are susceptible to chipping, care must be taken in handling. During re-assembly of the housing prior to deployment, certain procedures are necessary to maintain watertight integrity:
 - a. The glass sphere should be dry and warmed to room temperature using a heat gun to ensure adhesion of the sealing tape.
 - b. All mating surfaces must be cleaned with a solvent such as alcohol to remove any foreign matter, grease or oil.
 - c. Prior to sealing the sphere, careful inspection of all equipment, electrical connections, packing material and equipment settings should be made. The

use of check-off sheets and color-coding was found to be particularly helpful in avoiding operator error.

2. Electronic equipment - a general concern is the proper application of power supply voltages. Assembly of a large number of electrical components within the confines of a small glass sphere, necessitates careful planning and utilization of limited power resources. Improperly applied voltages may result in damage to electronic circuitry and/or loss of data. Certain pieces of electronic gear require particular considerations as follows:

a. Tape recorder- the recorder heads and capstan drive should be cleaned and demagnetized before each acquisition run. This action will help in reducing unwanted noise and distortion. High quality 60 minute tapes are recommended, since longer tapes appear to impose greater drag on the tape recorder used. Before sealing the instrumentation sphere, ensure the record button is depressed and the record levels have been properly adjusted.

b. Voltage controlled oscillator - the center frequency of the VCO should be adjusted to 1500 Hz prior to system deployment. This is accomplished by shorting the input, and adjusting the center frequency potentiometer.

c. Mixer - an amplifier stage is provided for the sensor and reference oscillator inputs to the mixer. While receiving inputs, the gain potentiometers should be adjusted for a 6-10 V peak-to-peak output difference frequency. This voltage output is required to drive the frequency-to-voltage converter downstream, in the system.

3. Batteries - Gelyte batteries were used for most power requirements. These batteries should be checked prior to system usage and a systematic approach regarding service use and charge interval should be taken. Mercury batteries were used in the sensor spheres. This type of battery provides a constant power source throughout its recommended life, but should be replaced at more frequent intervals to ensure successful system operation.

4. Connectors/cables: - before and after each use in a corrosive environment, all connectors should be thoroughly cleaned to extend service life. All rubber connectors should be lightly lubricated with silicon grease to ensure electrical continuity and prevent water intrusion. The use of color coding on cables and connectors lessen the possibility of error and is highly recommended. Care must be taken to avoid placing strain on the coaxial cable and associated connectors. A liberal amount of slack must be allowed between fixed points along the coaxial cables in order to avoid problems of intermittent and/or complete signal loss, due to cable strain.

APPENDIX C

A. THEORETICAL SENSOR SENSITIVITY

Faraday's Law of Induction states that the emf induced in a single turn of wire is equal to the following expression:

$$\text{emf} = - \frac{\partial \Phi}{\partial t} \quad (\text{C.1})$$

The flux passing through a surface bounded by the conductor is represented by:

$$\Phi = \int \vec{B} \cdot d\vec{a} \quad (\text{C.2})$$

For a coil of wire of N turns connected in series the total induced emf is equal to the sum of the emf induced in each turn. This leads to:

$$\text{emf} = -N \frac{\partial \Phi}{\partial t} \quad (\text{C.3})$$

If the assumption is made that magnetic fields vary in a sinusoidal manner with time, such a field may be written as:

$$\vec{B} = \vec{B}_0 e^{-j\omega t} \quad (\text{C.4})$$

B is a magnetic vector field which is a function of spatial coordinates and independent of time. Substituting equation (C.2) into (C.3) and applying equation (C.4) yields:

$$\text{emf} = -NB_0 j\omega A \quad (\text{C.5})$$

Where A is the area enclosed by the coil, hence the magnitude of the emf is:

$$\text{emf} = -NB_0 (2\pi f) A \quad (\text{C.6})$$

APPENDIX D

A. TRANSFER FUNCTION USAGE

The spectrum analyzer when in the dbV display mode provides a value:

$$N(\text{dbV}) = 20 \log \frac{A \text{ volt}}{1 \text{ volt}} \quad (\text{D.1})$$

In order to convert this to 0 dB (re: 1 nT vice 1 V):

$$\frac{A \text{ volts}}{1 \text{ volt}} \cdot \frac{x \text{ volts/nT}}{x \text{ volts/nT}} = \frac{A \text{ volts}}{x \text{ volts/nT}} \cdot \frac{x \text{ volts}}{1 \text{ volt/nT}}$$

where the magnetic field (B) measured by the system is:

$$B = (A \text{ volts}) / (x \text{ volts per nT}) \quad (\text{D.2})$$

Therefore referenced to 1 nT yields:

$$N(\text{dB}) = 20 \log (B/1 \text{ nT}) + 20 \log X \quad (\text{D.3})$$

where X is the system transfer function in units of volts/nT.

Most spectrum analyzers are capable of using various averaging windows over variable frequency ranges. They also possess a characteristic number of bins for which a correction must be made. This correction is developed as follows:

$$B^2 = \Phi(\text{BW})$$

and

$$(\text{BW}) = \frac{\text{Frequency range}}{\text{Number of}} \quad (\text{Window correction}).$$

Then:

$$N(\text{dB}) = 20 \log (\phi^{\frac{1}{2}}(\text{BW})^{\frac{1}{2}}) + 20 \log X$$

and finally after rearranging:

$$10 \log \phi = N(\text{dB}) - 20 \log X - 10 \log(\text{BW}) \quad (\text{D.4})$$

where $10 \log \phi$ is the corrected reading or the power spectral density and ϕ , the magnetic flux has the units of nT^2/Hz .

APPENDIX E

A. DATA CURVES

The figures within this appendix are a collection of representative data curves of measurements made on the floor of Monterey Bay and at a remote land station. The data for the measurements on the seafloor are displayed over two different bandwidths, 0.1 to 20 Hz (Figures E.1 to E.11) and .025-5 Hz (Figures E.12 to E.22). Figures E.23 to E.24 depict a sample of available land data. The individual data curves are appropriately anotated as to time, date, location, bandwidth, water depth and sea surface conditions.

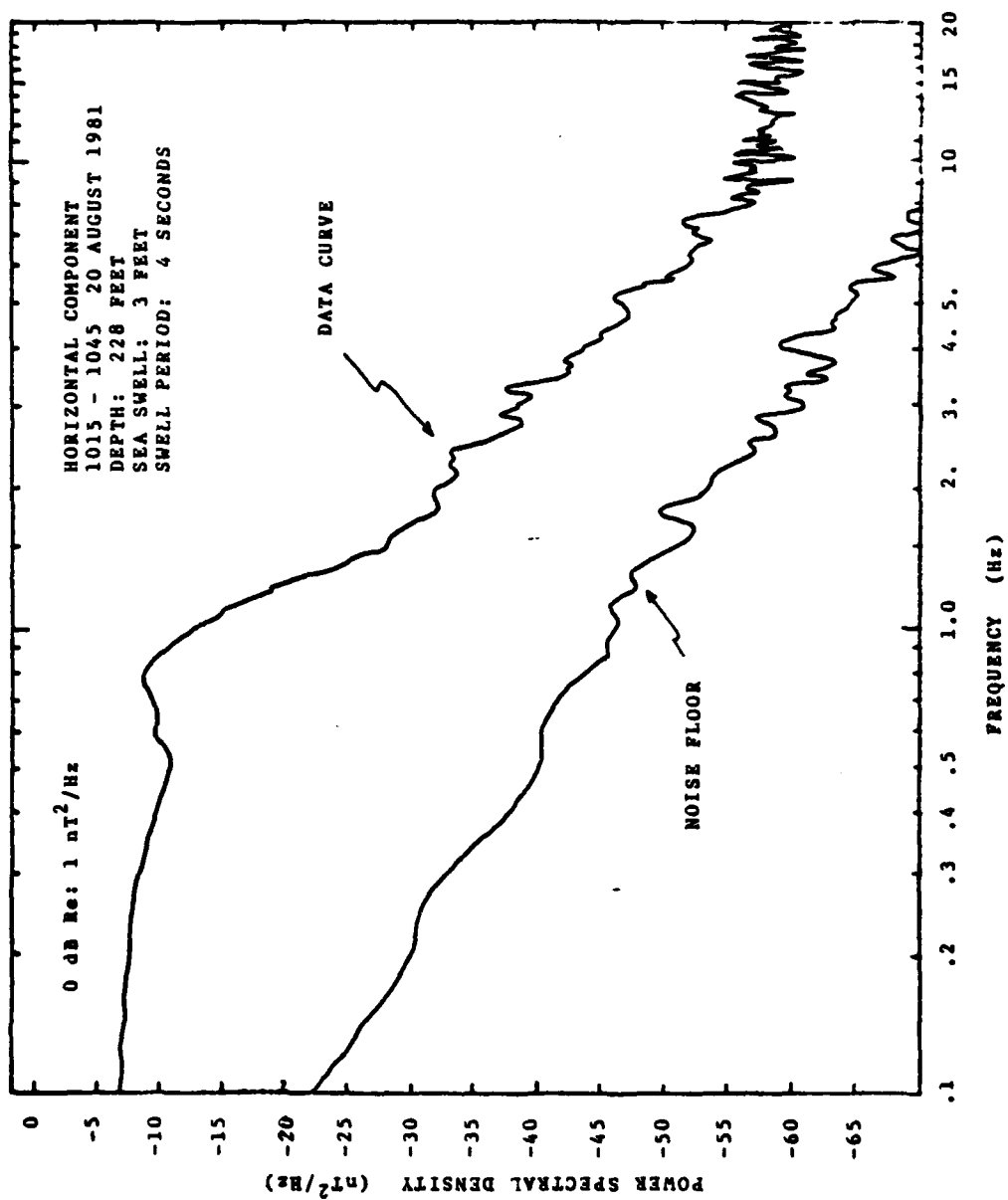


Figure E.1. Data Curve (9/20/81, horiz., .1-20 Hz)

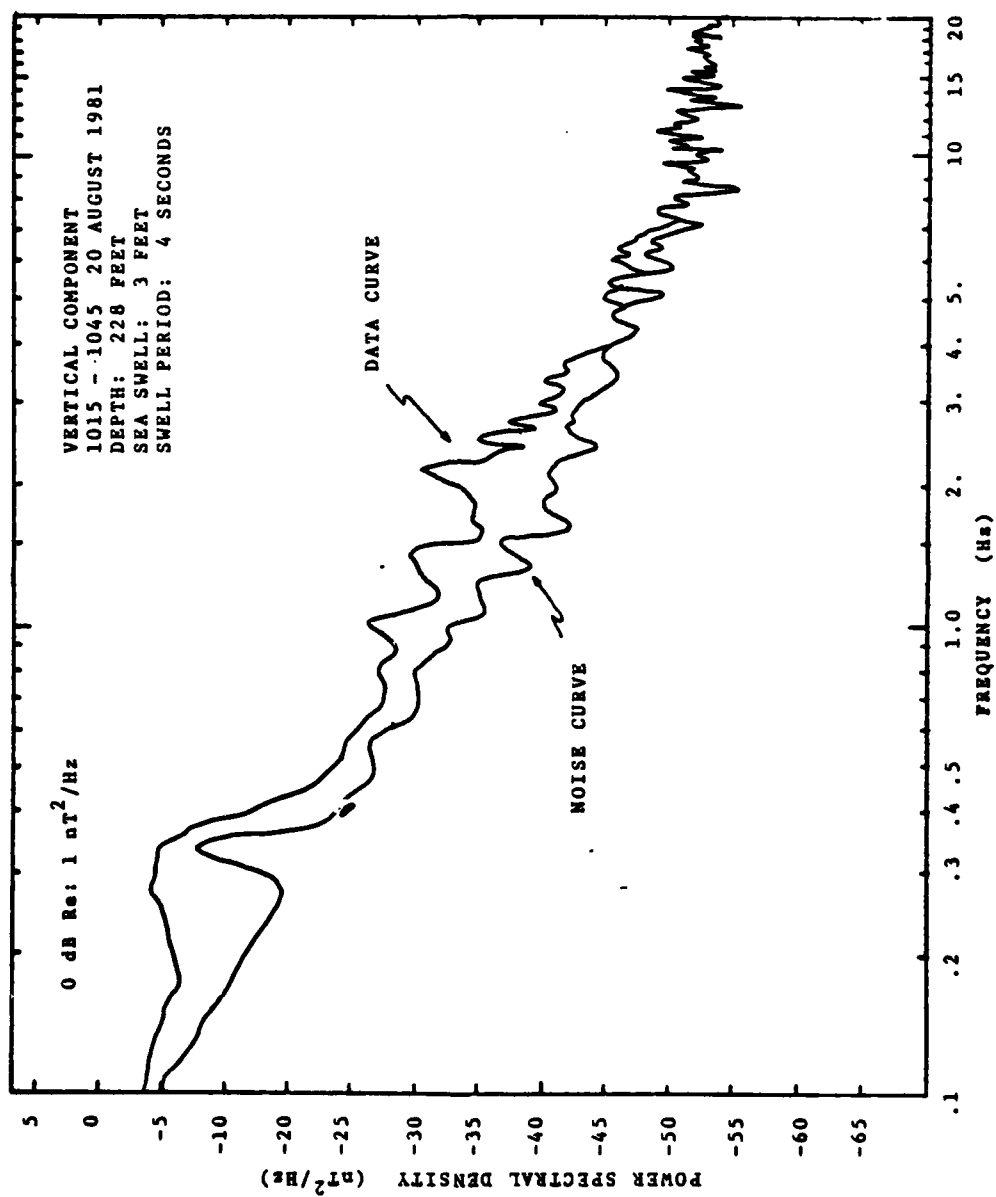


Figure E.2. Data Curve (9/20/81, vert., .1-20 Hz)

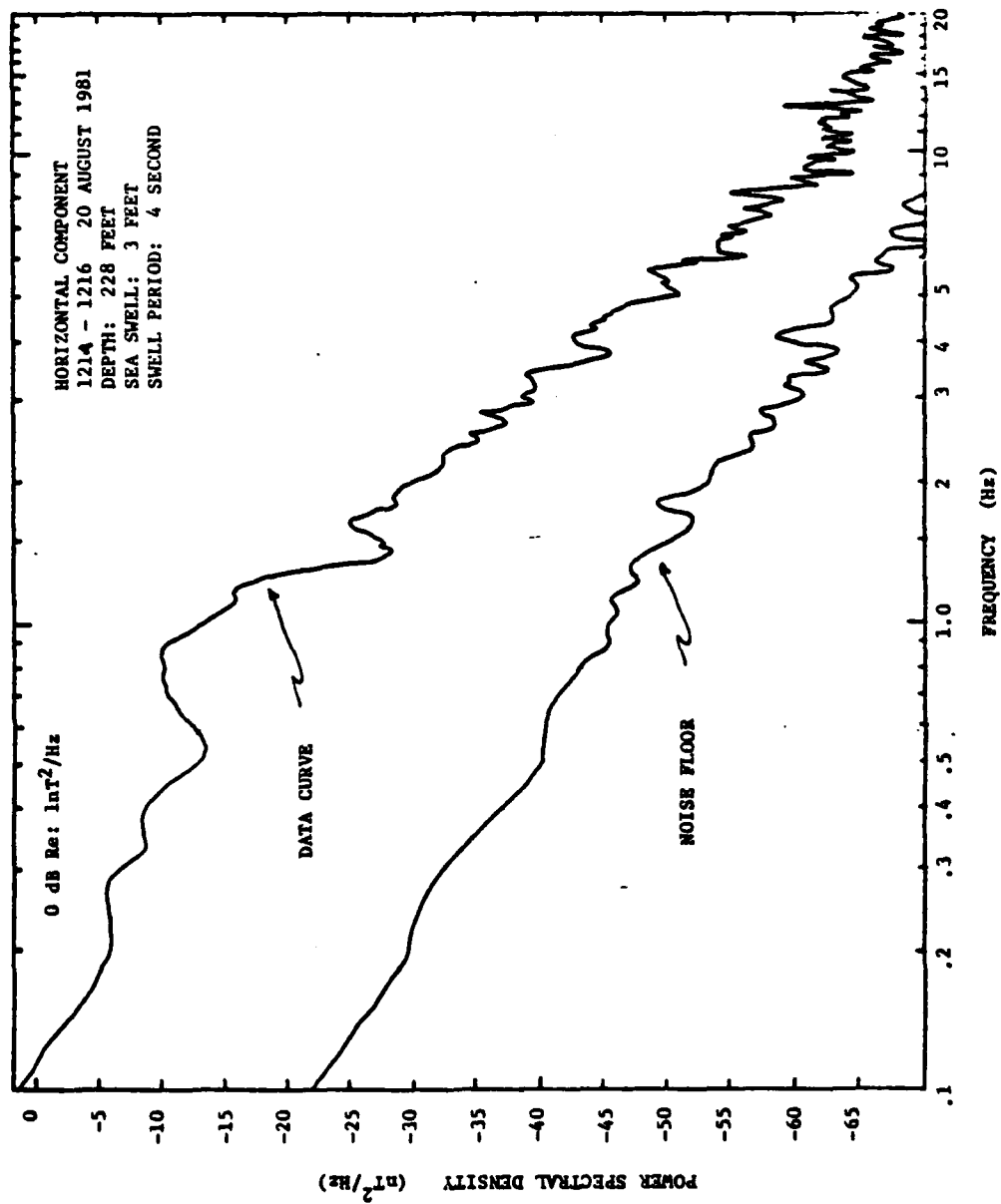


Figure E.3. Data Curve (9/20/81, horiz., 1-20 Hz)

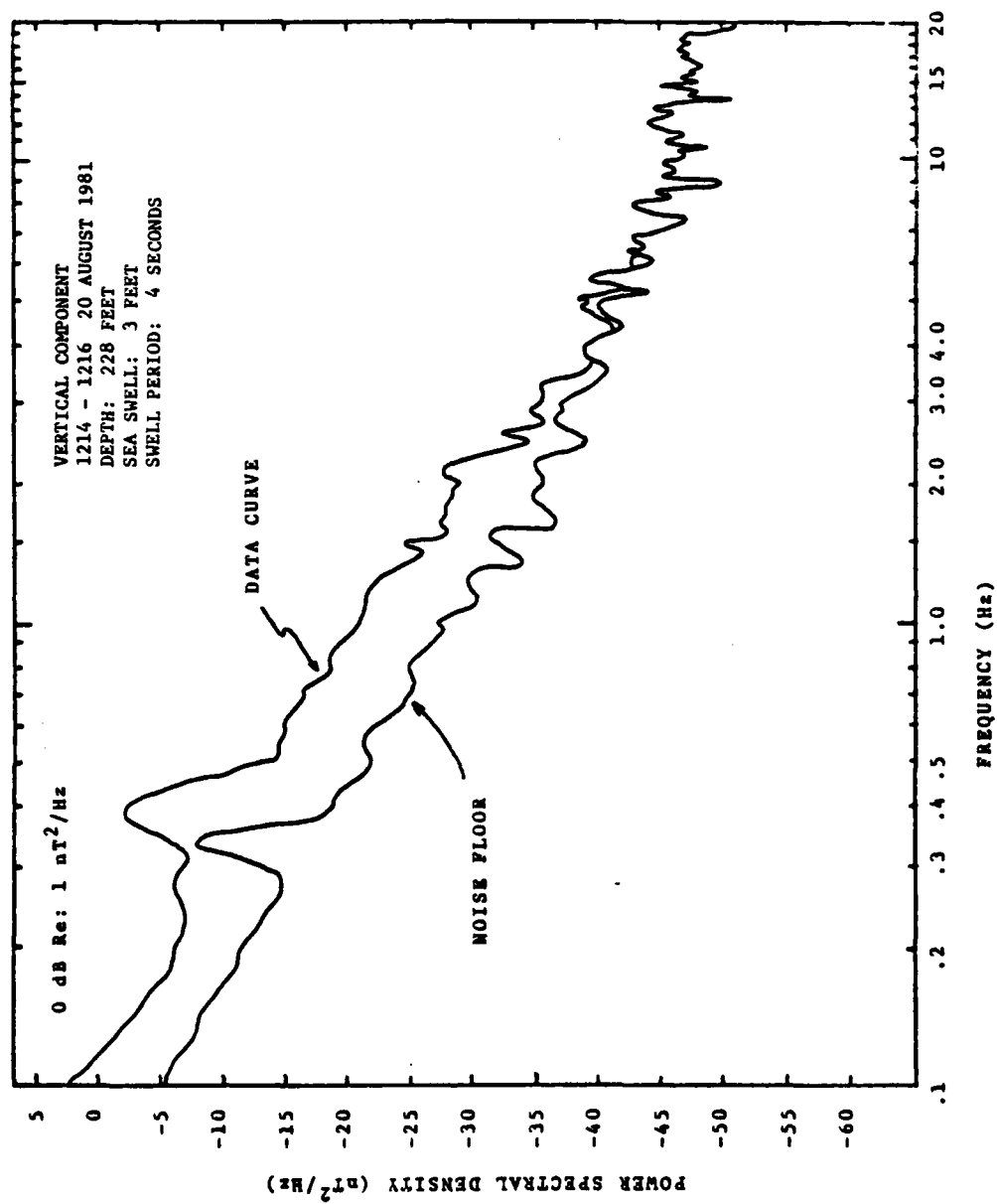


Figure E.4. Data Curve (9/20/81, vert., .1-20 Hz)

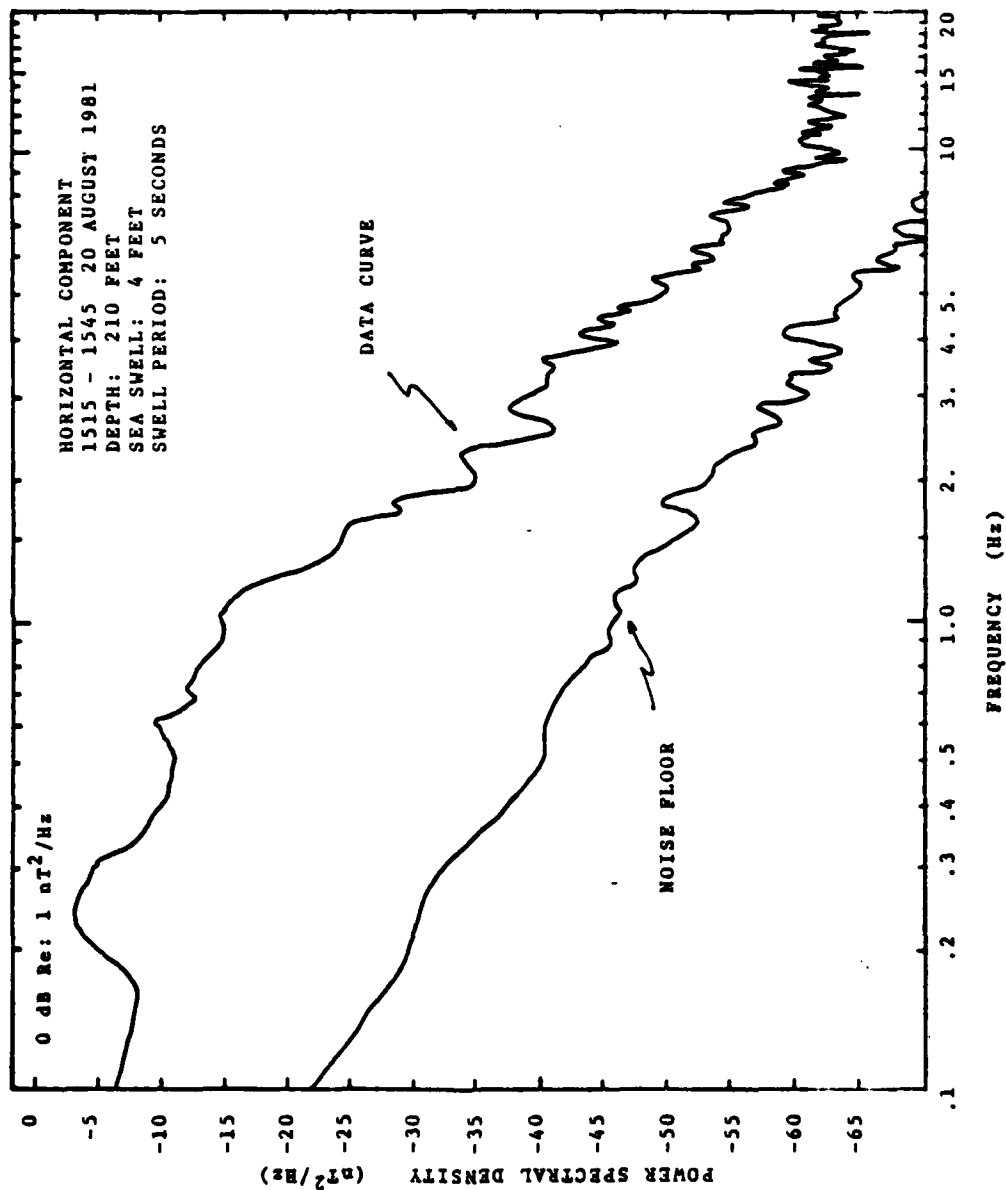


Figure E.5. Data Curve (9/20/81, horiz., .1-20 Hz)

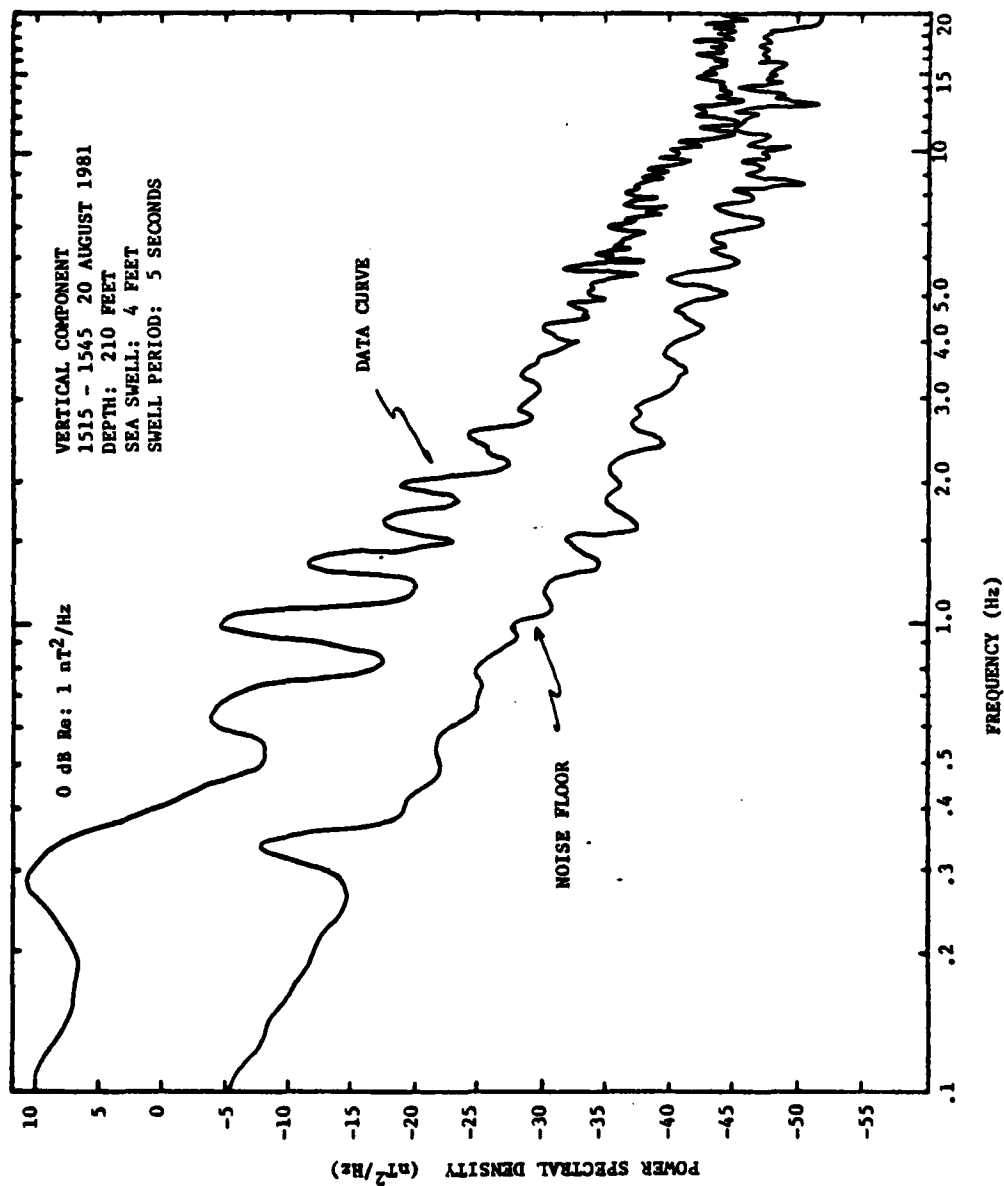


Figure E.6. Data Curve (9/20/81, vert., .1-20 Hz)

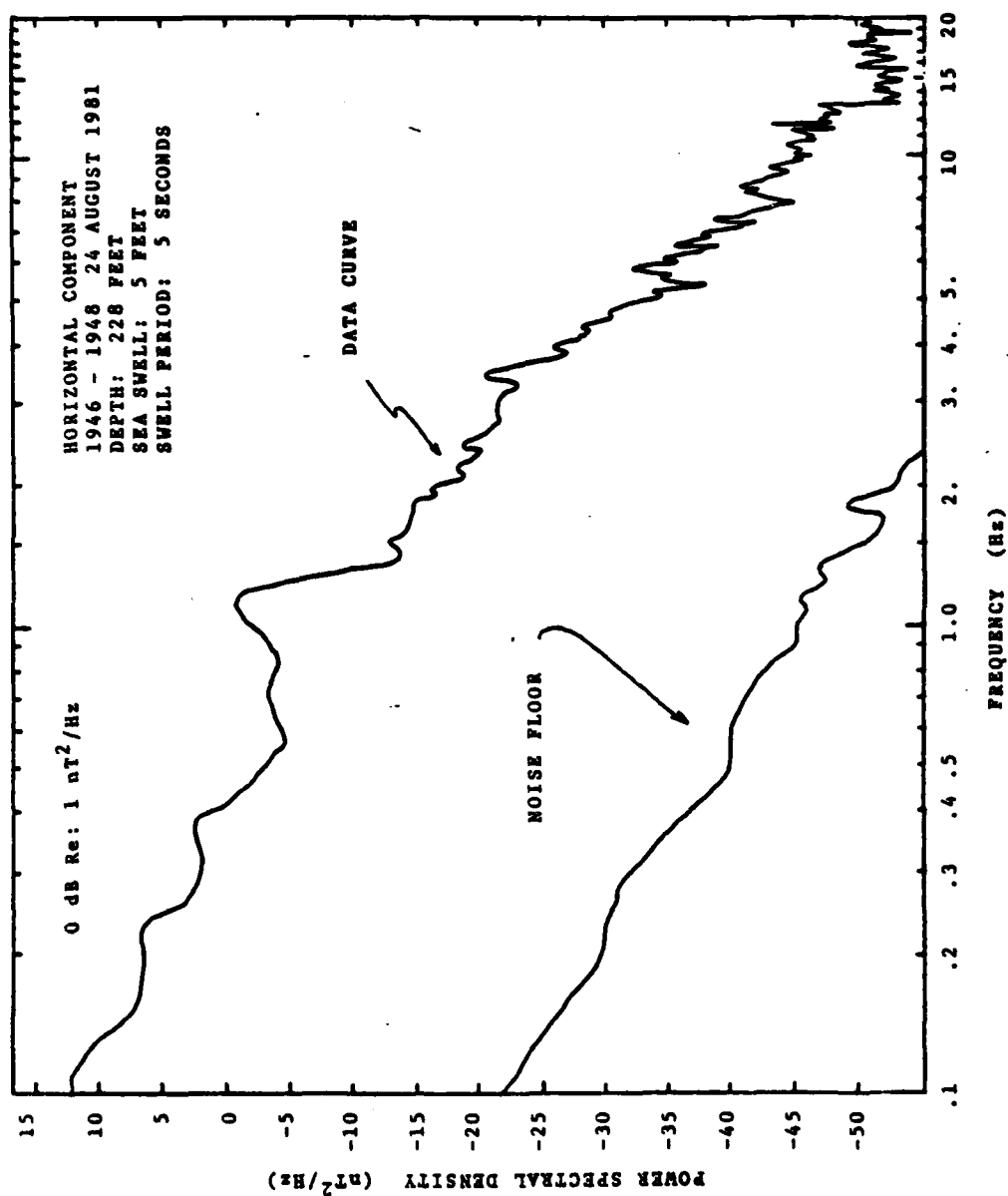


Figure E.7. Data Curve (9/24/81, horiz., .1-20 Hz)

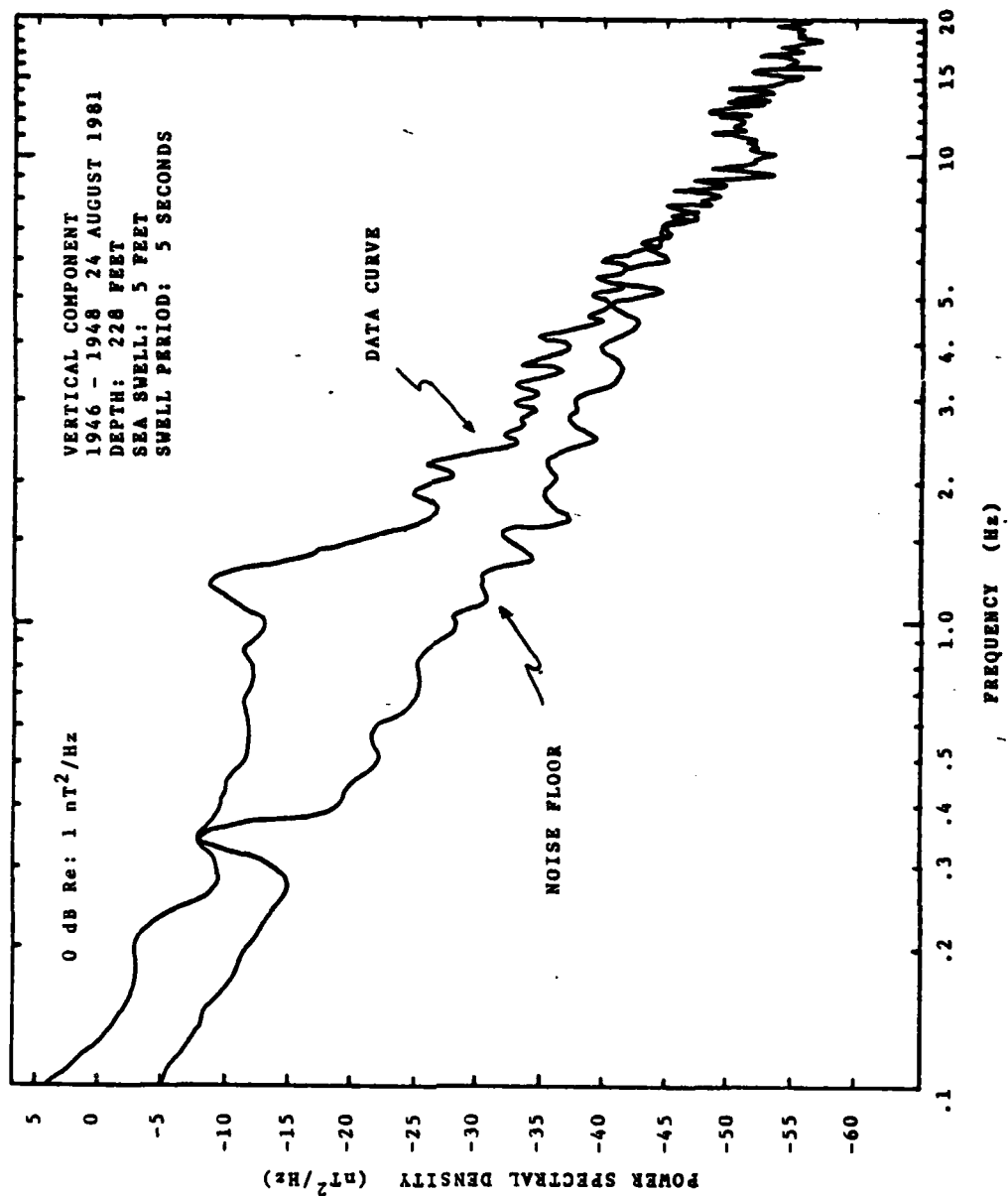


Figure E.8. Data Curve (9/24/81, vert., .1-20 Hz)

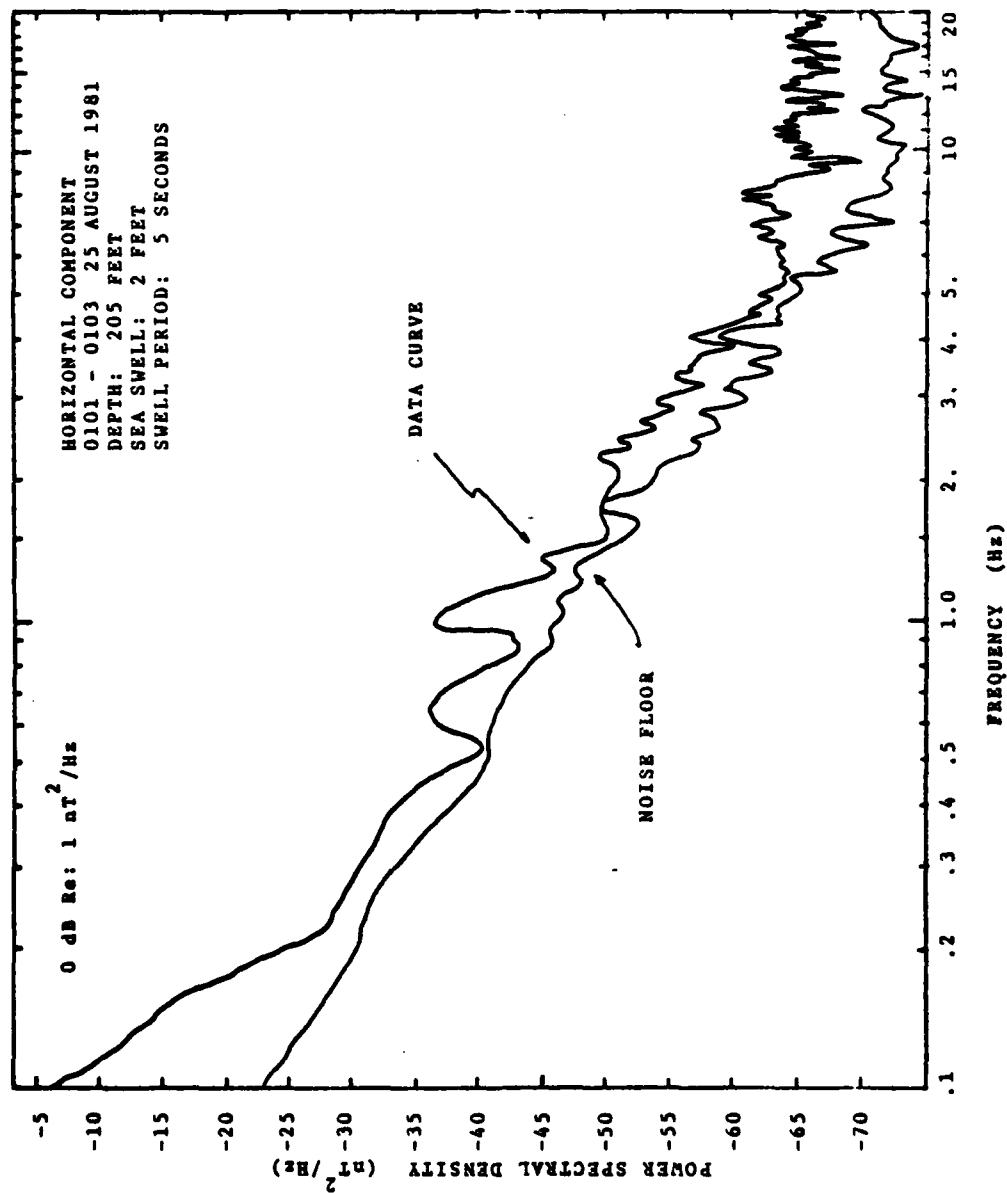


Figure E.9. Data Curve (9/25/81, horiz., .1-20 Hz)

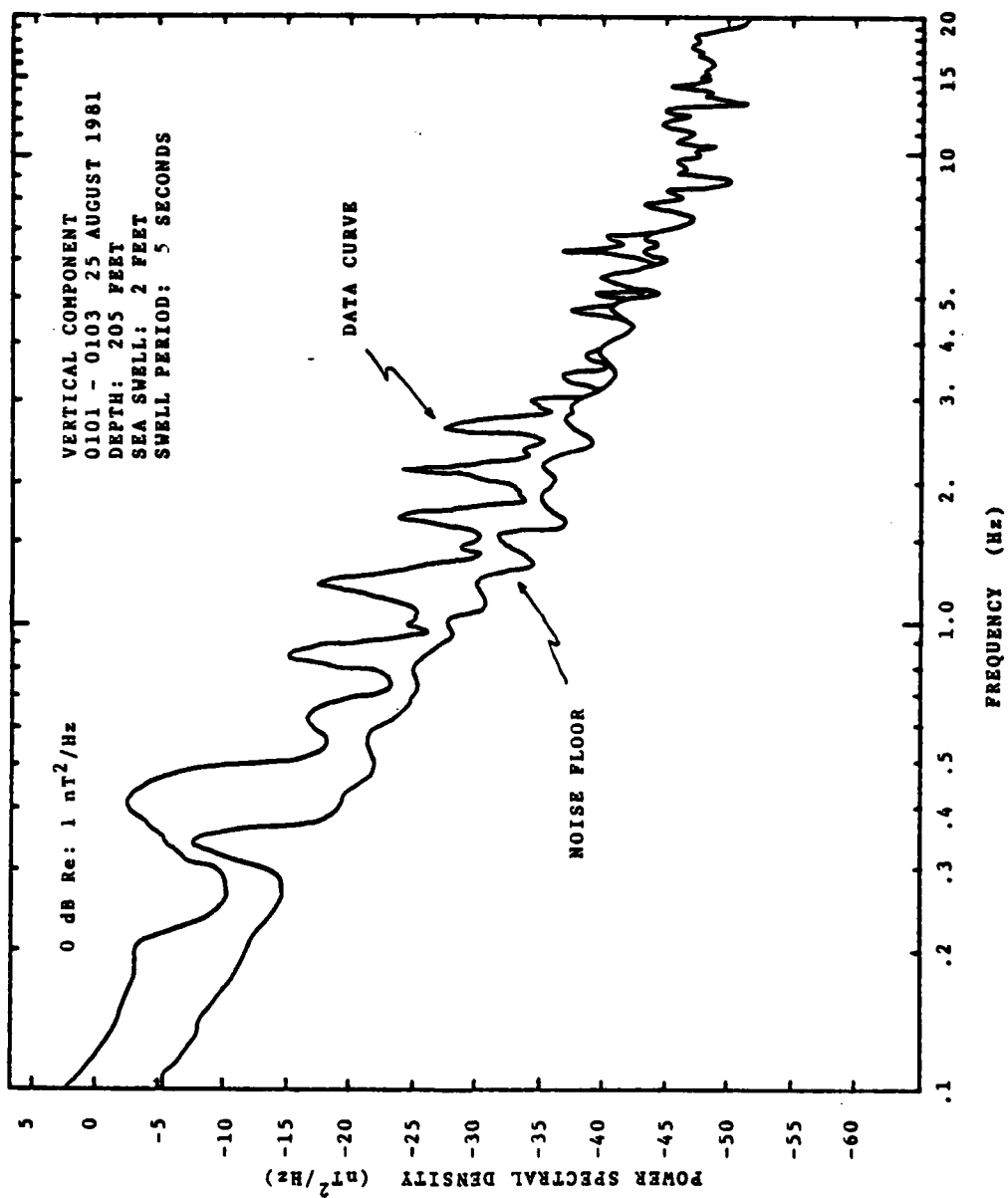


Figure E.10. Data Curve (9/25/81, vert., .1-20 Hz)

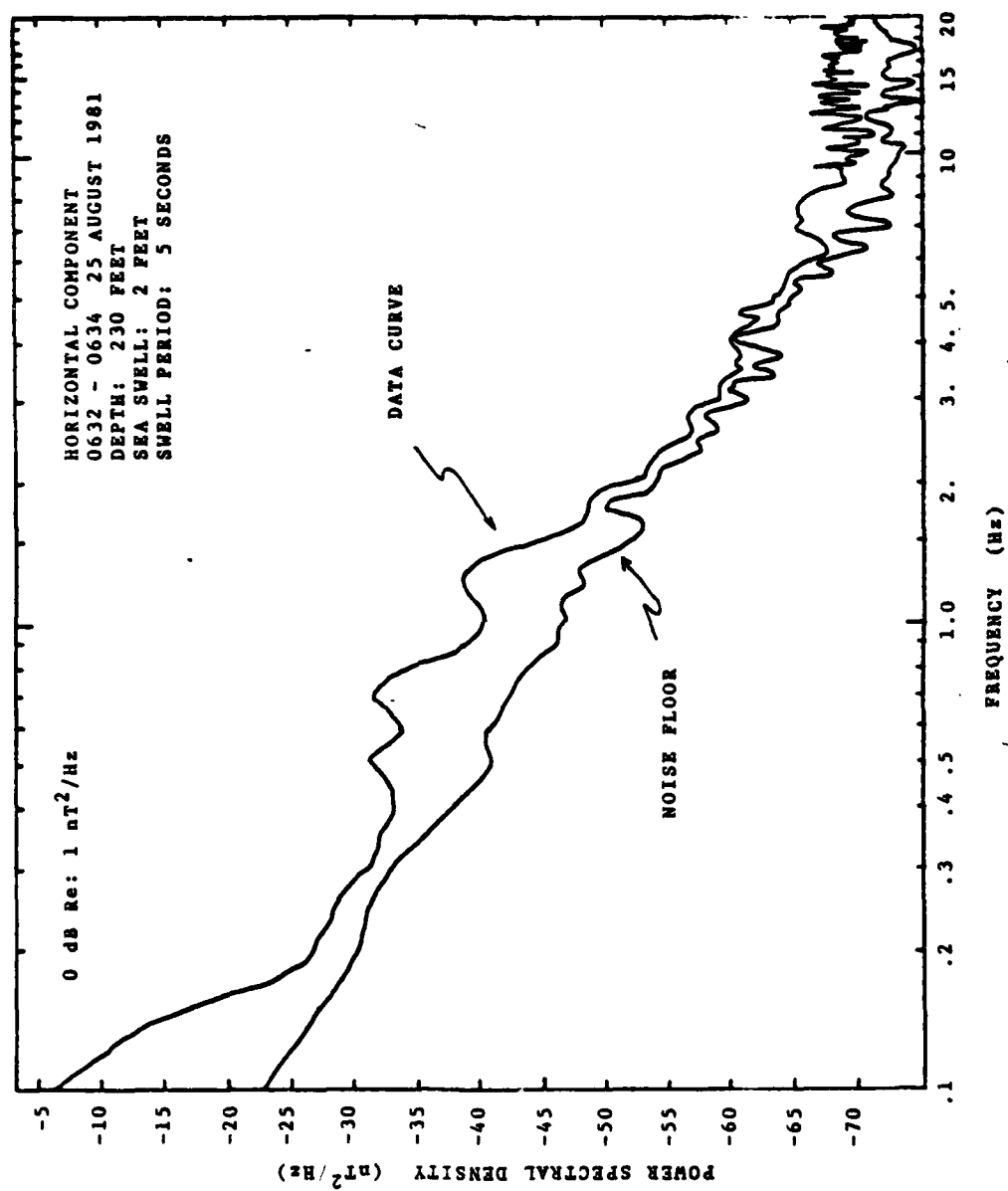


Figure E.11. Data Curve (9/25/81, horiz., .1-20 Hz)

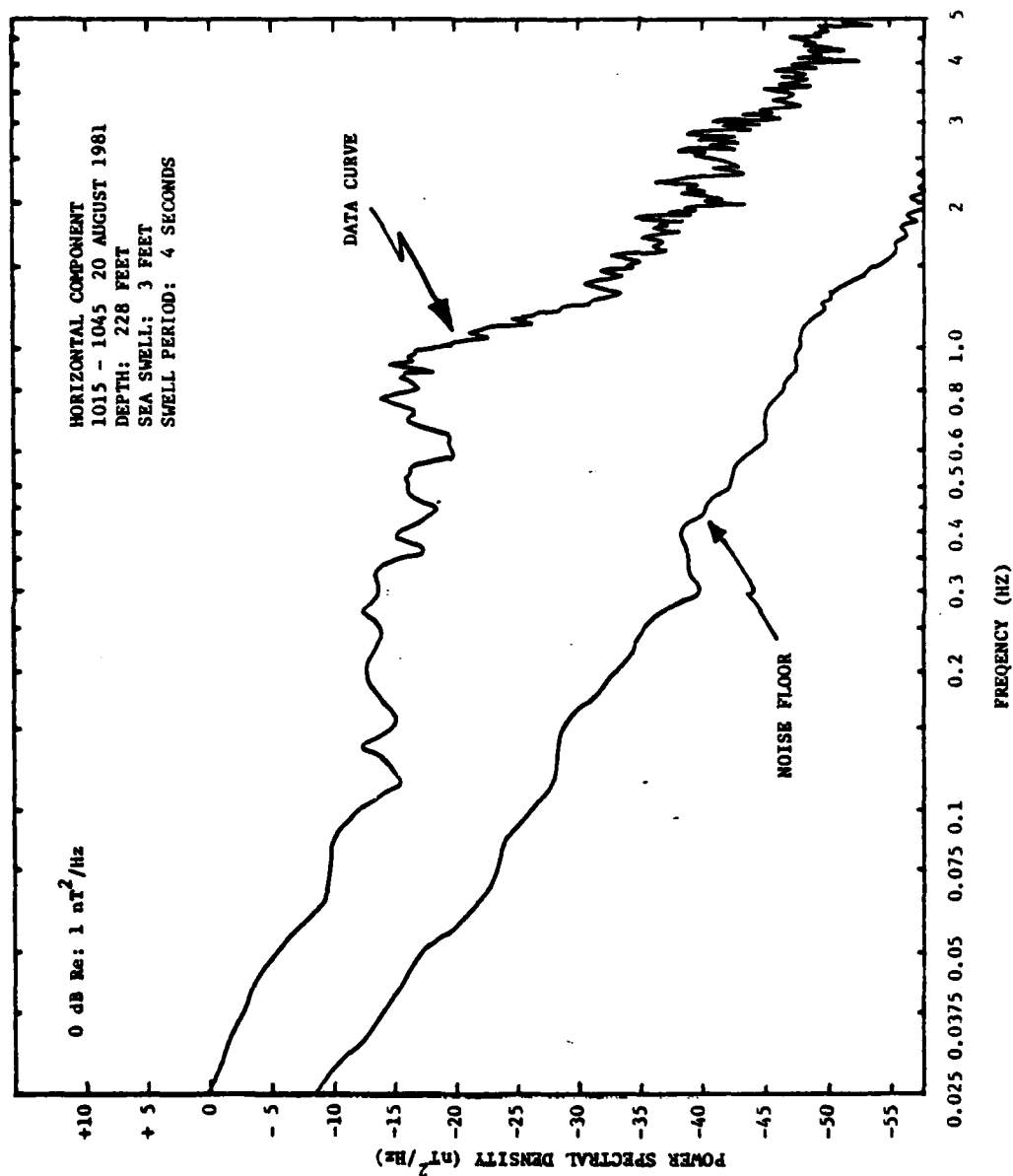


Figure E.12. Data Curve (9/20/81, horiz., .025-5 Hz)

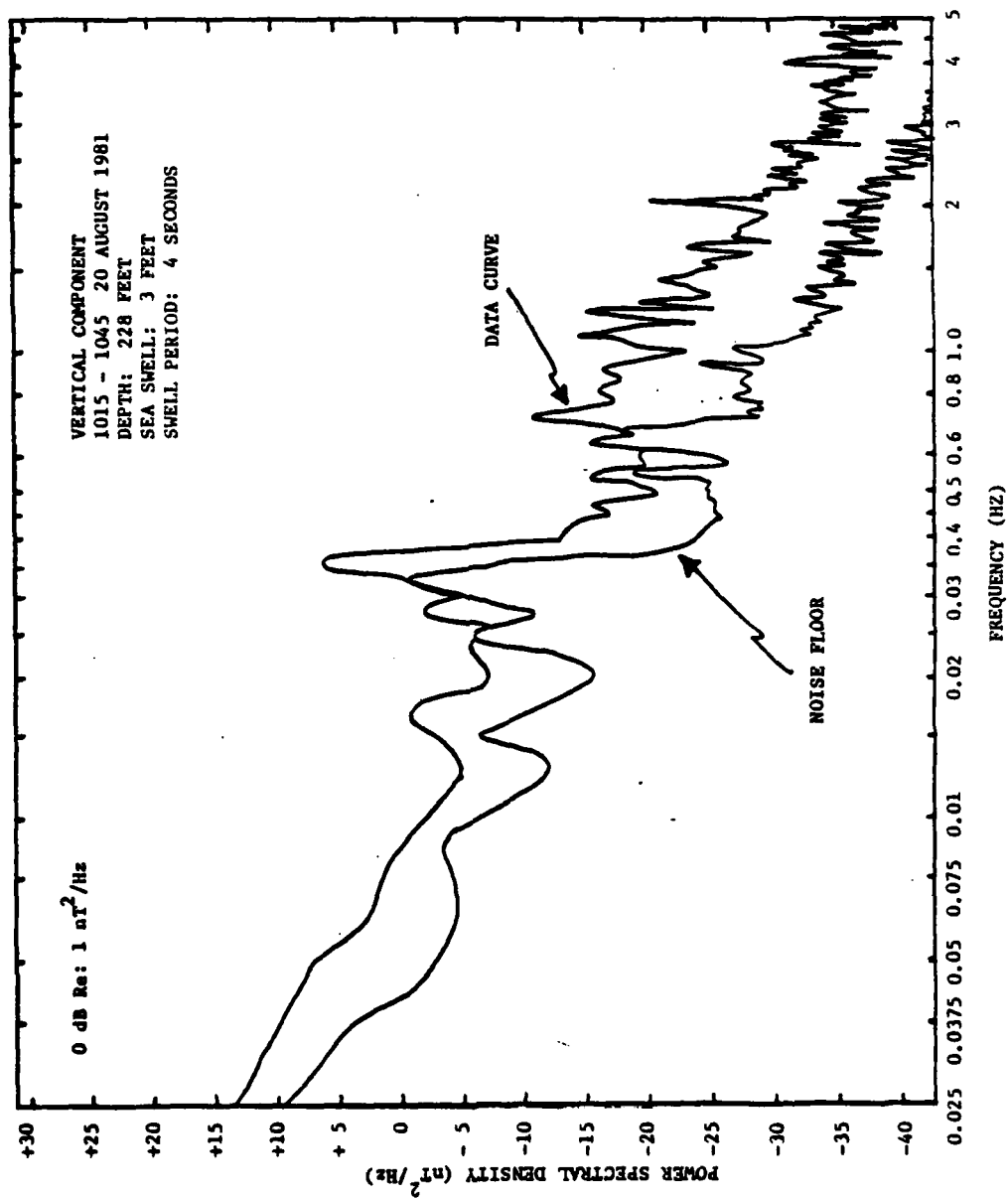


Figure E.13. Data Curve (9/20/81, vert., .025-5Hz)

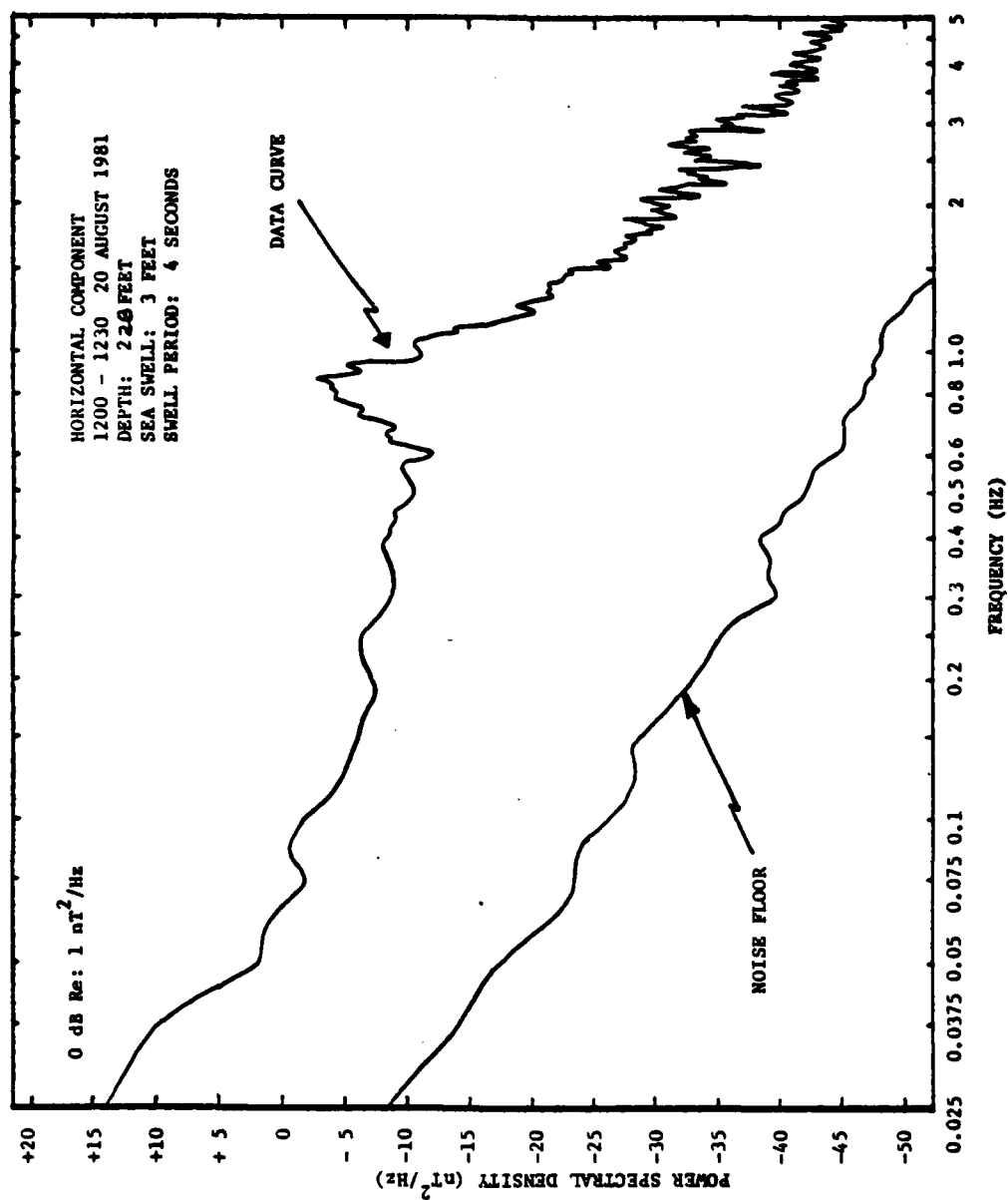


Figure E.14. Data Curve (9/20/81, horiz., .025-5 Hz)

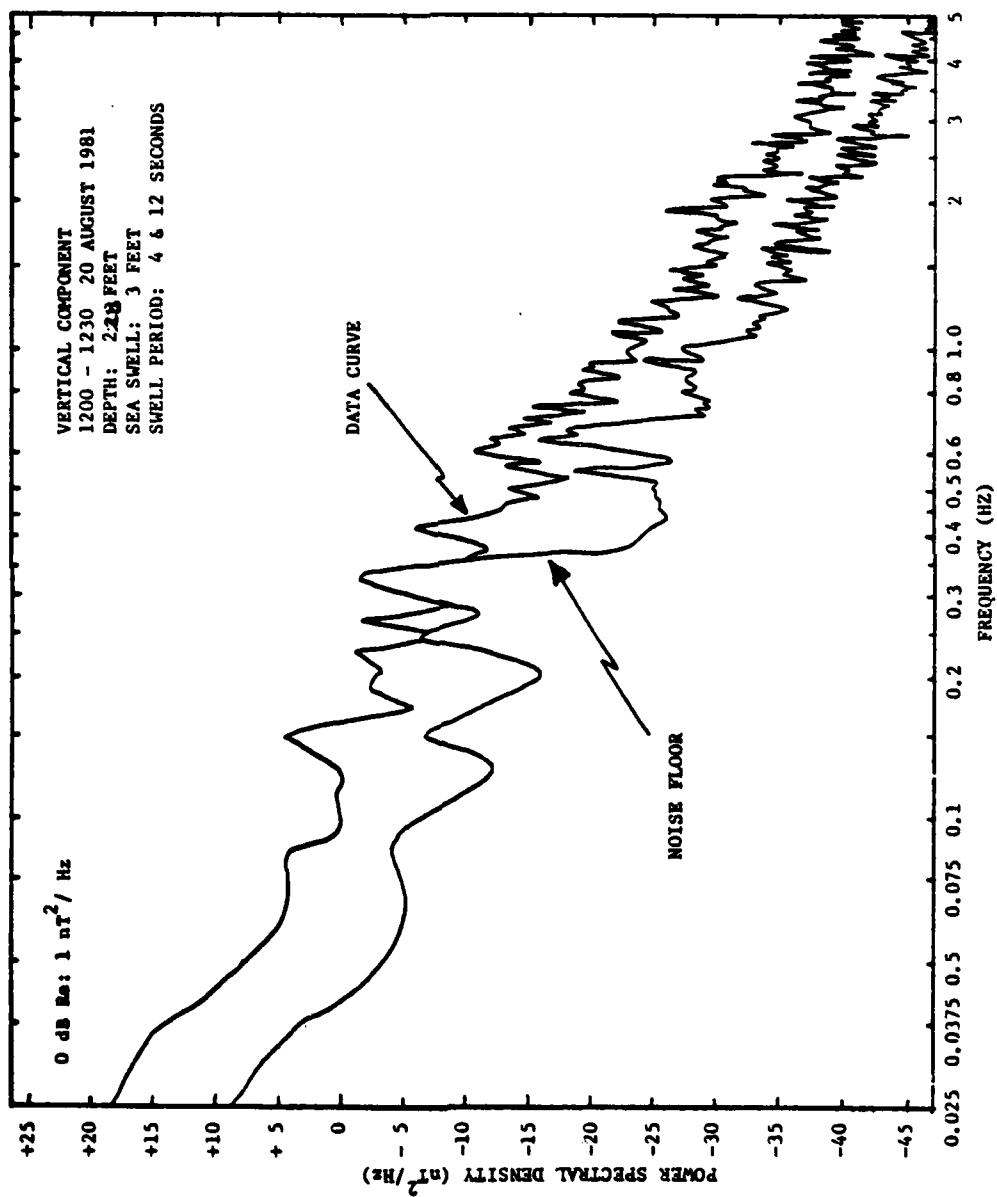


Figure E.15. Data Curve (9/20/81, vert., .025-5 Hz)

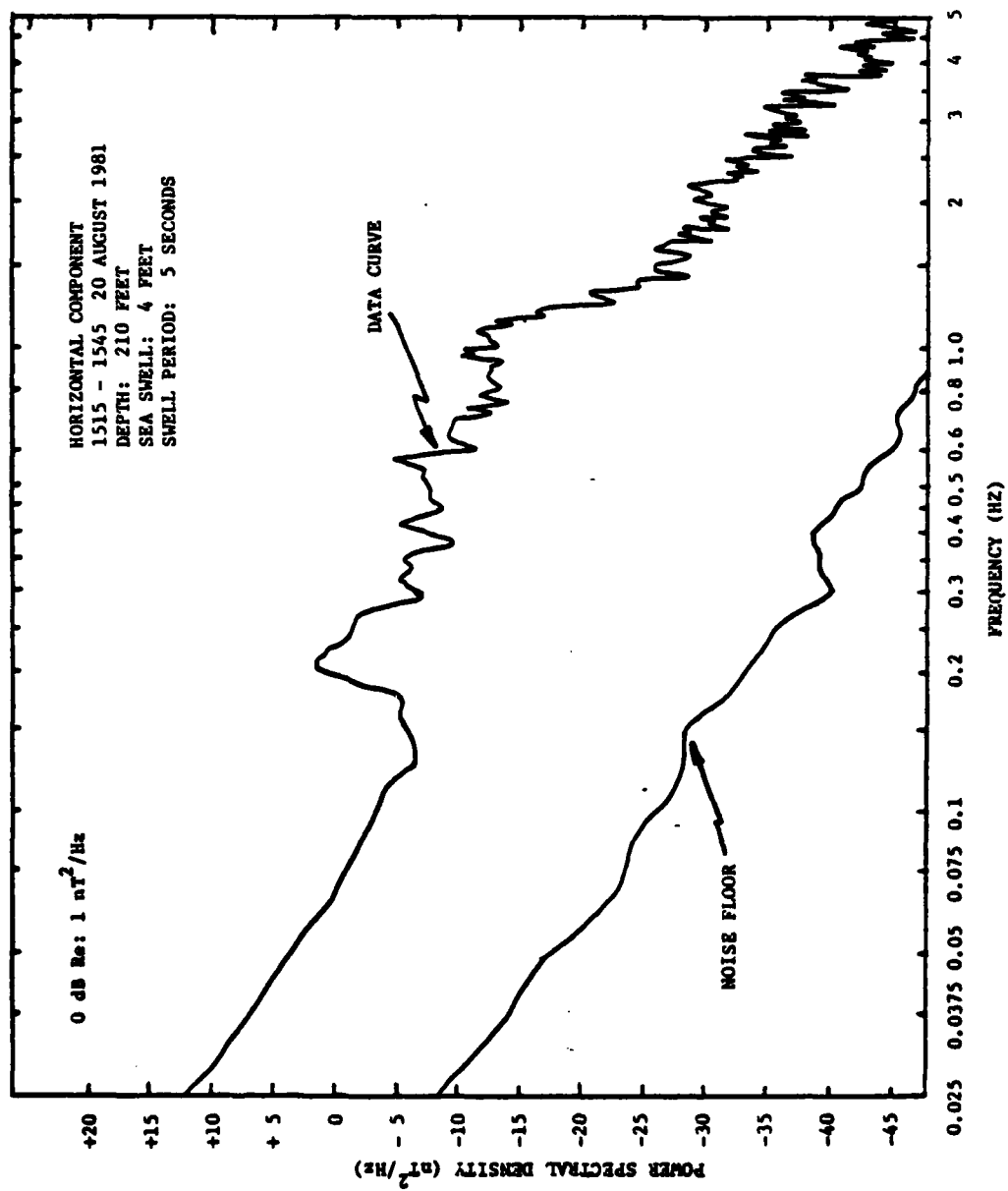


Figure E.16. Data Curve (9/20/81, horiz., .025-5 Hz)

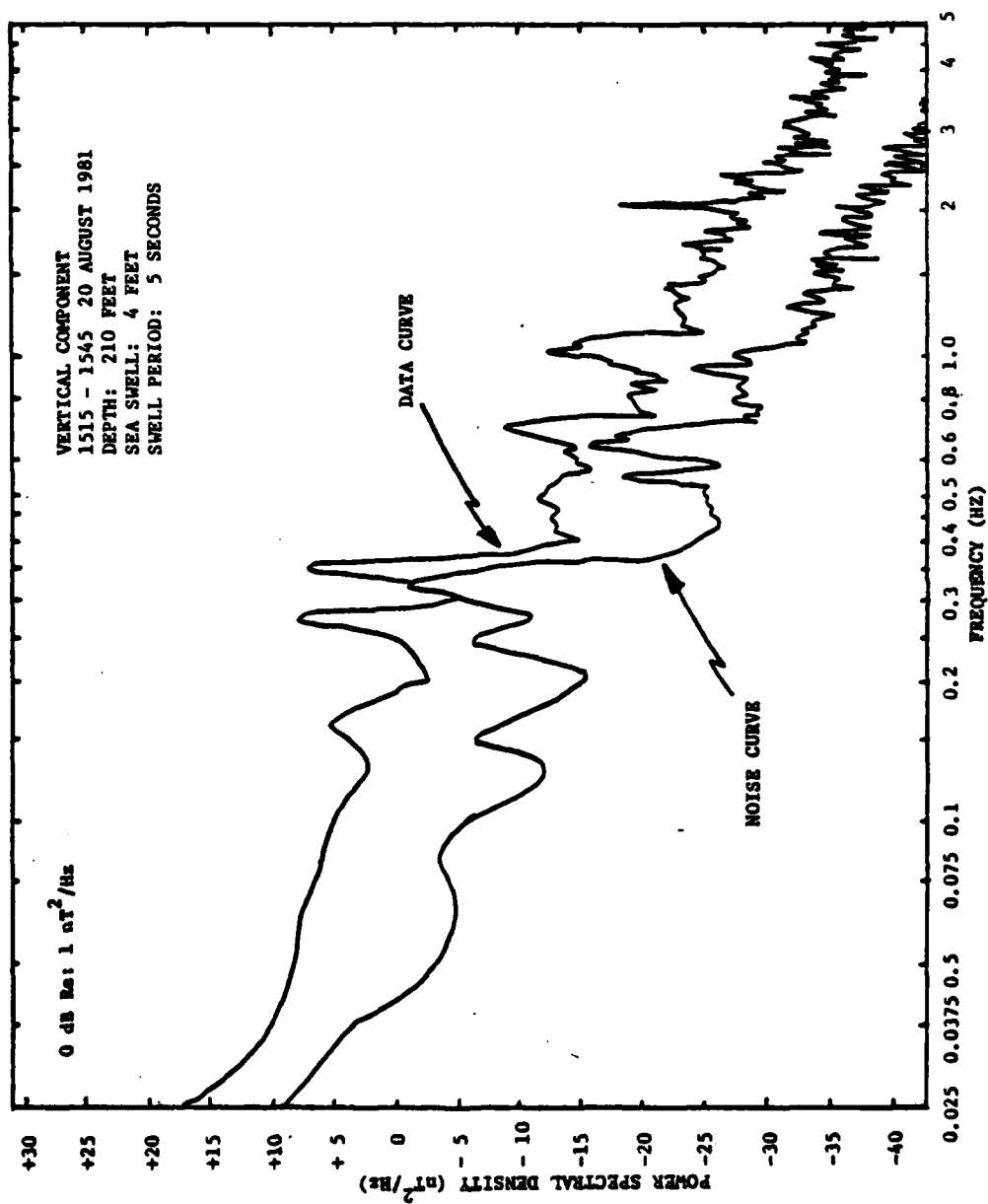


Figure E.17. Data Curve (9/20/81, vert., .025-5 Hz)

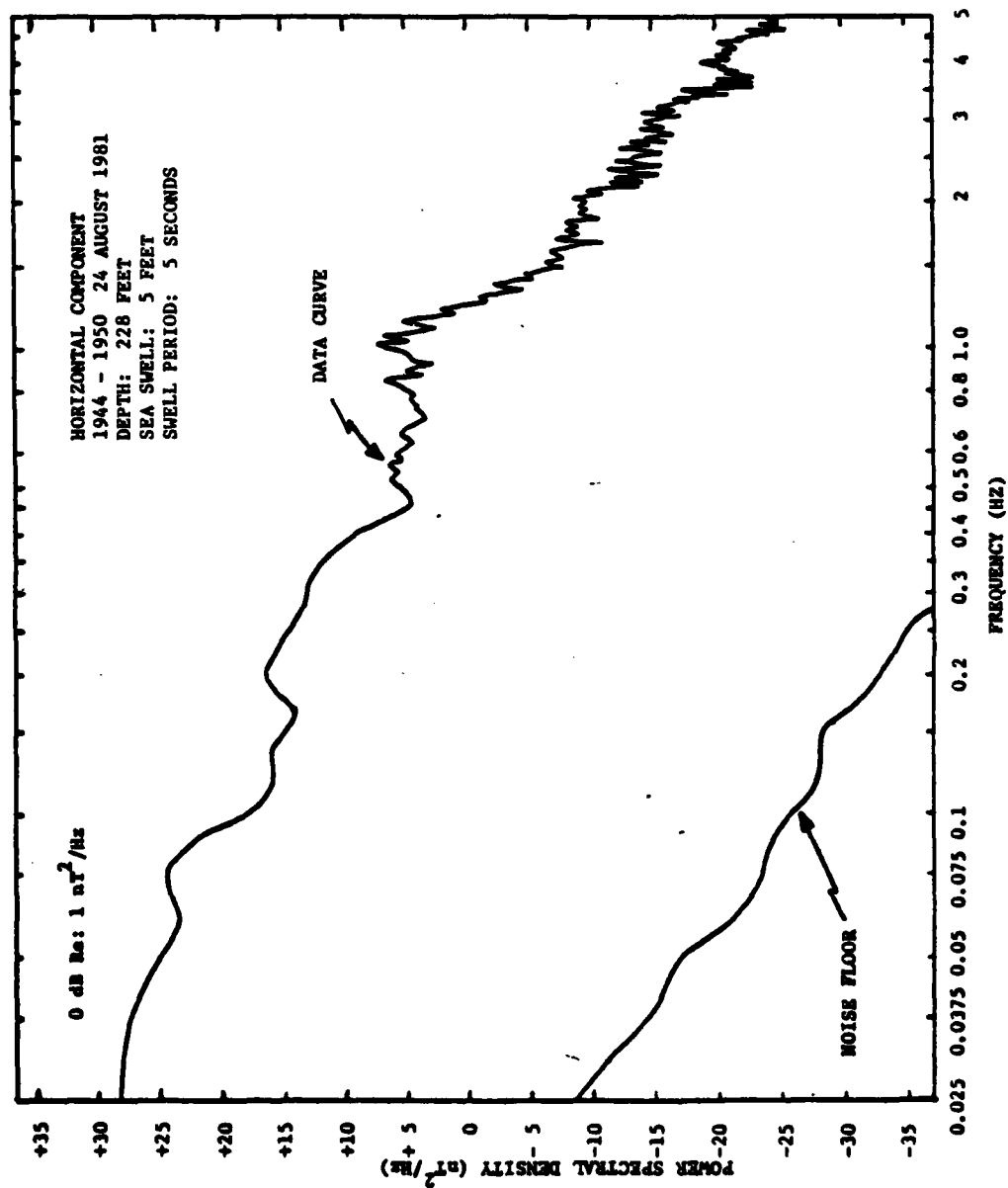


Figure E.18. Data Curve (9/24/81, horiz., .025-5 Hz)

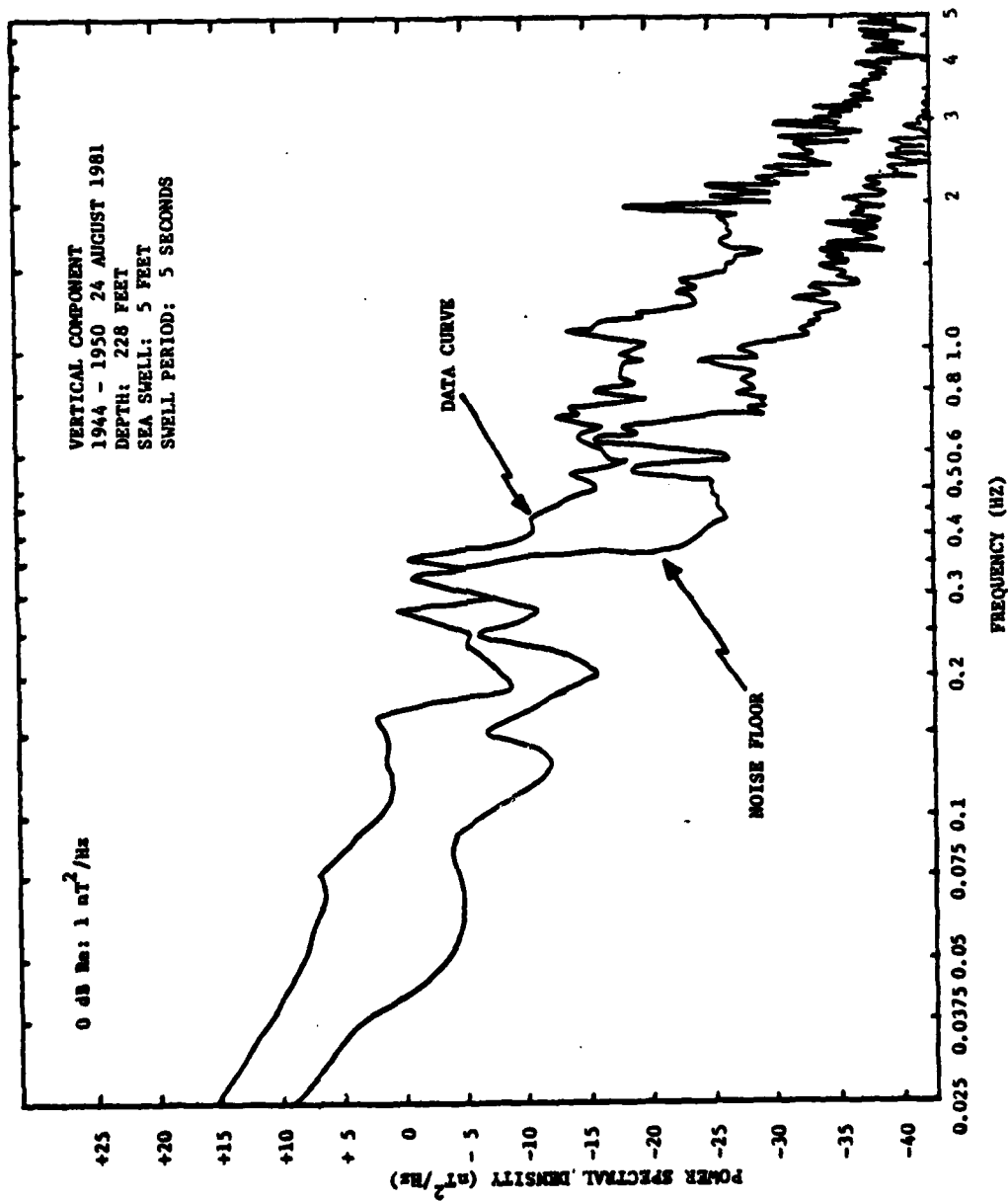


Figure E.19. Data Curve (9/24/81, vert., .025-5 Hz)

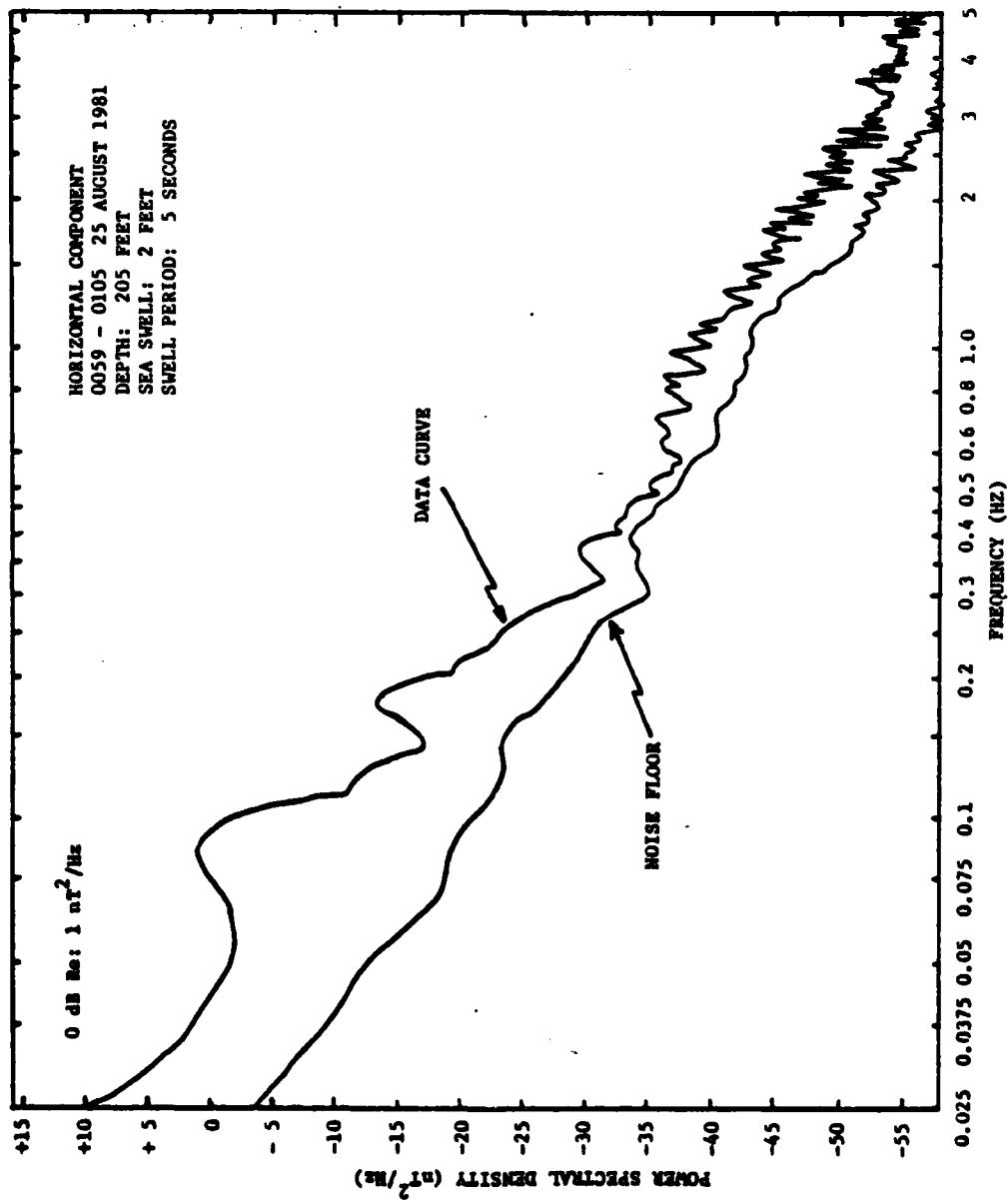


Figure E.20. Data Curve (9/25/81, horiz., .025-5 Hz)

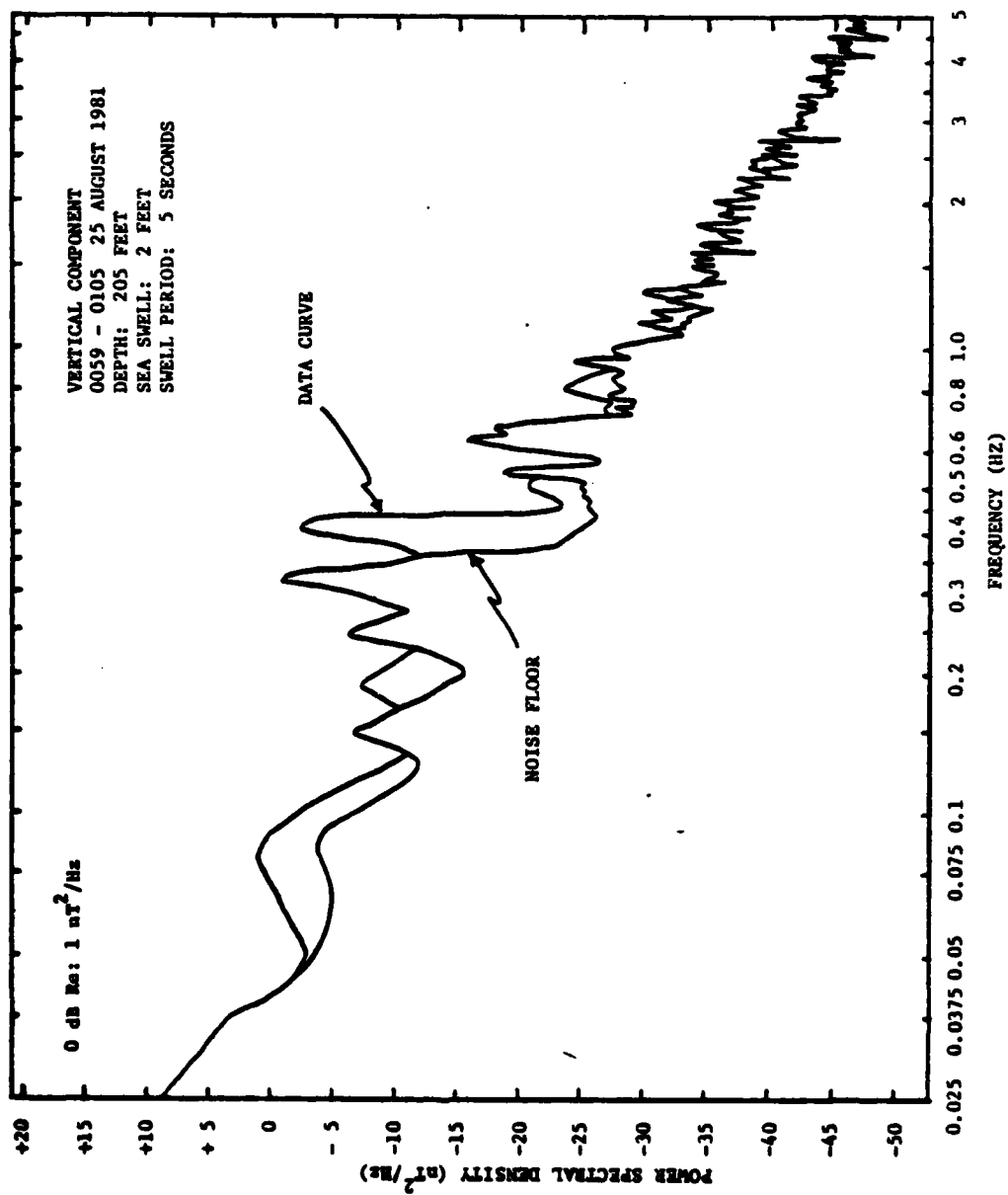


Figure E.21. Data Curve (9/25/81, vert., .025-5 Hz)

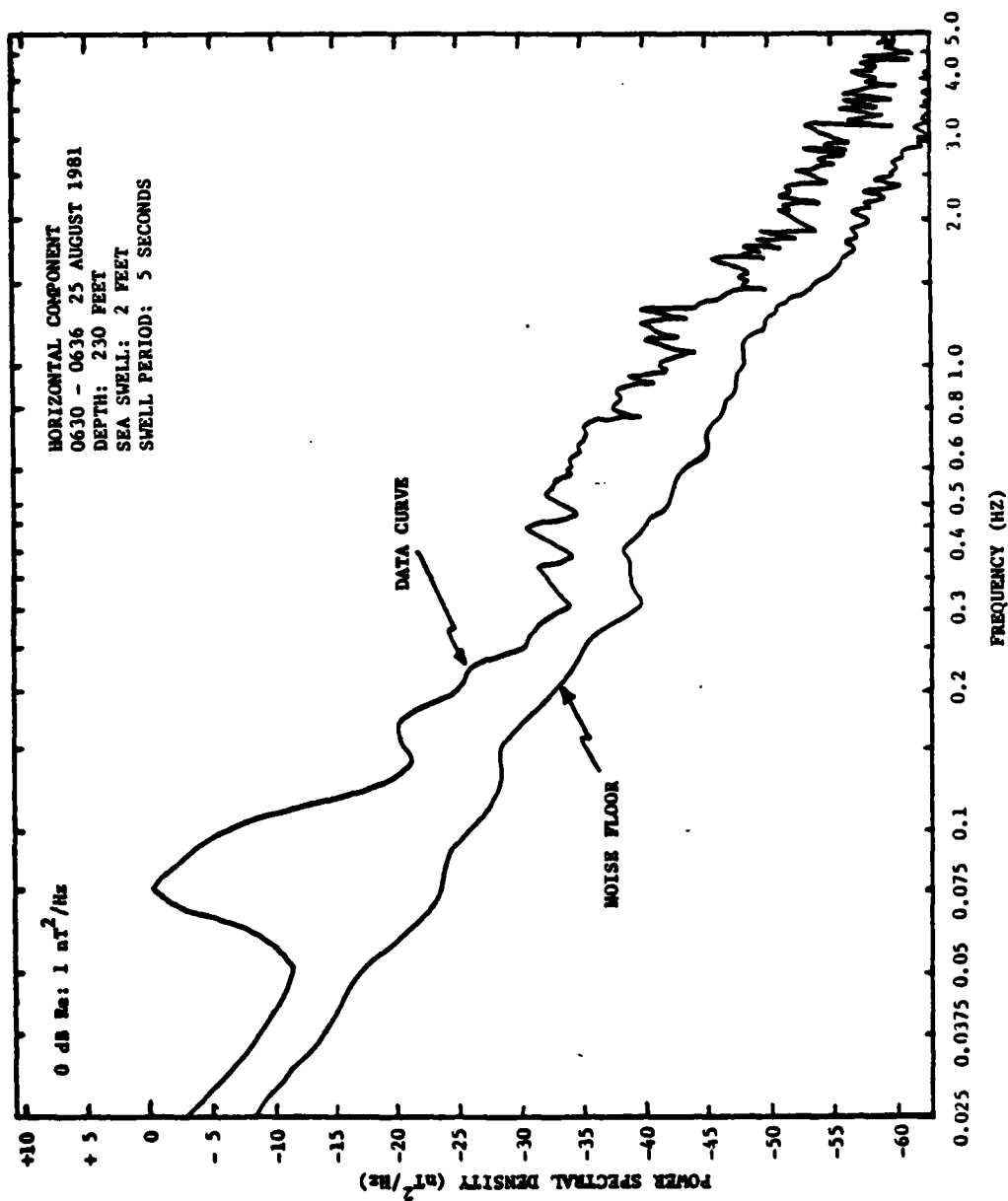


Figure E.22. Data Curve (9/25/81, horiz., .025-5 Hz)

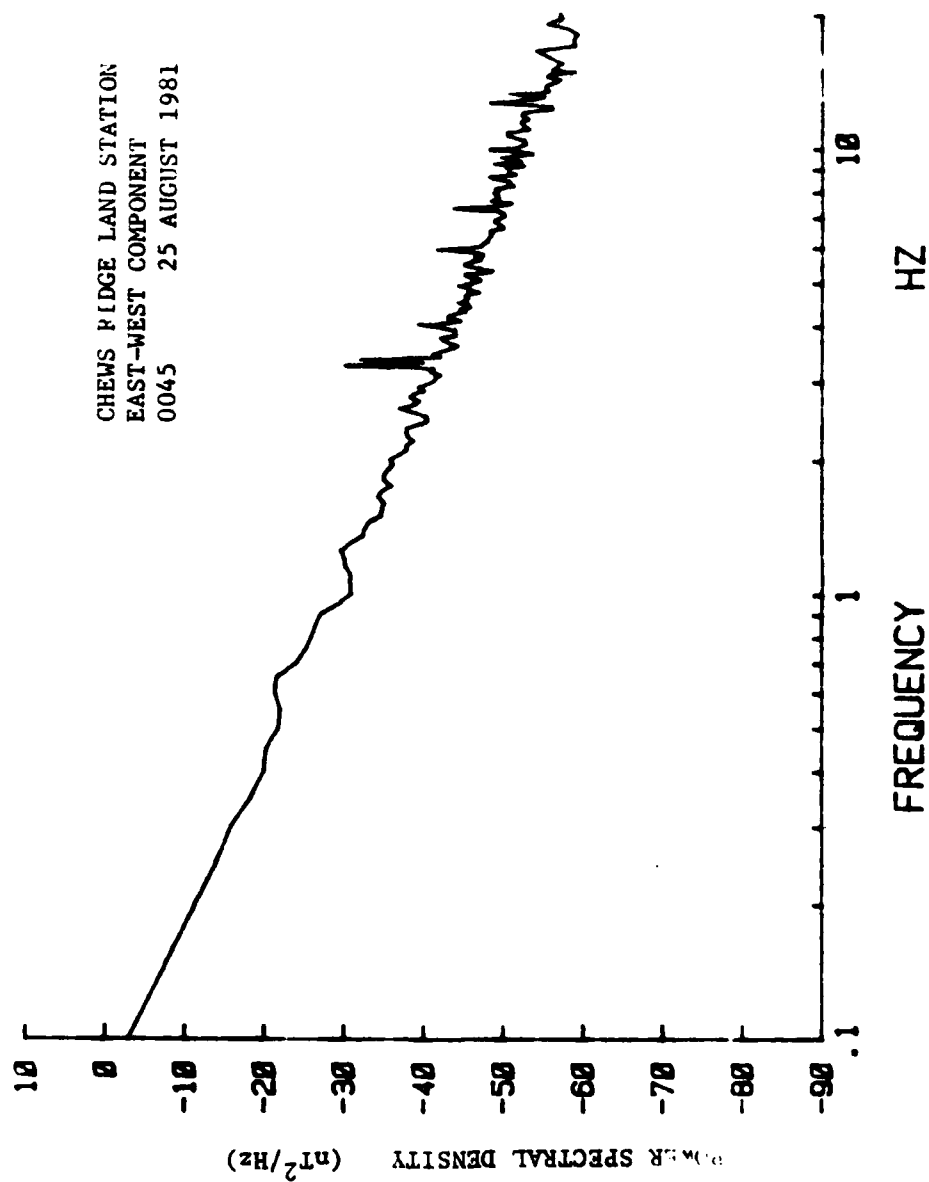


Figure E.23. Data Curve (9/25/81, Land Data, .1-20 Hz)
[Beard 1981]

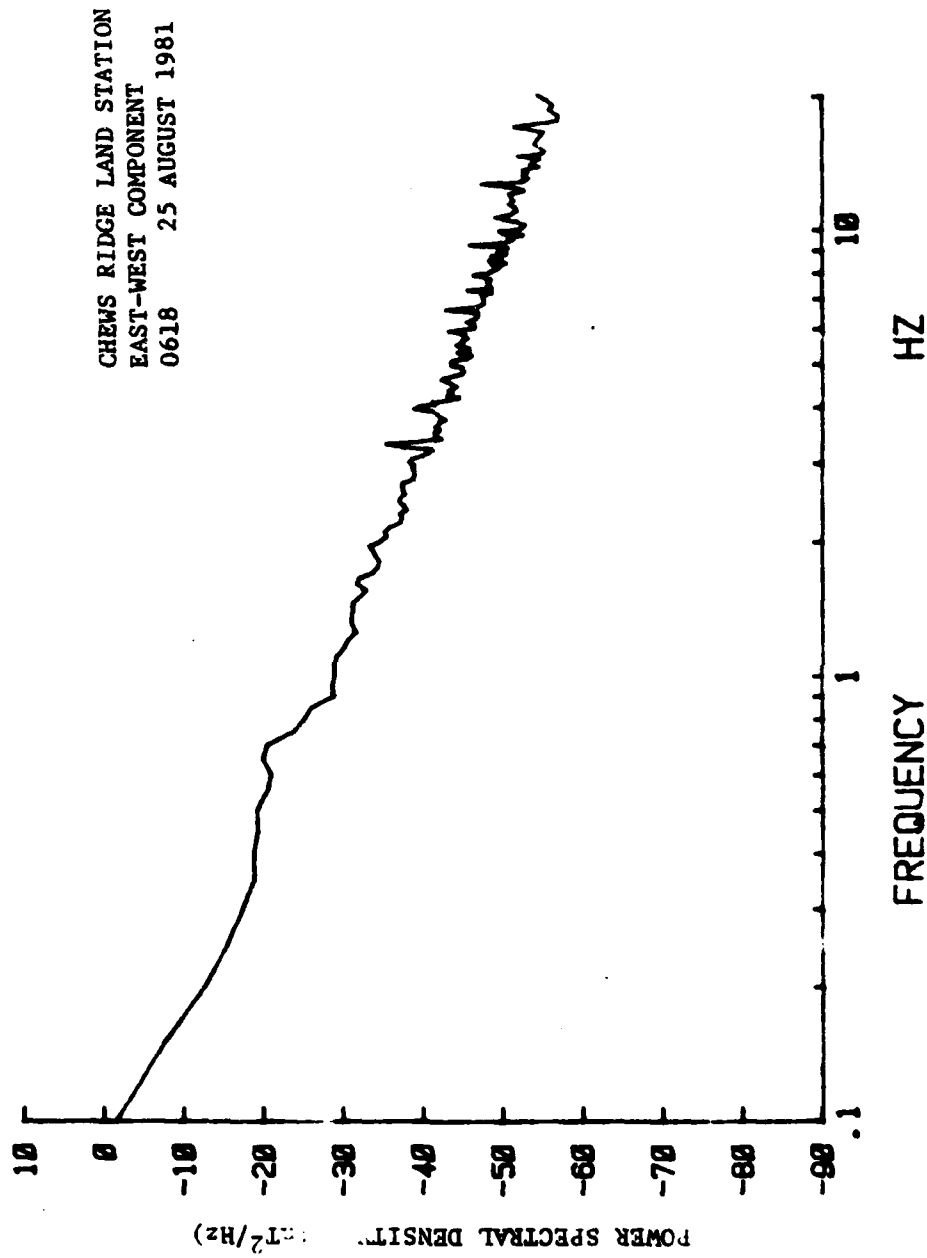


Figure E.24. Data Curve (9/25/81, Land Data, .1-20 Hz) [Beard 1981]

INITIAL DISTRIBUTION LIST

	No. Copies
1. Defense Technical Information Center Cameron Station Alexandria, VA 22314	2
2. Library, Code 0142 Naval Postgraduate School Monterey, CA 93940	2
3. Department Chairman, Code 61 Department of Physics and Chemistry Naval Postgraduate School Monterey, CA 93940	1
4. Professor O. Heinz, Code 61Hz Department of Physics and Chemistry Naval Postgraduate School Monterey, CA 93940	2
5. Professor Paul H. Moose, Code 61Me Department of Physics and Chemistry Naval Postgraduate School Monterey, CA 93940	2
6. Dr. Michael Thomas, Code 61 Department of Physics and Chemistry Naval Postgraduate School Monterey, CA 93940	1
7. LTJG P. M. Rutherford, Jr. USN Code 61Ru Department of Physics and Chemistry Naval Postgraduate School Monterey, CA 93940	1
8. LT M. P. Ames, Jr., USN 1977 Shippan Avenue Stamford, CT 06902	2
9. LT L. M. Vehslage, USN 1142 Shadyhill Drive Columbus, OH 43221	2

- | | | |
|-----|---|------------------|
| 10. | Dr. A. C. Fraser-Smith
Radio Science Laboratory
Stanford Electronics Laboratories
Stanford University
Stanford, CA 94305 | 1 |
| 12. | Chief of Naval Research
Department of the Navy
800 North Quincy Street
Arlington, VA 22217
Code 100C1
Code 460
Code 464
Code 480 | 1
1
1
1 |
| 13. | Dr. James Larsen
NOAA
Pacific Marine Environmental Lab
3711 15th Avenue, NE
Seattle, WA 98108 | 1 |
| 14. | Professor Charles S. Cox
Scripps Institute of Oceanography
University of California
La Jolla, CA 92037 | 1 |
| 15. | Professor George V. Keller
Colorado School of Mines
Department of Geophysics
Golden, CO 80401 | 1 |
| 16. | Dr. Jean H. Filloux
Scripps Institute of Oceanography
University of California
La Jolla, CA 92037 | 1 |
| 17. | Mr. William Andahazy
Naval Ship Research & Development Center
Annapolis Laboratory
Annapolis, MD 21402 | 1 |